Waste Glass as Partial Binder Precursor and Fine Aggregate Replacement in Alkali Activated Slag/Fly ash System

by

Shizhe Zhang

Submitted in partial fulfilment of the requirements for the degree of
Master of Science in Materials Science and Engineering
Specialized in Advanced Construction Materials
in
Faculty of 3mE – Department of Materials Science and Engineering
Faculty of CiTG – Department of Materials and Environment, Microlab
Delft University of Technology

December 2014 - September, 2015

Graduation Committee:

Prof. dr. ir. Klaas van Breugel	TU Delft, CiTG
Dr. Guang Ye, MSc	TU Delft, CiTG
Dr. Kamel Arbi, MSc	TU Delft, CiTG
Arno Keulen, MSc	Van Gansewinkel Minerals
Dr. ir. Michael Janssen	TU Delft, 3mE

Table of Contents

List of Abbreviations

AAMs	Alkali Activated Materials
AAS	Alkali activated slag
BSE	Backscattered electron
C-S-H	Calcium silicate hydrate
C-A-S-H	Calcium-alumino-silicate-hydrate
DTG	Differential thermogravimetry
ESEM	Environmental Scanning Electron Microscopy
EDX	Energy dispersive X-ray analysis
FTIR	Fourier transform infrared spectroscopy
GP	Glass powder
ICP-AES	Inductively coupled plasma atomic emission spectroscopy
L/S	Liquid to solid
LOI	Loss on ignition
MCL	Mean chain length
MIP	Mercury intrusion porosimetry
N-A-S-H	Sodium-alumino-silicate-hydrate
PSD	Particles size distribution
RH	Relative humidity
SSA	Specific surface area
TG	Thermogravimetry
XRD	X-ray diffraction
XRF	X-ray fluorescence

Abstract

Fast increasing of generation and release of undesirable pollutants by the industrialization raises concerns about the environmental consequences of waste disposal. Among these waste materials, non-recycled waste glass constitutes one of the majority wastes produced in many European countries and sets a major environmental issue. Although glass could be recycled into the packaging stream without significantly changing its chemical and physical properties, there is still a significant proportion, which does not meet the strict criteria for packaging glass, to be sent to landfill. Waste glass is not a biodegradable material, which made landfilling waste glass become a highly unsustainable option. To find a better solution to reduce the environmental issues caused by disposal of waste glass, alkaline activation technology is utilized to transform waste glass into alkali activated materials (AAMs) for construction. Waste glass is believed to have the potential to serve as precursor material in geopolymer production because of abundant amount of amorphous silica in waste glass. However, up till now, only limited research has been conducted on waste glass as precursor material in AAMs. Currently, the feasibility of using waste glass in geopolymer systems is still largely unknown.

This research project aims at a better understanding of the feasibility of using waste glass powder as partial binder precursor to create AAMs along with fly ash and slag and also the feasibility of using fine waste glass aggregate as partial aggregate replacement in geopolymer mortar. The main focus of this research is on the reactivity of waste glass powder and its influence on the microstructure development and gel formation, with correlation with mechanical strength.

Waste glass powder has been systematically characterized, including investigation on particles size distribution by laser diffraction, morphology by environmental scanning electron microscopy (ESEM) , chemical composition by X-ray fluorescence (XRF), crystalline phases by X-ray diffraction (XRD), amorphous phases content by selective chemical method, chemical bonds by Fourier transform inferred spectroscopy (FTIR) and dissolution properties by Inductively coupled plasma atomic emission spectroscopy (ICP). It has been found that: waste glass powder, which is dominantly in irregular polygonal shape, has much finer particles size distribution and larger specific surface area compared with fly ash and slag. It has abundant amorphous Si and Ca, and has higher reactivity than fly ash.

Microstructure development and gel formation has been analyzed, in order to study the influence of replacement of waste glass powder for fly ash. Crystalline phases, chemical bonds, and element distribution is characterized by XRD, FTIR and ESEM, respectively. Heat evolution and amount of gel product are studied by isothermal calorimetry and (differential) thermogravimetry (TG/DTG), respectively. Element distribution and binder morphology is obtained using ESEM. Strength data of paste at different curing ages are also acquired. Observations of pores in fly ash by mercury intrusion porosimetry (MIP) and ESEM before and after alkaline attack further assist in the understanding of the strength development. It has been confirmed by this study that C-A-S-H type gel is the main reaction products in alkali activated slag/fly ash/waste glass power ternary system. Waste glass powder in general leads to higher amount of gel formation and probably higher cross-linking of gel network,

and eventually lead to higher compressive strength. Inconsistency of strength development in binder with 10% waste glass powder replacement is found to be the result of competition between three factors, which are packing density, accommodation of reaction products by the fly ash and facilitated gel formation.

The effects of fine glass aggregate as replacement for sand in alkali activated slag/fly ash mortar is studied on workability and mechanical strength. It has been found that fine waste glass aggregate is feasible to be utilized in mortar preparation to replace sand while maintaining suitable mechanical strength and workability.

Finally, from this research, waste glass powder serves as effective precursor replacement for fly ash in alkali activated slag/fly ash system. Fine waste glass aggregate is possible to be utilized to replace sand in alkali activated mortars when suitable workability is taken care of. This study provides a better insight on properties of waste glass powder as well as promotes understanding of the influence of waste glass powder on microstructure and gel formation, which is essential for future research and engineering application of this kind of waste material.

1 General Introduction

1.1 Background

Fast increasing of generation and release of undesirable pollutants by the industrialization raise concerns about the environmental consequences of waste disposal. The biggest problem faced by industries today, as far as waste disposal is concerned is the safe and effective disposal of its effluent, sludge and by-products. These problems are especially According to the latest report of the year 2013 [1] released by Chinese Ministry of Environment Protection, the utilization ratio of industrial solid waste is 62.3%, which means there is still a huge amount of industrial solid wastes go to landfill. Landfilling will not only causes huge financial burden to the foundries, but also makes them liable for future environmental costs and problems. Moreover, the increasing load of toxic metals in the landfill potentially increases the threat to ground water contamination [2]. Except for environmental issues, economic factors also dictate that industry should look forward to recycling and reuse of waste material as a better option to landfilling and discarding.

Among these waste materials, non-recycled waste glass constitutes one of the majority wastes produced in many European countries and sets a major environmental issue. Although glass could be recycled into the packaging stream without significantly changing in its chemical and physical properties, recycling techniques require intricate cleaning and sorting glass of different colors and origins. Latest statistics from the European Union Container Glass Federation confirmed that the average glass recycling rates in the European Union have passed the 70% mark [3]. However, there is still a significant proportion, which does not meet the strict criteria for packaging glass, to be sent to landfill. Latest statistics from van Gansewinkel Minerals shows an annual waste glass production rate of up to 20,000 tons per year in the Netherlands along [4]. Since glass is not a biodegradable material, waste glass at the landfilling sites will not be decomposed for an extremely long period of time, which made landfilling waste glass become a highly unsustainable option.

A potential utilization of the waste glass is to use it to create construction materials. Previous studies [5-7] have already made attempts to incorporate waste glass into concrete, with general focus on replacement of fine aggregate in traditional concrete systems. In recent year, alkaline activation technology becomes a cost-effective solution for utilization of waste and by-products like fly ash, blast furnace slag, kiln dust, etc. Geopolymer based materials are environmental friendly and need only moderate energy for their production. It has been widely accepted that geopolymer is also one of the best alternatives for Portland cement-free binder for an 80 % reduction of greenhouse gases emission compared to ordinary Portland cement (OPC) [8].

1.2 Problem Description

To find a better solution to reduce the environmental issues caused by disposal of waste glass, alkaline activation technology is used to incorporate waste glass into geopolymer

systems as construction materials. Waste glass is believed to have the potential to serve as precursor material in geopolymer production because of abundant amount of amorphous silica in a structure that does not reflect long range order. However, limited research has been conducted on waste glass as precursor material in geopolymer systems, neither is the utilization of waste glass as replacement for binder precursor like fly ash. Currently, the feasibility of using waste glass in geopolymer systems is still largely unknown:

1. The reactivity of waste glass powder as binder precursor, i.e. content of amorphous phases (silica, alumina), dissolution of waste glass powder at certain condition for geopolymerization, etc.
2. The effects of waste glass powder replacement on the early age properties of geopolymer pastes, like setting time, mechanical strength and gel formation is not clear.
3. Dual function of waste glass in geopolymerization, both as activator and binder precursor
4. The feasibility of using waste glass aggregate as fine aggregate replacement in geopolymer mortar, its effects on workability and mechanical properties.

1.3 Research Goal and Objectives

The main goal of this project is to examine the feasibility of using waste glass to create geopolymer binder materials along with fly ash and slag and using waste glass cullet as partial aggregate replacement in geopolymer mortar.

The objectives are:

- Determination of both chemical composition and physical properties of waste glass powder;
- To study the reactivity and dissolution of waste glass powder in comparison with blast furnace slag and fly ash;
- Utilization of waste glass powder as partial binder precursor in slag/fly ash paste and characterization using multiple testing techniques to identify the effects of waste glass powder on early age microstructure and gel formation;
- Utilization of fine glass aggregate as sand replacement in geopolymer mortars and determination of effects on workability and mechanical strength.

1.4 Scope of this Research

There are two kinds of waste glass involved in this study, which are glass powder and glass aggregate. In this research, the utilization of waste glass material in geopolymer will be studied with the following restrictions:

- The glass powder serves as partial binder precursor replacement of FA;
- The glass aggregate serves as fine aggregate replacement;
- Liquid/Solid ratio was kept constant to be 0.42 for paste and 0.60 for mortar;
- All sample were cured at room temperature 20 °C with relative humidity of ≥95%;
- No superplasticizer or chemical admixtures were used in geopolymer paste and mortar mixtures.

1.5 Outline of Master Thesis

The outline of this master thesis is presented in Figure 1.1.

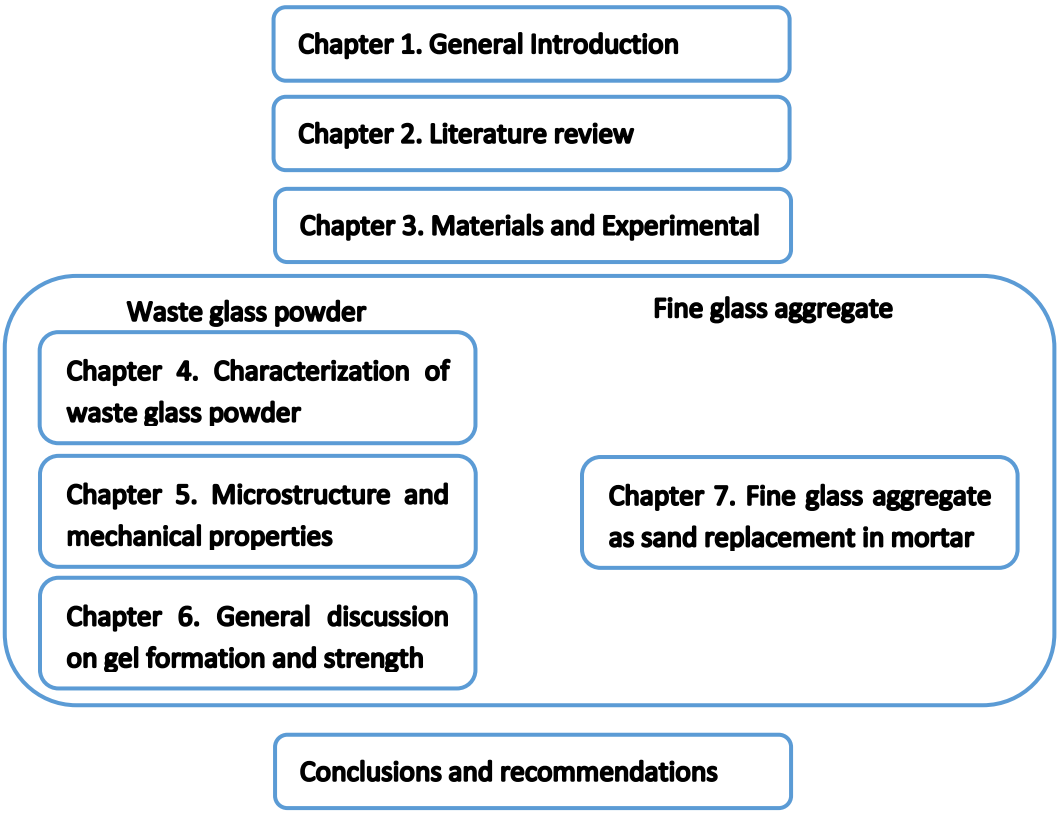

Figure 1.1 Outline of master thesis

Chapter 1 gives a general introduction of this graduation project with background, problem description and research objectives. Chapter 2 provides a short literature review of important aspects regarding to alkali activated materials and geopolymers, microstructure formation, dissolution mechanisms of precursors and waste glass powder in AMMs.

Chapter 3 gives an overview of the materials and experimental techniques used in this project. It also provides information on mixture design for pastes and mortars in later investigations. Sample preparation is also included in this chapter.

Systematic characterization of waste glass powder is given in Chapter 4, including investigation on particles size distribution by laser diffraction, morphology by environmental scanning electron microscopy (ESEM) , chemical composition by X-ray fluorescence (XRF), crystalline phases by X-ray diffraction (XRD), amorphous phases content by selective chemical method, chemical bonds by Fourier transform inferred spectroscopy (FTIR) and dissolution properties by Inductively coupled plasma atomic emission spectroscopy (ICP-AES).

Microstructure development is analyzed in Chapter 5 and Chapter 6. In Chapter 5, in order to study the influence of replacement of waste glass powder for fly ash, crystalline phases,

chemical bonds, and element distribution is characterized by XRD, FTIR and ESEM, respectively. Heat evolution and amount of gel product are studied by Isothermal calorimetry and Thermogravimetry (TG), respectively. Element distribution and binder morphology is obtained using ESEM. Strength data of paste at different curing ages are also acquired. Chapter 6 is the general discussion on gel formation and strength development of binder with waste glass powder as fly ash replacement. The strength development is correlated with microstructure development in Chapter 6. Observations of pores in fly ash by mercury intrusion porosimetry (MIP) and ESEM before and after alkaline attack further assist in the understanding of the strength development.

Chapter 7 presents the results from the use of waste glass aggregate as partial replacement for sand in selected mixture(s) and its effect on workability and strength of alkali activated slag/fly ash mortars.

Finally, the conclusions and retrospective research aspects of this project are summarized in Chapter 8.

2 Literature Review

2.1 Introduction

This literature review first provides a brief overview on important aspects regarding to alkali activated materials and geopolymers. A general introduction on the reaction mechanism and microstructure formation of gel network in alkali activated fly ash/slag binder is given. Reactivity and dissolution mechanism of precursors are reviewed. An overview of previous studies on incorporation of waste glass powder into construction materials is also shown.

2.2 Precursors for Alkaline Activation

2.2.1 Blast furnace slag

Slag, normally composed of calcium-magnesium aluminosilicate glass, is by-product of metallurgical industry. Blast furnace slag is specifically refers to those generated from iron ore reduction. Generally, calcium, magnesium, aluminum and silicon in oxides form add up to more than 95% of its chemical concentration. Ground-granulated blast-furnace slag (GGBS or GGBFS) is obtained by quenching molten iron slag (a by-product of iron and steel-making) from a blast furnace in water or steam, to produce a glassy, granular product that is then dried and ground into a fine powder. The structure and properties of slag is largely dependent on the raw materials used and also the industrial processing methods. The cooling rate as one of processing factors significantly influences the crystallinity of slag. Slow cooling of molten slag enhances the formation of crystalized Ca-Al-Mg silicates, which largely decrease their potential to be utilized as cementing component [9].

Blast furnace slag has been used as supplementary cementitious material blended with OPC. This kind of slag cement, locally typed as CEM III B cement in Netherlands, has been widely used especially in Western Europe. Another big application also lies in the field of construction materials, in which it serves as precursor in alkaline activation in alkali activated slag cements

2.2.2 Fly ash

Fly ash, as the solid by-product of the combustion of coal, is generally collected from the chimneys of coal-fired power plant. The fly ash particles are dominantly spherical in shape and range in diameter from 1 to 200 µm. Some of the fly ash particles are even hollow shaped. It contains both crystalline phases like quartz, mullite, hematite, etc. and also amorphous phases. Fernandez-Jimenez and Palomo found that fly ash with unburned material content lower than 5 wt%, Fe_2O_3 content less than 10 wt%, high reactive silica content and vitreous phase along with a fine particle size distribution was most suitable for alkali activation [10].

Two type of fly ash are specified according ASTM C618, which are Class C fly ash and Class F fly ash. The main difference lays in their different element contents. Class C fly ash is produced from lignite or subbituminous coal. The total content of SiO_2, Al_2O_3, and Fe_2O_3 in

Class C fly ash is greater than 50%. On the other hand, Class F fly ash has been produced from anthracite or bituminous coal with a total content of SiO_2, Al_2O_3, and Fe_2O_3 greater than 70%. In this research, Class F fly ash is used with consideration of higher amount of silica, alumina.

2.2.3 Waste glass powder

Glasses are non-crystalline silicates containing other oxides. Silicon atoms together with other elements (e.g. Al, Zr, B) that readily form bridging bonds with oxygen atoms provide the highly cross-linked glass network. Alkali cations (e.g. Li^+, Na^+, K^+) alter the network structure; they are usually present as ions, and are charge compensated by nearby non-bridging oxygen atoms.

The waste glass powder used in this project is a residue from the pre-processing of bottle glass recycling. Unlike normal glass powder manufactured by the crushing and milling of waste glass, glass is first dried before recycling process and this powder is sucked from the dried glass as residue.

2.3 Alkali Activated Materials & Geopolymers

Generally, alkali activated materials (AAMs), including geopolymer binders with other systems, are the broadest classification for any binder system derived from the reaction of an alkali metal source (solid or dissolved) with a solid silicate powder [11]. These materials maintain comparable performance to traditional cementitious binders but with added advantage on greenhouse gas emission reduction and sustainable utilization of industrial byproduct and residuals. The range of the solids varies largely from a calcium silicate as in alkali-activation of conventional clinkers to a more aluminosilicate-rich precursor. The common aluminosilicate precursors are metallurgical slag, natural pozzolan, fly ash, metakaolin, bottom ash, etc. The alkali sources are essentially any soluble substance which can supply alkali metal cations, raise the pH of the reaction mixture and accelerate the dissolution of the solid precursor [12]. Among all these alkali sources, alkali hydroxides, silicates, carbonates, sulfates, aluminates or oxides of sodium and potassium are most commonly used.

The history of alkali activation dates back to ancient times. As stated by Davidovits, the Egyptian pyramids are suggested to have been poured in place utilizing chemical reactions involved in alkali activation [13]. First systematic studies on AAMs began in 1940s when Purdon analyzed clinker free cement made from slag and NaOH [14]. A significant breakthrough was made in 1967 by Glukhovsky when Soviet Union was trying to find a substitution for OPC as construction materials. This study focused on binders from low calcium or calcium-free aluminosilicate (clay) and alkaline metal solutions. Glukhovsky called these binders “soil cements” and the respective concretes “soil silicates”. He also classified binders into two groups, depending on the composition of the starting materials: alkaline binding systems Me_2O-Al_2O_3-SiO_2-H_2O and “alkali-alkaline-earth” binding systems Me_2O-MO-Al_2O_3-SiO_2-H_2O (where Me=Na, K,⋯ and M=Ca, Mg,⋯) [15]. Similarly, two categories of AAMs based on their components of reaction products are defined later by Palomo: The first type being those based on silicon and aluminum composition (e.g.

metakaolin and fly ash), with main product as three dimensional aluminosilicate gel; and the second being those based on silicon and calcium composition (e.g. blast furnace slag), with C-S-H as the man reaction product [16]. Initially, most research upon alkali activation focused on the materials classified as in group 2 (alkali-alkaline-earth binding systems Me_2O-MO-Al_2O_3-SiO_2-H_2O). Alkali activated slag has already been applied in a great many constructions, including buildings; precast road slabs and blocks, etc. The research on the first group became popular only after the work of Davidovits on alkali activated metakaolin in 1760s, with the initial purpose to synthesize a fire-resistant material as an alternative to organic thermosetting polymers.

Davidovits named this kind of material "geopolymer" in 1978 considering its structural similarities with organic polymers. According to him, they are polymers because they transform, polymerize and harden at low temperature. Nonetheless, they are also geopolymers, since they are inorganic, hard and high temperature resistant and also nonflammable [17]. Based on his research work Davidovits elaborated a structural model of the geopolymer (in this case, the model was designed for a poly-sialate-silox type formed by alkali activation of metakaolin). Davidovits suggests the name ''polysialates'', in which sialate is an abbreviation for aluminosilicate oxide. The sialate network is composed of tetrahedral anions $[SiO_4]^{4-}$ and $[AlO_4]^{5-}$ sharing the oxygen, and positive ions such as (Na^+, K^+, Li^+, Ca^{2+}, Na^+, Ba^{2+}, etc.) These cations associated with aluminium to serve as positive change balancer for Al^{3+} in tetrahedral coordination. An empirical formula for the polysialate is shown as following:

$$M_n\{-(SiO_2)_z - AlO_2\}_n, wH_2O$$

where n is the degree of polymerization, z is 1, 2 or 3, and M is an alkali cation, such as potassium or sodium, generating different types of polysialates [18]. As shown in Figure 2.1, these polysialates are distinguished by different Si/Al ratio, which representing the number of silicon atoms being replaced by aluminium.

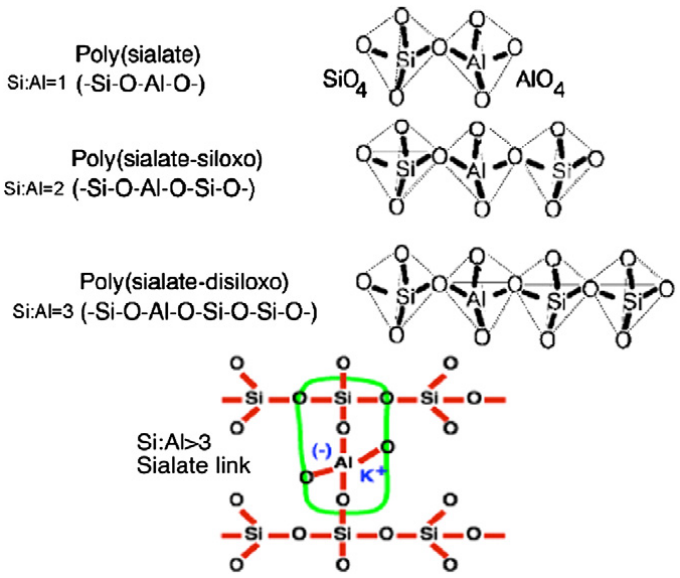

Figure 2.1 Chemical structures of Polysialate (PS), polysialate-siloxo (PSS) and polysialate-disiloxo (PSDS) by Davidovits [18].

The reaction mechanism of alkali activated aluminosilicate material was proposed by Glukhovsky with a general model in 1967. In this model, the reaction process is divided into three main steps: (i) destruction-coagulation, (ii) coagulation-condensation and (iii) condensation-crystallization [15].

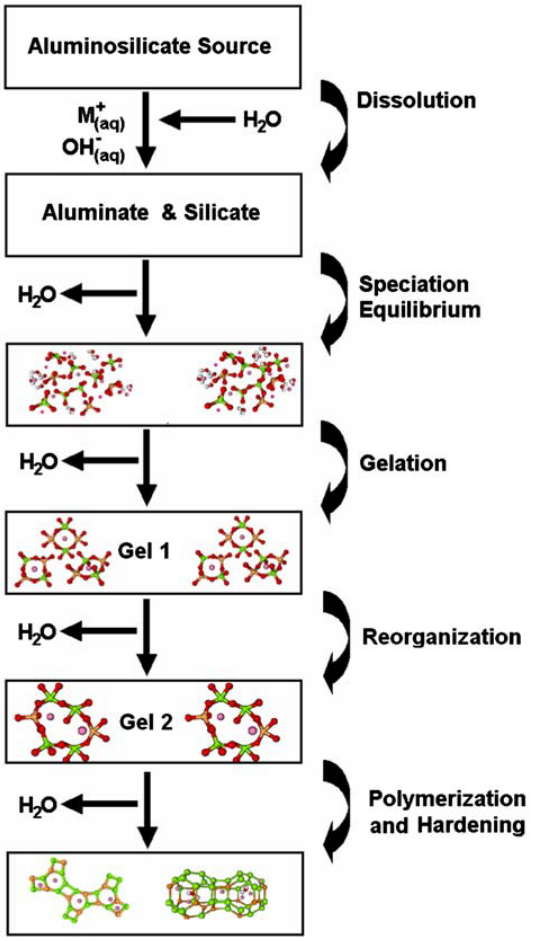

Figure 2.2 Conceptual model for geopolymerization after Duxson [19]

Combining with knowledge of zeolite synthesis, recent research expanded this theory to explain the formation of alkali activated aluminosilicate. A detailed model for the geopolymerization is explained by Duxson et al [19]. The scope of this discussion is limited to geopolymers synthesized from aluminosilicate precursors, especially fly ash-based and metakaolin-based materials. Part of conceptual geopolymerization model is shown in Figure **2.2**. The first stage is the dissolution of vitreous/amorphous phases in the solid particles in the alkaline solution. The dissolution of solid particles at the surface leads to the liberation of aluminate and silicate (most likely in monomeric form) into solution, which will enable later geopolymerization. These source materials, after speciation equilibria in the solution, may exist in several kinds of forms, like monomer, dimer or trimers [15]. When the saturation occurs, the second stage gelation starts and aluminosilicate gels forms.

2.4 Alkali Activated Fly ash/Slag

Fly ash and blast furnace slag are most popular choices as main raw materials for production of AAMs. Previous studies on alkali activated fly ash/slag are mostly on the microstructure and mechanical properties, also give insights into the chemical makeup and formation mechanism of the reaction products. A number of researchers [20, 21] found that the incorporation of GBFS to FA geopolymer resulted in additional calcium in the system and the mechanical properties and microstructure of geopolymer were improved.

Microstructure and nature of gel formation in alkali activated fly ash/slag binder was also characterized in previous studies. Lloyd [22] identified increasing amount of slag as a calcium source will lead to the formation C-S-H products with certain degree of aluminum substitution. Kumar et al. [20] researched on effect of slag replacement of fly ash geopolymers, and found that C-S-H gel to be dominant reaction products, coexisting with aluminosilicate gels. A similar result on the dominance of slag is also reported by Provis et al. [23] with blends of fly ash and slag of ratio 1:1. Puertas et al. [21] studied the hydration products of alkali activated fly ash/slag with ratio 50/50 (wt%) activated with NaOH. The main reaction product in the pastes is a hydrated calcium silicate, like C-S-H gel, with high amounts of tetra-coordinated Al in its structure as well as Na ions in the interlayer spaces. Other reaction product was detected in later research as result of fly ash activation, which is an alkaline aluminosilicate hydrate with three-dimensional structure [24]. The C-S-H products with certain degree of aluminum substitution in above research papers is also treated as aluminum modified C-S-H gel or C-A-S-H gel in later publications.

Metakaolin has been regarded as a more pure Si and Al source than fly ash. Bernal et al. [25] studied alkali silicate-activated slag/metakaolin pastes, both C–A–S–H and (C, N)–A–S–H type gels are formed in activated binders solely based on slag, along with the zeolitic products gismondine and Garronite. In activated blended pastes with 0.8 or 0.9 slag/metakaolin ratio formed a (C, N)–A–S–H type gel. Two distinct binding products were confirmed, where the “inner” products and the “outer” products consistent with (C, N)–A–S–H and C–A–S–H type gels, respectively. Yip et al. studied the alkali activated metakaolin/slag binder and found that by a moderate amount of calcium source, i.e. slag, will improve the mechanical properties [26]. It has also been confirmed that C-S-H gels were the main products when metakaolin was alkali activated in the presence of calcium hydroxide under low alkalinity. The dominant reaction product become aluminosilicate gel with alkali hydroxide increased from 5 M to 10 M [27, 28].

Recent research on the phase modification of alkali-activated slag by fly ash incorporation indicates that the nature of this gel is strongly dependent on the slag/fly ash ratio. With slag contents $\geqslant$50 wt%, the main binding product is a calcium silicate hydrate gel substituted with Al and Na (C-N-A-S-H), or N-C-A-S-H gel, or intermixed gel of this two. With increased contents of fly ash, the main product tend to be a hybrid binding phase described as N-C-A-S-H gel, with a higher degree of crosslinking than C-A-S-H gel formed in AAS [29]. Other studies suggested that, with moderate fly ash content, the coexistence of C-A-S-H gel with a more aluminosilicate type gel is possible. These gels are intermixing towards the formation of a third hybrid binding phase and do not remain independent of each other,

thus could not be differentiated using only ESEM/EDX [20, 30, 31]. C-A-S-H type gel is preferred over aluminosilicate geopolymers at high pH (>12) and it is reported that Ca ions could degrade geopolymeric gel on the fly ash spheres and disrupt the three-dimensional structure of geopolymers [32].

2.5 Reactivity of Precursors

Previous studies on reactivity of precursors focus on element dissolution process and on amorphous phase content, especially amount of reactive silica and alumina. When it comes to alkali activation of aluminosilicate precursors, reactive silica and alumina amount is of great significance because their ability to react simultaneously with alkalis and introduce cementitious properties to the products.

Lee and van Deventer [33] conducted a leaching test of fly ash in varying concentrations of soluble silicate solution (pH=13.95) at room temperature. Ca and Si were found to dissolve followed by Al, and the dissolution process was inhibited by the secondary precipitates formed on the surfaces when soluble silicate solution of low molarity was utilized. High molarity greatly enhanced the dissolution followed by a gel-phase precipitate being produced similar to geopolymeric gel. Mikuni et al. [34] studied the dissolution properties of three kinds of fly ash in NaOH solution with different concentrations. The results showed that Ca^{2+} was dissolved in relatively large amount in neutral water and decreased with increase of NaOH concentration; however, the dissolution of Al^{3+} and Si^{4+} was both enhanced with the increase of solution concentrations and reaction temperature. In addition, Chen-Tan et al. [35] conducted a similar research using chemical treatment with NaOH solution and quantitative XRD in conjunction with XRF to determine the amorphous phase content. They found that even under ideal conditions (high pH, extended time, elevated temperature, and stirring), the maximum amount of material that could be dissolved from fly ash was lower than quantitative analysis. This suggested that less of the amorphous component would be available to take part in the dissolution and polycondensation reaction. Of critical importance was the observation that the amorphous iron oxides did not appear to play a significant role in the geopolymerization process.

Except for element dissolution of precursors, amorphous phase content is also another indicator for the reactivity of precursors. Selective chemical attack analysis and XRD combined with the Rietveld methods [36-38] are two ordinary approaches for determine reactivity of precursors, which have been most intensively used. Fernández-Jimenez et al. [39] studied vitreous and crystalline components of fly ashes using three techniques: Chemical analysis with selective HF acid solution, Rietveld X-ray powder diffraction quantification and nuclear magnetic resonance (NMR) and confirmed NMR are also highly effective in characterizing and quantifying the phases present in fly ash.

2.6 Dissolution Mechanism

The dissolution of solid particles at the surface is assumed to be the mechanism responsible for conversion of the solid particles into available source material during geopolymerization. This assumption does have overwhelming scientific merit based on the literature describing

alkaline dissolution. The dissolution mechanism of aluminosilicate minerals in acidic or alkaline solution has already been studied intensively in geological research. These former researches have provided a solid foundation for understanding dissolution of geopolymer precursors in under the attack of alkaline activator.

2.6.1 Dissolution of aluminosilicate precursors

Although aluminosilicate precursors like fly ash and slag as industrial by-products have more complicated structures than natural minerals like feldspar, basaltic glass, etc., they share similar dissolution mechanism because they are all multi-oxide aluminosilicate in nature. In general, the metals are liberated by metal/proton exchange reactions by analogy with single hydro (oxide) [40-42].

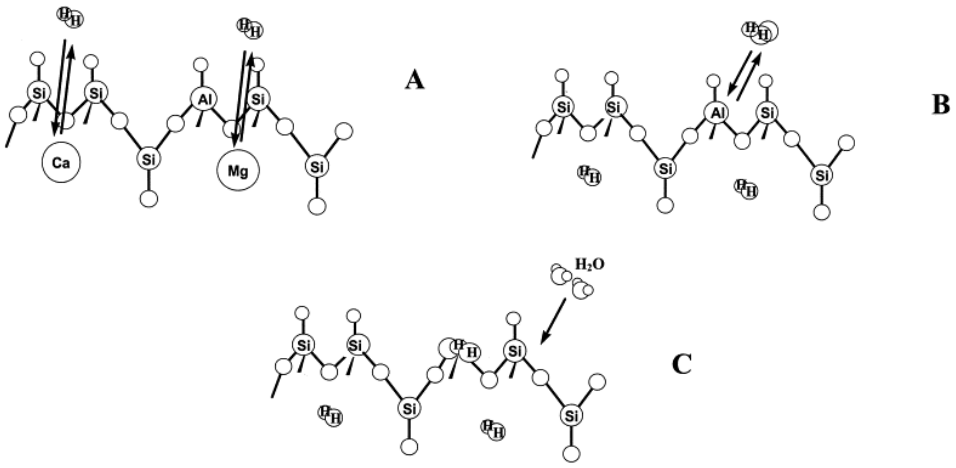

Figure 2.3 Mechanism of basaltic glass dissolution as an schematic illustration of aluminosilicate precursors by Oelkers and Gislason [43].

A schematic illustration of aluminosilicate precursors is shown in Figure 2.3, which is the dissolution basaltic glass in acidic solutions constructed by Oelkers and Gislason. Dissolution process begins by exchanges of monovalent and divalent cations via metal-proton exchange reactions (Step A in Figure 2.3). Afterwards, the framework rich in Al and Si is destroyed by partial removal of Al by Al-proton exchange reactions (Step B in Figure 2.3) and also liberation of partially detached Si tetrahedral (Step C in Figure 2.3) [43]. Step B and C can be further explained as follows: The attack of OH^- ions from the liquid phase on the solid/liquid interface causes breaking of the surface Si-O-Al and Si-O-Si bonds of the precursor and formation of soluble aluminate and silicate species. Owing to agitation of the suspension, soluble silicate and aluminate species so formed leave the solid/liquid interface and tend to be homogeneously distributed throughout the bulk of the liquid phase [44]. Possible gel formation may exist when concentration of soluble silicate and aluminate species reach certain limits.

It is worth noting that although Figure 2.3 indicates the mechanism of dissolution of aluminosilicate precursor under acidic conditions, the one under alkaline conditions have similar mechanism. Protons, instead of from acid, now come from hydroxyl ion. They are also available for metal-proton exchange reactions, albeit probably change the reaction pathway depending on different structures of aluminosilicate material [45].

Since metal-proton exchange reactions largely depend upon the availability of proton, the pH of the solutions largely affect the dissolution rate under both acidic and alkaline conditions. The reaction rate is comparably higher in a more acidic or more alkaline liquid. Other factors on dissolution rate like Al/Si ratio, specific surface area, etc. are also of significance.

2.6.2 Dissolution of waste glass

Most of the theoretical work on glasses dissolution was concentrated on the short-term diffusion controlled alkali leaching as an initial step of the glass/water reaction. In this project, the dissolution of waste glass is focused in dissolution in alkaline solutions of high pH value.

Corkhill, et al [46] studied the dissolution of UK waste glass at simulated hyper-alkaline conditions. The initial dissolution process is the interdiffusion process, resulting in an alkali depleted, silicon-rich zone at the glass surface.

$$\equiv \mathrm{Si} - \mathrm{O} - \mathrm{Si} \equiv + OH^- \rightarrow \equiv Si - OH + \equiv Si - O^-$$

Hydrolysis of the glass leads to the rupture of Si bridging bonds, leading to the release of orthosilicic acid, $Si(OH)_4$. For that reason, the resistance to alkaline media is much higher than in acidic one. In alkaline media, glass is able to be depolymerized, resulting in a total destruction of its network.

$$\equiv \mathrm{Si} - \mathrm{O}^- + \mathrm{H}_2O \rightarrow \equiv Si - OH + OH^-$$

Resulting in silicate solution:

$$\equiv \mathrm{Si} + 2\, H_2O \rightarrow Si(OH)_4$$

Bunker et al. [47] also explained that the tetrahedral SiO_4 sites common to all silicates glasses were susceptible to nucleophilic attack primarily by OH^- to form a reactive five-coordinated intermediate which can be decomposed to rupture the Si-O-Si bond. Therefore, a significant quantity of OH^- could improve the formation of a five-coordinated intermediate which could lead to a great dissolution of the glass.

A number of studies have considered the effect of high pH on the early dissolution of simulant waste glasses of varying composition. Dissolution rates are found to be pH dependent, with significantly higher dissolution rates observed above pH 9. It has been suggested that enhanced dissolution is likely due to a breakdown of the silicate network. Like this project, these studies used hydroxides of sodium and potassium to buffer the pH to higher values, which are not expected to interact with dissolved glass components significantly during early stages of dissolution.

2.7 Waste Glass Powder in Alkali Activated Materials

Waste glass powder has been reported to have the potential to serve as precursors for AAMs [12]. Nonetheless, limited research has been conducted with waste glass powder as binder precursor AAMs. Tashima et al. [48] investigated the properties and microstructure of alkali-activated glass fiber waste using NaOH and KOH solution as activators. The mortar samples showed compressive strengths of up to 77 MPa after three days of curing at 65°C

when 10mol/L NaOH solution was used as activator. Pascual et al. [49] used metakaolin (MK) to replace a part of the glass powder in order to introduce Al and also to stabilize alkali ions in the system. Compressive strength of the mortars increased with MK content up to 8%. In contrast, without MK or with less than 3% MK content, the compressive strength decreased with time.

Redden and Neithalath [50] utilized silica-rich glass powder to produce sustainable binders through alkaline activation. Glass powder activated using NaOH provides higher compressive strengths than NaOH activated fly ash binders at lower heat curing temperatures. Sodium silicate gel is the reaction product when glass powder alone is used as the source material, while a combination of sodium silicate and sodium aluminosilicate (N-A-S-H) gels form in activated glass powder-fly ash blends. Inferior moisture stability and corresponding strength loss is compensated by doping the systems with Al containing (metakaolin) and Ca containing (slag) source materials, while retaining glass powder as the major component (≥50%).

On the other hand, researchers also explored the potential of using waste glass powder to produce alkali activator. Puertas and Torres-Carrasco [51, 52] activated blast furnace slag with three activators: commercial water glass, a $NaOH/Na_2CO_3$ mixture, and the solutions derived from dissolving waste glass in $NaOH/Na_2CO_3$. The compressive strength was over 60 MPa at 28 days when the $NaOH/Na_2CO_3$ mixture and the glass waste mixed solution were used as activators, indicating that this glass was potentially useful as a supplementary silica source in place of commercial silicate solutions.

These results confirms the potential for waste glass powder to be utilized in alkaline activation technology to produce AAM with stable properties, which serves as theoretic basis when design an AAM involving waste glass powder as precursor or alkali activator.

3 Materials and Experimental Methods

3.1 Materials

Three different kinds of raw materials as binder precursors are used throughout this research projects, namely blast furnace slag, fly ash and waste glass powder (GP). Waste glass powder serves as replacement in slag/fly ash paste. Normalized sand and 0.1-2 mm fine glass aggregates (GA) were used in producing mortars. Fine glass aggregate serves as sand replacement in mortars.

The following materials were used in this study:

- Blast furnace slag (Orcem B.V.)
- Class F Fly ash (Vliegasunie B.V.)
- Waste glass powder (Van Gansewinkel Maltha B.V.)
- CEN Reference sand
- Fine waste glass aggregate (Van Gansewinkel Maltha B.V.)
- Sodium Hydroxide (analytical grade, purity≥98%, supplied by Sigma-Aldrich)
- Distilled water

Although waste glass powder and fine glass aggregate are all from recycling stream of waste glass, a few distinctions exist between them. Waste glass powder, as sucked by the vacuum cleaner after the drying process when recycling; consist of really fine particles of size under 10 µm. While the fine glass aggregates are 0.1-2mm fractions crushed waste glass cullet.

As one of the main objective to study the chemical and physical properties of waste glass powder, the detailed characterization of waste glass powder in comparison with slag and fly ash will be given in Chapter 4.

3.2 Mixture Design

Microstructure development of alkali activated slag/fly ash binder with different level of GP for fly ash was characterized in order to study the influence of GP on microstructure and gel formation. Paste made only with solid precursors and alkali activator was used for these microstructural tests to eliminate the influence by aggregate or other chemical admixtures. The feasibility of using GA as sand replacement is evaluated in mortar, to study its influence on workability and mechanical strength.

The mixture design of both paste and mortar are presented in this section.

3.2.1 Activating solutions preparation

From the previous experiments in alkali activated binder based on slag (50 wt. %) and fly ash (50 wt. %) by Van Gansewinkel Minerals, 4 M NaOH solutions is regarded to be the optimum for this type of mixture cured at ambient temperature since it provide a balance between good mechanical properties and cost benefit. Therefore, 4 M NaOH solutions were chosen to be the alkali activator for all mixtures in this project, both for paste and mortar.

4 M NaOH solutions were prepared one day before casting of both pastes and mortars. The amount of solid NaOH and distilled water needed were first calculated from the molar concentration. After weighing all the materials using electric balance, the solid NaOH pellets were dissolved in distilled water. As dissolving of NaOH is exothermic, a magnetic stirrer was used for better dissolving and heat convection while at the same time the solution was cooled by water bath. Afterwards, the solution was left to further cool to room temperature before use.

3.2.2 Paste design

7 different geopolymer pastes were prepared with mixture proportion listed in Table 3.1. The pastes prepared using slag (50 wt. %) and fly ash (50 wt. %) as binder precursors were set as the reference. GP served as partial precursor replacement for fly ash in the binder. The GP to fly ash replacement level was 0, 10%, 20% and 30% respectively with respect to total mass of solid precursors. The obtained mixtures were names R, G10, G20 and G30, respectively.

The precursors were activated by 4M NaOH solutions. Through trial and error, the liquid to solid (L/S) ratio was fixed constant at 0.42 in order to guarantee adequate workability for all mixtures.

The replacement for fly ash was limited to maximum 30% for several reasons. The first is because of the fine particles size distribution of GP. Fine particle size distribution generally has a major effect on water demand since finer particle size can significantly increase the specific area, which may further lead to higher liquid demand and worse workability. Another reason according previous studies is that GP can react with sodium hydroxide to form sodium silicate, also known as water glass [50, 52]. Compared with original sodium hydroxide solution, the sodium silicate solution has higher viscosity which can make it hard to flow. This phenomenon also occurred in mixing procedure in this project. In this way, if too much GP is involved in the reaction, the workability of paste will be reduced.

Table 3.1 Mixture proportions of paste with different level of GP replacement

Sample	L/S ratio	Activator	Slag (wt. %)	FA (wt. %)	GP (wt. %)
R	0.42	100% 4M NaOH	50	50	0
G10				40	10
G20				30	20
G30				20	30

Weight percentage is with respect to the total mass of solid precursors.

3.2.3 Mixing and curing of pastes

After weighing all precursors and activating solution, the raw materials were first mixed for 5 min using a HOBART® mixer at low speed. Activating solution was then gradually added and the raw materials were mixed with activating solution for another 5 min at middle speed. Afterwards, the pastes were cast in prismatic molds of 40mm x 40mm x 160mm. The fresh mixtures were put on vibration for 4 times with each time to be 30s in order to remove

entrapped air. Since the L/S ratio is more than needed for the reference samples, they were only vibrated twice, each for 60s to prevent possible bleeding. Afterwards, the molds were sealed with plastic foam for curing. The paste samples were removed from the molds after 24 hours and transferred to a climate room (20°C and 95% RH) until testing age at 1, 7 and 28 days curing for compressive strength. Fractured pieces and powder of mixtures after 1, 7 and 28 days curing were used for mineralogical and microstructural characterization which is elaborated in Chapter 5.

3.2.4 Mortar design

As particles size distribution (PSD) of fine aggregate influence on mechanical strength of mortar, the fine waste glass aggregate (GA) with exactly the same PSD as CEN reference sand is used as replacement. GA is first separated in a sieving machine equipped with sieves of different sizes.

Table 3.2 Particle size distribution of CEN Reference sand [53]

Square mesh size (mm)	2.00	1.60	1.00	0.50	0.16	0.08
Cumulative sieve residue (%)	0	7±5	33±5	67±5	87±5	99±1

Each fraction retained in the sieves was weighed and was mixed afterwards according to the standard for the particle size distribution of CEN Reference sand, as shown in Table 3.2. These mixed GA was used as sand replacement in mortar preparation.

Table 3.3 Mixture proportions of mortar with different level of GA replacement

Sample	L/S ratio	Activator	Precursors (g)			Aggregate (g)	
			Slag	FA	GP	Normalized Sand	GA
R-0	0.6	100% 4M NaOH	225	225	-	1350	-
R-10						1215	135
R-20						1080	270
R-30						945	405
G-0				90	135	1350	-
G-10						1215	135
G-20						1080	270
G-30						945	405

8 different geopolymer mortars in two groups were prepared according to the mixture proportion as shown in Table 3.3. The two groups are name as R (Reference) and G30 (30% GP replacing fly ash). 450 g of precursors were used in each batch of mortar preparation. The proportions of precursors were exactly the same as were those described in R (Slag 50 wt%, FA 50 wt%) and G30 (Slag 50 wt %, FA 20 wt% and GP 30 wt%) paste, as is shown in Table 3.1. Within each group, four different replacement levels of GA to reference sand were chosen, which were 0, 10%, 20% and 30% with respect to the total mass of fine

aggregate. Accordingly, the obtained mortar samples in group R were further named R-0, R-10, R-20 and R-30. The sample names were likewise for the G30 group.

All mortar mixtures were prepared according to the European standard (EN 196-1): methods for testing cement [53]. The L/S ratio was fixed at 0.6 in order to provide suitable workability for all mixtures, despite of the different water absorption capacities of the precursors.

3.2.5 Mixing and curing of mortars

In the mixing procedure, the raw materials were first mixed for 5 min using a HOBART® mixer at low speed. Activating solution was then gradually added and the raw materials were mixed with activating solution for another 5 min at middle speed. Afterwards, the pastes were cast in prismatic molds of 40 mm x 40 mm x 160 mm. The fresh mixtures were put on vibration for 4 times with each time to be 30s in order to remove entrapped air. Since the L/S ratio is more than needed for the reference samples, they were only vibrated twice for 60s to prevent possible bleeding. Afterwards, the molds were sealed with plastic foam for curing. The paste samples were removed from the molds after 24 hours and transferred to a climate room (20° C and 95% RH) until testing age at 1, 7 and 28 days curing for compressive strength. Fractured pieces and powder of mixtures after 1, 7 and 28 days curing were used for mineralogical and microstructural characterization which is elaborated in Chapter 5.6.1.

3.3 Experimental Methods

Determination of the physical and chemical properties of solid precursors as well as microstructural development and mineralogical characterization of geopolymer paste were performed utilizing a series of experimental techniques. The tests performed on solid precursors, pastes and mortars are listed in Table 3.4, Table 3.5 and Table 3.6, respectively.

Table 3.4 Tests performed on solid precursors

Properties	Experimental Methods
Crystalline phases	X-Ray Diffraction (XRD)
Chemical composition	X-ray fluorescence (XRF)
Amorphous phase content	Selective chemical attack method with XRF
Particle size distribution	Laser Diffraction
Specific area and density	BET nitrogen absorption
Element dissolution	Inductively coupled plasma atomic emission spectroscopy (ICP-AES)
Pore structure of fly ash	Mercury Intrusion Porosimetry (MIP)

Table 3.5 Tests performed on the paste

Properties	Experimental Methods
Crystalline phases	XRD
Microstructure	Environmental scanning electron microscopy (ESEM)
Gel formation	Fourier transform infrared spectroscopy (FTIR), Energy dispersive spectroscopy (EDX)
Element distribution	EDX
Heat evolution	Isothermal Calorimeter
Strength	EN-196-1

Table 3.6 Tests performed on the mortar

Properties	Experimental Methods
Strength	EN-196-1
Workability	EN-1015-3

3.3.1 Particle size distribution

Particle size distributions of solid precursors were measured by Laser diffraction, which was performed on a laser diffraction machine as shown in Figure 3.1. This instrument can measure powders with a size distribution ranging from 0.1 to 1,000 µm. The chosen dispersant was ethanol. The sample is insoluble in ethanol and the ethanol does not react with the sample itself. An external ultrasonic bath was used for the de-agglomeration of the particles, increasing the dispersion efficiency.

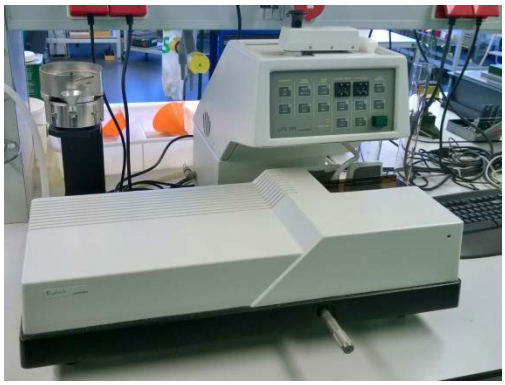

Figure 3.1 Eye Tech Laser Diffraction Machine

The instrument was first rinsed with ethanol until reaching a required cleanness of the system. 500 ml ethanol was poured into the upper sink afterwards and 0.5 gram solid precursor was weighed and put into the ethanol for 5 min ultrasonic bath. The measurement started right after ultrasonic bath and the settings for the instrument is listed in Table 3.7. The system was drained and cleaned with distilled water after each measurement. For each precursor, experiments were repeated at least 5 times to ensure reproducibility of the results.

Table 3.7 Laser Diffraction Instrument settings

Flow speed	15	Stirrer speed	15 rpm	Time per cycle	180 s
Flow direction	Backwards	Ultrasonic bath	5 min	Number of cycles	3

3.3.2 Specific surface area

The specific surface area (SSA) of solid precursor powder was studied using nitrogen absorption method established upon BET theory, in which the physical adsorption of gas molecules on a solid surface. Physical adsorption depends on the forces between the gas molecules and the adsorbent surface of the powder, in this way the measurement of the SSA of a material is possible. The measurements were conducted on a Micrometrics Gemini VII 2390 V1.03, which is shown in Figure 3.2.

Figure 3.2 Micrometrics Gemini VII 2390 V1.03

The determination is performed at the temperature of liquid nitrogen (-195.75 °C). The specific surface area was determined according to the BET equation:

$$\frac{1}{V(\frac{p_0}{p}-1)} = \frac{1}{V_m} + \frac{C-1}{V_m C}\frac{p}{p_0}$$

Where p and p_0 are the equilibrium and the saturation pressure of adsorbates at the temperature of adsorption, V is the adsorbed gas volume, V_m is the monolayer adsorbed gas volume and C is the BET constant.

The SSA is calculated as following:

$$S_{BET} = \frac{S_{total}}{a} = \frac{V_m \cdot N_A \cdot s}{V} \cdot \frac{1}{m}$$

Where V is the molar volume of N_2 (2.242 m^3); N_A is the Avogadro's number; s is the area of cross section of the N_2 molecule (0.162 nm^3); m is the mass of solid precursors used in the tests.

3.3.3 Pore structure analysis of fly ash

The pore size distribution of fly ash was examined using mercury intrusion porosimetry (MIP). Covering a broad range of pore sizes, MIP for characterizing the pore structure has

been proved to be quite useful in cementitious materials for several decades. MIP can measure a pore diameter ranging from 0.001 μm to 1000 μm according to variable pressure applied. The MIP machine is shown in Figure 3.3.

Figure 3.3 Micrometrics Pore Sizer® 9320

The relation between pressure p (MPa) and the pore diameter D (μm) is correlated by the Washburn equation:

$$\mathrm{p} = -\frac{4\gamma \cos\theta}{d}$$

In which γ is the surface tension of the mercury (mN/m) and θ is the contact angle between mercury and the pore surface of tested solid. In this specific case, γ=480 N/m and θ=139 were used.

The total porosity was calculated from the maximum total volume of mercury intruded into the solid. The pore size distribution was determined by the following equation：

$$\mathrm{dV(d)} = -\frac{V_{pore}}{d} \cdot \frac{dV}{dp}$$

Where V_{pore} is the pore volume and d is the pore diameter.

3.3.4 Crystalline phases analysis

Crystalline phases in both solid precursors and paste mixture after 1, 7 and 28 days were determined by using X-ray diffraction (XRD). As a nondestructive testing method for crystalline phases in the solid, XRD determines the scattered intensity of the electron beam as a function of incident and scattered angle, through which reflects information of crystalline phases. By comparing differences in XRD patterns, characterization of crystalline phases can be made and it can also provide useful information about gel formation and microstructure development.

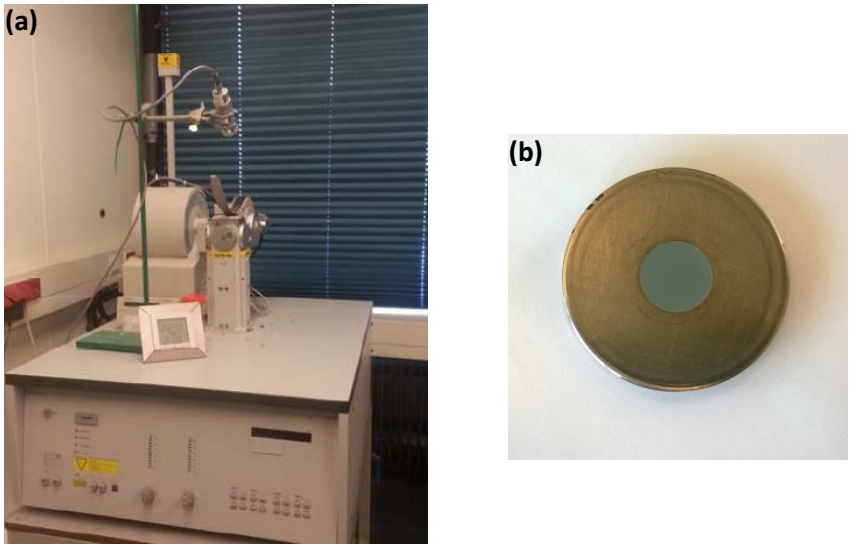

Figure 3.4 (a) Philips PW 1830 powder X-ray diffractometer; (b) Aluminum sample holder with sample

XRD is conducted using a Philips PW 1830 powder X-ray diffractometer, which is shown in Figure 3.4 (a), with Co Kα (1.789Å) radiation, tube setting to be 40kV and 40mA, a step size of 0.030°,a rate of 2.0 seconds per step and a 2θ range of 5-70°. The powder sample was compressed and placed into the center of aluminum sample holder which is shown in Figure 3.4 (b).

3.3.5 Amorphous phase content

The amorphous content in both GP and fly ash were measured by chemical dissolution treatment outlined in EN 196-2 Chemical Analysis of Cement [54]. In this method, the solid precursors were dissolved in the concentrated acid solution and were afterwards treated with the boiling potassium hydroxide solution. The residue was heated up to 1050 °C and was allowed to cool to room temperature before weighing. The dissolved fraction, which is the mass loss after chemical dissolution treatment, is the amorphous content. This method has also been used to characterize amorphous content in fly ash in previous studies [39, 55]. Amorphous content of raw materials could also be determined by quantitative Rietveld analysis; however, due to the limitation of analyzing software, only chemical dissolution method was used.

XRF analysis was conducted on the residues. Combined with SiO_2 and Al_2O_3 content in XRF results of GP and fly ash, the reactive SiO_2 and Al_2O_3 content can be calculated.

3.3.6 Element dissolution of fly ash and GP in NaOH

The element dissolution of precursors in alkali activator solution, in this case, the 4M NaOH solution was studied by element leaching test modified according to NEN 7375 leaching test [56]. At the beginning of the test, 5 g of solid precursors were added into 50 ml 4M NaOH solution with stirring speed at 300 rpm on a magnetic stirrer. A plastic bottle with cap was used as container. For each precursor, different dissolution times were set as 5 min, 30 min, 1 h, 2 h, 6 h and 12 h. After reaching certain dissolution time, the solutions were separated

from the remaining solids through vacuum filtration using a glass micro-filter paper. The solution was afterwards acidified and the Si, Al, Ca concentrations were measure using inductively coupled plasma optical emission spectrometry (ICP-OES). The experimental instrument is Optima 5300 DV ICP-OES, as is shown in Figure 3.5.

Figure 3.5 Optima 5300 DV ICP-OES

3.3.7 Chemical bond changes monitoring

The chemical bonds in both solid precursors and paste mixtures from a curing age of 1, 7 and 28 days were measured by Fourier transform infrared spectroscopy (FTIR). FTIR identifies different chemical bonds in a molecule from the absorption of infrared radiation at different wavelengths. With assistance of attenuated total reflectance (ATR), the solid state powder samples can be examined. The FTIR spectra at different curing ages can reflect how the gel network is developing by monitoring certain shift of chemical bonds.

FTIR spectra were collected using Spectrum TM 100 Optical ATR-FTIR spectrometer, which is shown in Figure 3.6. Spectra analysis was performed over the wave length range of 400 cm^{-1} to 4000 cm^{-1} with a resolution of 4 cm^{-1}. An average of 20 scans was performed on each sample in order to give more accurate results.

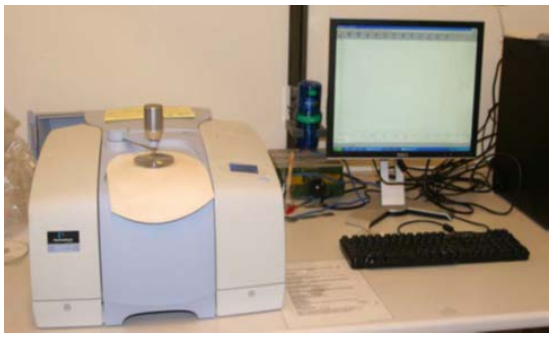

Figure 3.6 Spectrum TM 100 Optical ATR-FTIR spectrometer

3.3.8 Element distribution and gel formation

Gel formation and element distribution is studied by environmental scanning electron microscopy (ESEM) using a Philips-XL30-ESEM electron microscope equipped with Energy dispersive X-ray spectroscopy (EDX) detector. The facilities are shown in Figure 3.7. The

acceleration voltage was 20 keV and the water vapor pressure in the sample chamber was at 1 Torr. The working distance (WD) was kept at 10 mm.

Figure 3.7 Philips-XL30-ESEM

Images of paste samples at different curing ages were required with different magnifications using backscattered electrons (BSE) mode. BSE images give the qualitatively composition and phase distribution of the sample surface by reflecting the differences in grey level. The grey level intensity depends on the local atomic number of the area, the higher the atomic number, the brighter the images.

Simultaneously along with BSE imaging, EDX spot analysis on element distribution was conducted using an EDX detector in order to determine chemical composition of the gel formed in a quantitative way. Multiple selected points within the binder region were used for the EDX spot analysis. The results were later used for the construction of SiO_2, Al_2O_3 and CaO ternary phase diagram for determination which kind of gel was formed in the system.

3.3.9 Heat evolution

The heat evolution of all paste mixtures were monitored by an isothermal conduction calorimeter, which is shown in Figure 3.8. Calibration was first done at 20°C before measurements. The materials for testing were stored in the same room for 24 hours before testing. In the testing procedure, L/S ratio was 0.42 and proportion of solid precursors were exactly the same as described in paste design. Heat evolution for single precursors were also studied by mixing with 4M sodium hydroxide solution, whereas a L/S ratio of 0.6 was used to assure adequate mixing.

Figure 3.8 TAM-Air-314 thermometric isothermal conduction calorimeter

A detailed plan for all material used is shown in Table 3.8.

Table 3.8 Material proportions for heat evolution testing

Sample	Mass of Precursors (g)			L/S ratio	Total mass (g)
	Slag	FA	GP		
Slag	4.7368	-	-	0.6	10
FA	-	4.7368	-		
GP	-		4.7368		
R	3.521	3.521	-	0.42	
G10		2.817	0.704		
G20		2.113	1.048		
G30		1.408	2.133		

After mixing with 4M NaOH solution, the mass of each mixture was 10 g. The mixtures were first transformed into the glass ampoule and then transferred into the chamber in calorimeter. The measurement lasted for a period of 120 hours and the data were recorded every 1 min. Two replicates for each mixture were measured.

3.3.10 Thermogravimetric analysis

The powder of paste G10, about 30 mg, at a curing age of 1, 7 and 28 days were put in an small aluminum oxide crucible and heated from 40 °C to 1100 °C in the TG-449-F3-Jupiter instrument for thermogravimetric analysis. The instrument is shown in Figure 3.9. The rate of heating was 10°C/min. Argon served as protection atmosphere with a flow speed of 50 µL/min.

Figure 3.9 : NETZSCH Thermal Analyzer TG-449-F3-Jupiter

3.3.11 Strength and workability

Flexural and compressive strength of all pastes and mortar samples were measured according to the procedure described in NEN-EN-196-1 Methods of testing cement–Part 1: Determination of strength [53].

Workability of fresh mortar mixtures were determined according to the procedure outlined in NEN-EN-1015-3 Methods of test for mortar for masonry part 3: Determination of consistence of fresh mortar (by flow table) [57].

3.4 Sample Preparations

3.4.1 Stopping the reactions and drying

Paste samples were small crushed pieces from the paste prisms at curing age of 1 day, 7 days and 28 days right after flexural and compressive strength tests. These specimens were then immersed into liquid nitrogen for 5 minutes to stop further reactions. They were transported to the vacuum freeze-dryer (-24 °C and 0.1 Pa) immediately afterwards and were allowed to be dried for 14 to 20 days before they were taken out for microstructural tests. The value of water loss at the end of drying process was lower than 0.05% per day.

For element dissolution test and pore structure analysis by MIP, original fly ash was put into the oven at temperature 105 °C to remove free water for 24 hours before testing.

3.4.2 Sample preparation for microstructural tests

The solid precursors were manually grinded using an agate pestle and mortar set until mean particles size was smaller than 125 µm. The powder samples were used in XRD, XRF and FTIR analysis.

The crushed pieces were used for ESEM with EDX. Some of the crushed pieces were grinded into powder manually using an agate pestle and mortar set until reaching a very fine particles size of 125 µm or under. These powder specimens were used for XRD, FTIR and TGA tests.

3.4.3 Sample preparation for ESEM with EDX

3.4.3.1 For powered precursors

The samples of powdered precursors were prepared by spray a homogenous layer of powder onto the surface of carbon sticker. Unattached particles were removed by blowing air onto the surface in case of possible determination of sample chamber. Each carbon sticker was then clung to the surface of a special made sample holder and later transported onto the sample chamber for observation.

3.4.3.2 For paste

Sample preparation for ESEM is crucial for a proper examination and interpretation of micros rural features. Proper preparation includes epoxy impregnation, cutting, grinding and polishing [58].

The epoxy impregnation was done inside a vacuum chamber, in which the dried sample pieces in small plastic bottles were first evacuated at 30 mBar for 1 hour. The epoxy was first made using a base liquid with a hardener fluid. Afterwards, the epoxy fed into the plastic bottles one by one though a direction-adjustable plastic tube until the sample was fully immersed by epoxy. After 10 min holding at vacuum, air was gradually let in until atmospheric pressure. The impregnated samples were cured at 40 °C for 24 hours before cutting, grinding and polishing.

The samples were cut to ensure cross sections of all pieces of samples in the epoxy. Since ESEM using backscattered electrons requires a highly polished surface for optimal imaging, a series of SiC grinding papers (P320, P500, P800, P1200 and P4000) were used on a middle-speed wheel for grinding of samples. All samples after grinding process were further polished on a special cloth using diamond paste with a particle size from 6, 3, 1 and 0.25µm. Ethanol was used as lubricant throughout the whole process.

4 Characterization of Waste Glass in Comparison with Fly ash and Slag

4.1 Introduction

This chapter presents the study on characterization of all solid precursors, with a special focus on waste glass powder (GP) to evaluate its suitability to be utilized as binder precursor replacement in AAMs. Fly ash and slag in this study were also characterized.

The particle size distribution (PSD), specific surface area (SSA), chemical compositions and physical properties of all precursors were determined. Crystalline phases and amorphous phases were characterized and compared. Reactivity of GP is studied by measuring the amorphous phases content (Reactive Si and Al) as well as element dissolution properties of Si, Al and Ca. Chemical bonds in amorphous phases is further for determination of reactivity.

4.2 Results and Discussion

4.2.1 Particle size distribution

The particle size distribution curve of GP measured by laser diffraction is presented in Figure 4.1. In comparison, the PSD curves of fly ash and slag are also plotted in the same figure.

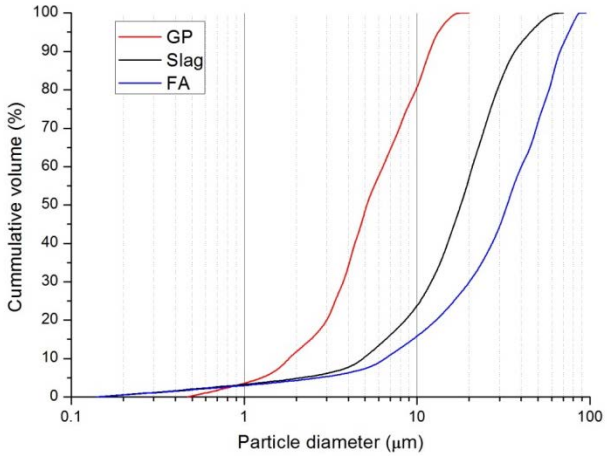

Figure 4.1 Particle size distribution of waste glass powder, fly ash and slag

Compared with fly ash and slag, GP has a much finer particle size. The particle size ranges from 0.5 to 16 μm with a mean particle diameter of 6.16 μm. Such fine particle distribution is associated with processing and collecting of glass dust from the waste glass recycling process. Slag used in this project is similar in particle size distribution compared with many previous studies. Fly ash, with a mean diameter of 35.61 μm, however, is quite coarse compared with ordinary Class F fly ash in the market. A detailed volume weighted dimensions including the median size of all precursors are listed in Table 4.1.

Table 4.1 Volume dimensions of precursors with median size

Precursor	D_{10} (µm)	D_{50} (µm)	D_{90} (µm)
GP	1.77	5.07	11.81
FA	6.52	33.19	66.39
Slag	4.90	17.88	36.20

PSD is one of the most crucial physical properties affecting the reactivity of precursors and later geopolymerization products, because major part of reactions occurs at the liquid/solid interface. Normally, finer particles yield greater surface area and also higher reactivity of precursors. The reactivity of GP in this study is in line with these findings, which will be further discussed in Section 4.2.5.

4.2.2 Morphology of precursors

Morphology of precursors was studied by taking BSE images at a magnification of 500X, which is shown in Figure 4.2.

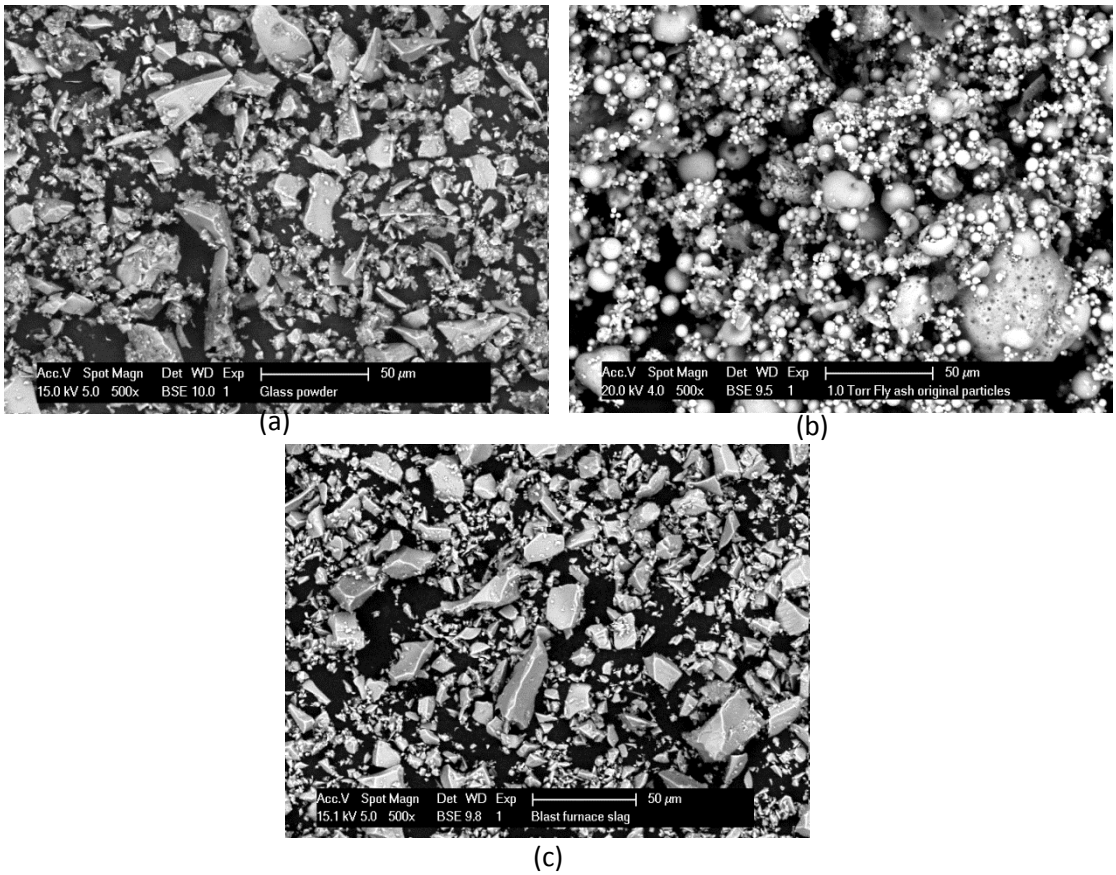

Figure 4.2 BSE images of precursors: (a) Glass powder, (b) Fly ash, (c) Blast furnace slag

Figure 4.2 (a) indicates that GP consist mainly of fine angular particles with a narrow particle size range. Very fine glass powder particles could be observed which are partially agglomerated together. Compared to GP, fly ash particles have very different particle morphology, which are mainly spherical in shape as shown in Figure 4.2 (b). Fly ash particles

are Light gray in color and generally have regular spherical shapes and have a diameter range from 5 to 50 µm. Some of the fly ash particles are also in irregular shapes. Similarities exist between GP and slag in morphology. Slag particles, as is illustrated in Figure 4.2 (c), are irregular polygonal in shape, generally with a different particles size range from 5 to 30 µm compared with GP. GP, on the other hand, also share this morphology whereas with some particles to be like irregular triangle in shape.

4.2.3 Chemical compositions and physical properties

The chemical compositions of three precursors were analyzed by X-ray fluorescence (XRF) and results are shown in Table 4.2. It is noted that the most abundant oxides in GP are those of Si and Ca, followed by Al, Fe, Mg, S and alkali (Na, K). GP shows a significant higher amount of SiO_2 in composition compared with fly ash and also a higher Ca content. However, the aluminium content is only 2.37 wt%, even lower than slag. According to ASTM C618, GP may be classified as Class N natural pozzolan if Na_2O content is not a concern.

Chemical composition of fly ash in this project meets the recommended values of fly ash for alkali activation ($Fe_2O_3 \leq 10\%$ and LOI ≤ 5%) proposed by Palomo [10].

Table 4.2 Chemical compositions of solid precursors

Oxide (wt %)	SiO_2	Al_2O_3	Fe_2O_3	CaO	MgO	SO_3	Na_2O	K_2O	LOI
GP	65.60	2.37	2.40	22.06	2.174	0.39	1.99	0.86	2.00
FA	52.90	26.96	6.60	4.36	1.50	0.73	0.17	-	3.37
Slag	32.91	11.84	0.46	40.96	9.23	1.60	-	0.33	1.15

The physical properties are shown in Table 4.3.

Table 4.3 Physical properties of solid precursors

Oxide (wt %)	Density (g/cm^3)	Surface area (m^2/g)
GP	2.40	2.874
FA	2.44	1.737
Slag	2.89	2.539

4.2.4 Crystalline phases

The mineral compositions of all precursors are identified using X-ray diffraction (XRD) technique, which is shown in Figure 4.3. It is revealed that the main crystalline phases in GP are quartz (SiO_2, PDF# 01-085-0930) and calcite ($CaCO_3$, PDF# 01-086-2334). Some minor crystalline phases like chamosite ($Fe_3Si_2O_5(OH)_4$, PDF# 00-010-0404), tobermorite ($Ca_5Si_6O_{16}(OH)_2$, PDF# 00-029-0329) and tremolite ($CaMg_3(SiO_4)_3$, PDF# 00-002-0455) are also detected. These minor crystalline phases, which are not originally from waste glass, may be introduced in the recycling process, since they are highly unlikely to exist in ordinary container glass or flat glass. Crystalline phases in fly ash are mainly quartz (SiO_2, PDF# 01-085-0930), mullite ($Al_6Si_2O_{13}$, PDF# 00-015-0776) and hematite (Fe_2O_3, PDF# 01-073-0603). Slag used in study mainly contains glassy phase, minor calcite existence could

be detected possibly because of carbonation. Instead of mullite commonly found in FA, GP contain calcite phase. As mullite is aluminium rich phase while calcite is actually all calcium carbonate, this is consistent with the chemical composition results determined by XRF, in which lower aluminium amount and higher calcium amount is found within GP.

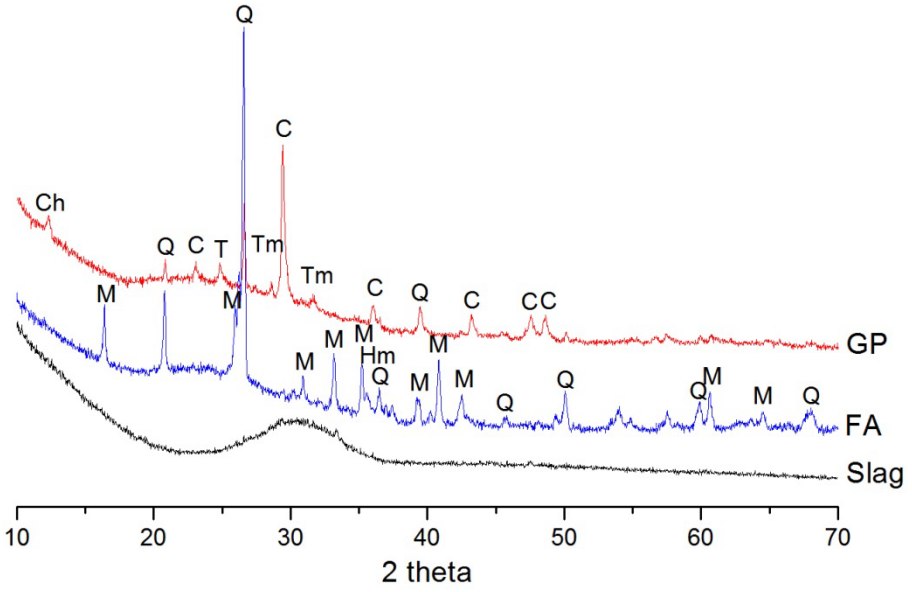

Figure 4.3 XRD patterns of unreacted GP, fly ash and slag, Q=Quartz; C=Calcite; M=Mullite; Ch=Chamosite; T=Tobermorite; Tm=Tremolite; Hm=Hematite

Furthermore, all precursors contain considerable amount of amorphous phases as can be reflected from the wide amorphous hump in each XRD spectra. In case of GP and fly ash, the hump is from approximately 17° to 35° 2θ degree. This hump is found in between 25° to 35° 2θ degree for slag. It is accepted that the difference positions of amorphous humps are associated with different structure of amorphous phases in precursors. The amorphous/glassy phases in the solid precursors can contribute to the potential for alkali activation which directly links with the reactivity of raw materials. Study on amorphous phases and reactivity will be discussed in Section 4.2.5.

4.2.5 Amorphous Phases Content and Reactivity

The amorphous phase in GP and fly ash was measured by chemical dissolution method according to EN 196-2. The insoluble residue (I.R.) fractions of GP and fly ash were derived from the Dissolution tests. Combined with the SiO_2 and Al_2O_3 content in the residue already obtained by XRF shown in Table 4.2 and also the XRF result on the insoluble residue listed in Table 4.4, the reactive SiO_2 and Al_2O_3 content can be calculated.

Table 4.4 Chemical composition of insoluble residue of GP and fly ash by XRF

Oxide (wt %)	SiO_2	Al_2O_3	Fe_2O_3	CaO	MgO	SO_3	Na_2O	K_2O	TiO_2
GP	62.24	7.96	0.77	18.01	3.86	0.16	0.592	3.29	1.82
FA	43.59	50.59	3.18	0.189	-	0.12	-	0.69	1.46

The reactive amount of reactive SiO_2 is calculated as following:

$$\omega_{reactive}^{SiO_2} = \frac{m_{total} \times \omega_{total}^{SiO_2} - m_{residual} \times \omega_{residual}^{SiO_2}}{m_{total}} = \omega_{total}^{SiO_2} - \omega_{residual} \times \omega_{residual}^{SiO_2}$$

Likewise is for the calculation of reactive Al_2O_3 amount.

Table 4.5 Reactivity of GP and fly ash determined by chemical dissolution and XRF (wt%)

Precursor	I.R.	Amorphous content	Total SiO_2	Reactive SiO_2	Total Al_2O_3	Reactive Al_2O_3	Total CaO	Reactive CaO
GP	18.14	81.86	65.60	54.31	2.37	0.92	22.06	18.81
FA	22.63	77.37	52.90	43.04	26.96	15.51	0.189	-

The reactivity of GP and fly ash are indicated in Table 4.5 with reactive SiO_2, Al_2O_3 and CaO content. The reactivity of slag almost 100% and is not listed in the table. It is commonly acknowledged that aluminosilicate precursor exhibit higher reactivity with higher reactive Si and Al content, since higher reactive content represent higher silica and alumina availability at early age and should lead to a faster conversion of solid aluminosilicate source into gel products [33, 59]. Reactive CaO content is quite high in GP with 85% of total CaO to be reactive while FA contains almost no reactive CaO. Therefore, the results clearly imply that GP can serve as good precursor material with high reactivity of Ca and Si. On the other hand, fly ash in this project is abundant with reactive silica and alumina, like fly ash used in enormous previous studies.

4.2.6 Chemical bonds in amorphous phases by FTIR spectra subtraction

Spectra subtraction was performed to further understand the amorphous phases dissolved in selective chemical treatment described in Section 3.3.4. Subtraction was performed on both GP and fly ash considering their comparability in chemical composition. The spectra of components dissolved during the selective chemical treatment were obtained by subtracting the FTIR spectra obtained after attack from the original spectra, using OMNIC software following procedure by Puligilla and Mondal [60]. For both GP in Figure 4.4 and fly ash in Figure 4.5, the spectra collected before treatment is noted as ‘original’, while the spectrums after treatment are noted as ‘residue’. The resultant spectrum obtained through subtraction is referred to as ‘Dissolved’. Spectra subtraction helps to uncover the hidden information for the dissolved amorphous phases.

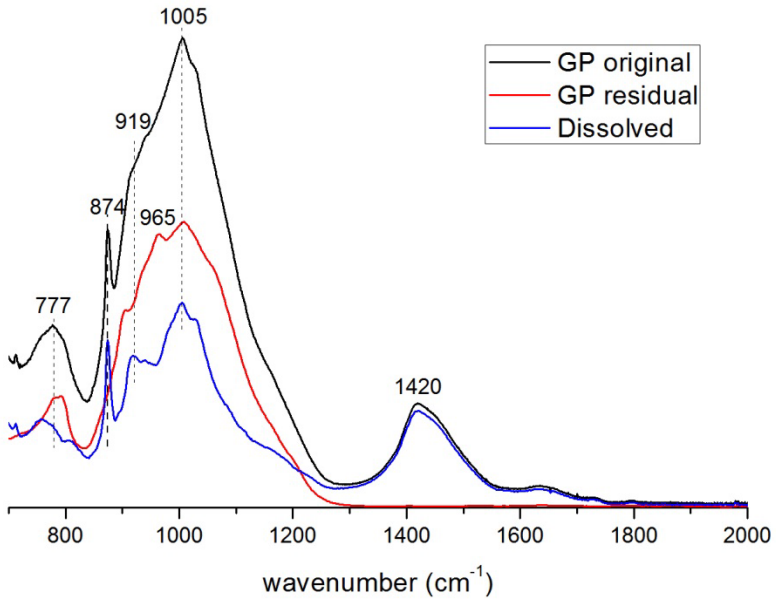

Figure 4.4 Subtraction spectrum of GP after extraction of all amorphous phases

FTIR spectra for GP original, GP residual after treatment and dissolved phases in GP are shown in Figure 4.4. Spectrum for GP original indicates a broad band at 1005 cm^{-1} with a peak shoulder at 919 cm^{-1} and also a really sharp peak at 874 cm^{-1}. Existence of quartz is detected with peak at 777 cm^{-1} [61]. Both the sharp peak at 874 cm^{-1} and the relative broad hump at 1420 cm^{-1} are associated with presence CO_3^{2-} with different vibration mode: $v_2[CO_3]^{2-}$ for 874 cm^{-1} and $v_3[CO_3]^{2-}$ for 1420 cm^{-1} [62]. They possibly exist in calcite detected in XRD patterns. Peak at 1005 cm^{-1} may be in correlation with asymmetric stretching of Si-O-Si bonds in amorphous glasses [63]. Stretching of Si-O-M (M as alkali metal or alkali-earth metal) is found at wavenumber 919 cm^{-1} [63]. Considering GP is rich in calcium, it is highly likely they could be Si-O-Ca bonds.

Peak at 965 cm^{-1} in GP residual may be associated with v_3(Si-O) stretching vibrations in SiO_4 tetrahedral, also more often be regarded as Q^2 structure of Si. The existence peak may be owing to inactive Si in crystalline phases like tremolite, etc.

As shown in dissolved spectrum, it is evident that peak at 1005 cm^{-1} and 919 cm^{-1} are attributed to active silica content in GP. Peaks indicating the existence of CO_3^{2-} in GP disappeared after treatment with acid.

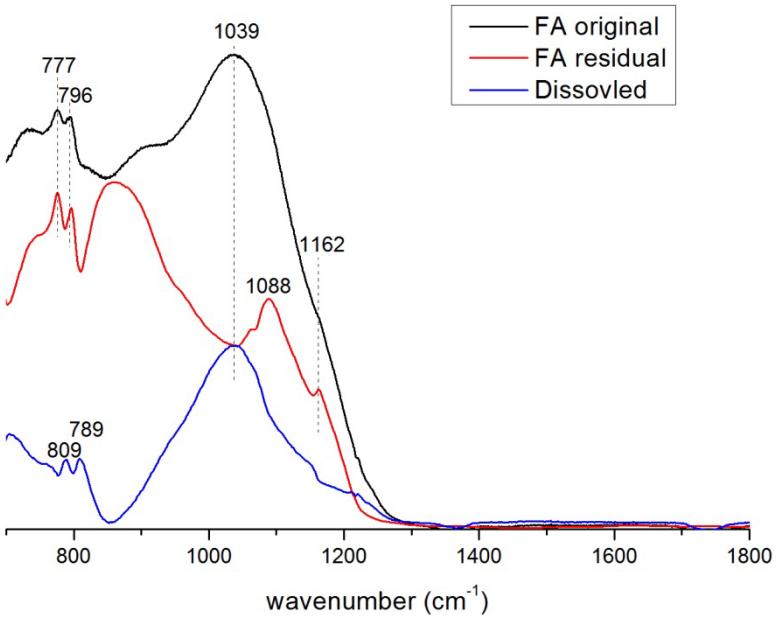

Figure 4.5 Subtraction spectrum of fly ash after extraction of all amorphous phases

As a comparison with GP, FA original, FA residual after treatment and dissolved phases are plotted in Figure 4.5. Quartz is again identified as had been detected in XRD pattern, with two typical peaks at 777 cm^{-1} and 796 cm^{-1}, which remained in the residual after chemical treatment. The broad hump centered approximately in 1039 cm^{-1}, also known as the main band, represent (Si, Al)-O-Si in glass, which could be composed of higher Al concentration [63]. A huge drop of this broad hump is found after chemical treatment because the dissolution of enormous amount of silica and alumina from the structure. Peak at 1088 cm^{-1} and 1162 cm^{-1} are associated with asymmetric stretching of (Si, Al)-O-Si in mullite phase in fly ash, which is in line with the XRD study. Band near 800 cm^{-1} may be attributed to Si (Al)-O bonds or Si-O-Al stretching bonds with limited reactivity compared with bonds inside the main band.

For both GP and fly ash, the reactive chemical bonds in precursor revealed by FTIR spectra subtraction generally fall in the range at 1085-1092 cm^{-1}, 997-1001 cm^{-1} and 900-915 cm^{-1}. Chemical bonds within these position ranges mostly corresponds with (Si, Al^{IV})-O-Si bonds or (Si, Al^{IV})-O-M (M=Na or Ca) bonds, which has been confirmed to be highly reactive and largely determine the activity of aluminosilicate precursors [64].

4.2.7 Element Dissolution of Si, Al and Ca

The aim of study on element dissolution behavior of GP in comparison with fly ash is to understand how precursors react with high concentration alkali activator solution. Element dissolution is crucial to later geopolymerization process since it provides available source element for further reactions. The study on element dissolution is of more importance at early ages. Although the environment for precursors are not identical between dissolution process with a higher liquid to solid ratio and real blending of mixtures, however, the dissolution can reveal similar trend at the early age.

Dissolution performance of fine glass aggregate (GA) was studied to determine its potential to make contribution for element release. The concentrations of different element dissolved,

namely Si, Al and Ca in 4M NaOH solution for different periods of time were measured. 5 g raw materials were added into 50 ml solution.

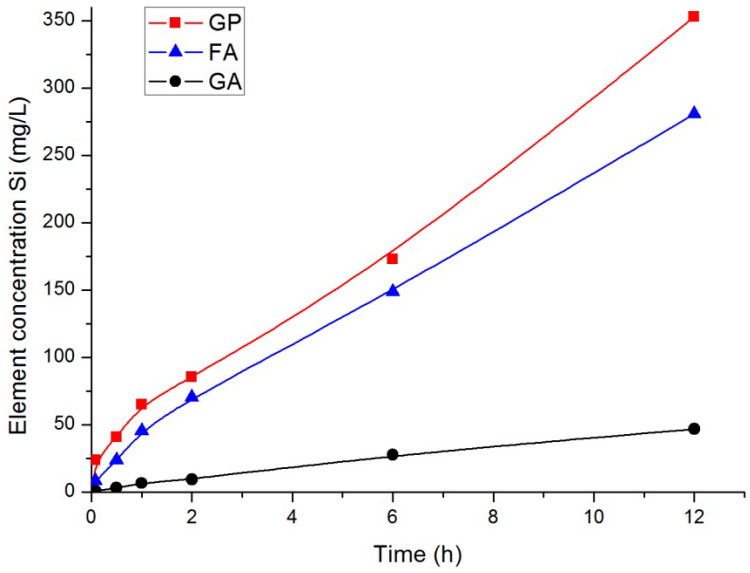

Figure 4.6 Element concentration of Si in solution after different dissolution time

Element concentrations of Si in solution dissolved from GP, fly ash and GA after 5 min, 0.5h, 1h, 2h, 6h and 12h is shown in Figure 4.6. It is evident from the figure that GP dissolved more Si than FA and GA up to 12 hours dissolution time. As has been discussed in section 4.2.5, the active SiO_2 content is higher in GP than in FA, which indicates that GP will have a higher Si dissolution capacity than fly ash. It can be seen from Figure 4.6 that the dissolution of Si for both GP and FA is not completely finished since the curves do not reach the plateau which indicate the maximum potential of element release under current condition.

GA has limited potential to for Si release, since it is observed that the Si concentration is lower than 50 mg/L after 12h dissolution. It has already been proved that fine particle size lead to better solubility of waste glass [65]. The solubility is directly linked with the specific surface of particles for reaction. For the smaller the particle size, the specific surface is greater. As the mean particle size for GP is 5 µm while for GA it is 2 mm. Consequently, GP with a much higher specific surface area leads to more intense contact between the NaOH solution and the glass which result in higher solubility and enhanced element release.

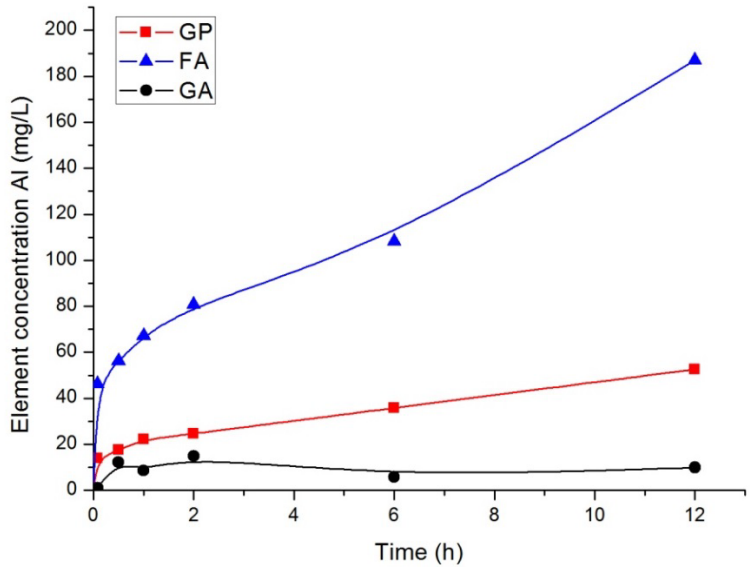

Figure 4.7 Al concentration in solution after different dissolution time

Figure 4.7 illustrate the element release of Al in 4M NaOH solutions for a different period of dissolution time. Apparently, FA has a higher Al release rate from the start and also shows a higher dissolution capacity compared with GP. This phenomenon is consistent with the chemical composition of two precursors. GA exhibits a lower Al release rate at all ages compared with GP and FA, which is due to the lower scarce Al content in GA.

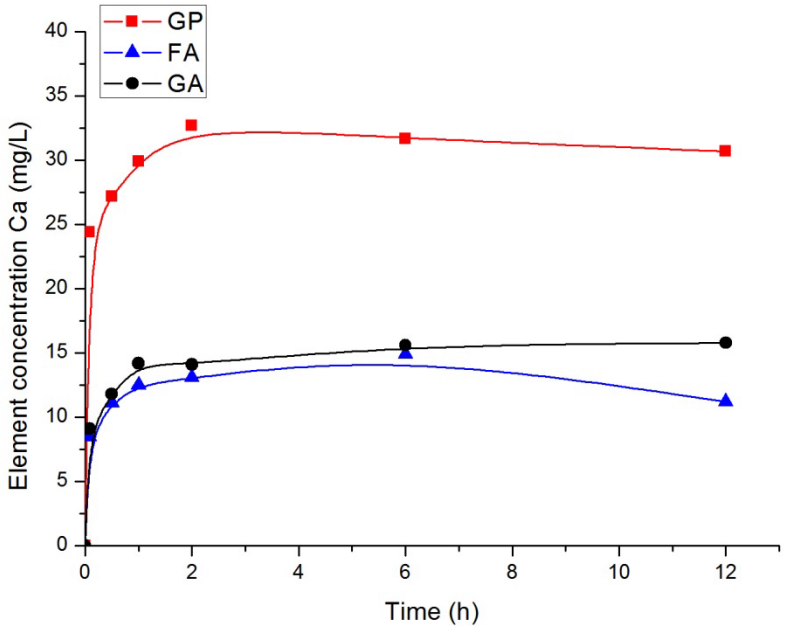

Figure 4.8 Ca concentration in solution after different dissolution time

Figure 4.8 illustrate the element release of Ca in 4M NaOH solutions for a different period of dissolution time. As the curve indicates, the rate of Ca dissolution is higher for GP than for FA at early age. The dissolution curves reaches a plateau after 2-hour dissolution, indicating the Ca dissolution capacity if higher in GP than FA. This phenomenon is reasonable since the GP has higher CaO in chemical composition. Ca is treated as a network modifier in the

(alumino) silicate network and Ca-O bond energy is lower than Al-O or Si-O bond energy. Furthermore, dissolution of Ca is by exchanges via metal-proton exchange reactions. Thus, Ca will start to dissolve at first contact to the NaOH solution.

Dissolution curves of GA is also included in the figure, which shows a slightly higher Ca dissolution potential than FA. Since GA is mainly soda-lime glass from recycled container glass and flat glass, the Ca content is much higher than FA and even GP. However, due to coarse particle size distribution of GA, the dissolution is suppressed; consequently lead to a lower Ca release capacity compared with FA.

It should be mentioned that the deviation of Ca concentration after 2-hour dissolution is due to the variation in chemical concentration of precursors and GA. Although the chemical concentration of different element can be maintained at more or less same level in large quantity of materials, it is impossible to have exactly the same chemical composition for each specimen of small amount for dissolution tests. This reason explains the decrease in Ca concentration for FA dissolved for 12 hours and GP dissolved for 6 and 12 hours.

4.3 Concluding Remarks

A systematic characterization on both chemical and physical properties of waste glass powder utilizing a series of different techniques leads to following conclusions:

1. GP has much finer particles size distribution and larger specific surface area compared with fly ash and slag. This leads to a higher water demand within binders containing GP as precursor.
2. GP has irregular polygonal shape, like blast furnace slag.
3. Quartz and Calcite are the main crystalline phases in GP.
4. GP is rich in Si (65.60%) and Ca (22.06%) and has limited Al content (2.37%). The total amorphous content in GP is higher than that in fly ash. The reactive Si content is higher than that of fly ash, which is up to 54.31%. Due to these reason, the dissolution potential of Si and Ca is higher in GP than in fly ash.
5. Reactive chemical bonds in amorphous phases in precursor characterized by FTIR spectra subtraction mostly corresponds with (Si, Al^{IV})-O-Si bonds or (Si, Al^{IV})-O-M (M=Na or Ca) bonds, which has been confirmed to be highly reactive and largely determine the activity of aluminosilicate precursors.

5 Characterization of Alkali-activated Slag/Fly ash Paste using Waste Glass Powder as Partial Binder Precursor

5.1 Introduction

The partial replacement of precursors with waste glass powder may influence early age properties and microstructural development of alkali activated slag/fly ash paste. Therefore, in order to meet the second objective of this project, the alkali activated slag/fly ash paste with GP replacement of fly ash are intensively characterized in this chapter to provide further insights on early age properties and microstructure development. The characterization is conducted with respect to strength development, heat evolution, mineral composition, chemical bonds, element distribution and gel formation.

Isothermal calorimetry is used to examine the heat evolution. Along with thermogravimetric analysis (TG), the amount of gel formation is determined. Fourier transform infrared spectroscopy (FTIR) and X-ray diffraction (XRD) are applied to analyze chemical bonds and mineral composition of reaction products. Element distribution and gel formation are examined by Environmental scanning electron microscopy (ESEM).

5.2 Crystalline Phases Analysis

5.2.1 Introduction

As a major testing method for crystalline phases in the solid, XRD determines the scattered intensity of the electron beam as a function of incident and scattered angle, through which reflects information of crystalline phases. Crystalline phase development can be affected by many factors and characterization of crystalline phases helps the interpretation of microstructure development and may provide useful information for linking microstructure with macro properties in cementitious materials.

In this section, XRD has been used to identify crystalline phases in paste mixture. XRD patterns of paste mixtures with different amount of GP replacement are studied in order to provide useful information about gel formation and microstructure development.

5.2.2 Results and discussion

The XRD patterns of all investigated paste samples cured for 1, 7 and 28 days are illustrated in Figure 5.1, Figure 5.2 and Figure 5.3, respectively. All of the X-ray patterns of paste cured for different ages evidently exhibit predominately amorphous products formed by alkali activation as well as formation of several crystalline phases. All XRD spectra are stacked for comparison purposes to analyze the effect of the replacement of fly ash by GP. It is worth noting that huge percentage of amorphous and semi-crystalline phases existed in the paste after alkaline activation, therefore some the crystalline phases might not be identified.

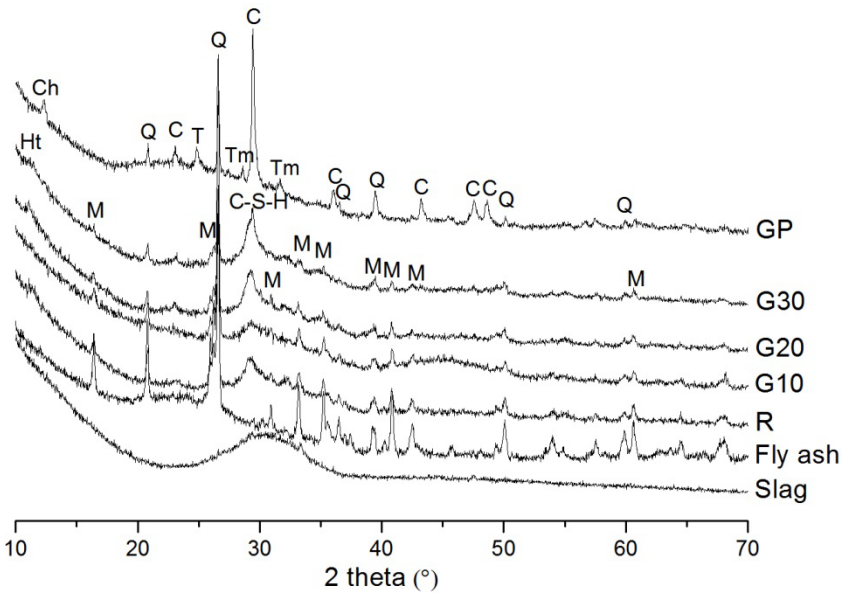

Figure 5.1 XRD pattern of alkali activated slag/fly ash paste with various amount of GP as replacement for fly ash at 1 day with XRD patterns of unreacted precursors, C-S-H=Calcium Silicate Hydrate; Q=Quartz; M=Mullite; C=Calcite; Ch=Chamosite; T=Tobermorite; Tm=Tremolite; Ht=Hydrotalcite.

Compared with original crystalline phases in unreacted precursors, new crystalline reaction products marked as C-S-H and Ht are identified after one day alkaline activation as shown in Figure 5.1. No significant changes in intensities of crystalline peaks are detected within same paste mixture over time of curing, suggesting a relative fast reaction kinetics. Therefore, XRD patterns on evolution over curing time are not shown.

After alkaline activation, a poorly crystalline calcium silicate hydrate (C-S-H) phase ($1.5CaO{\cdot}SiO_2{\cdot}xH_2O$, PDF# 00-033-0306) is found near 29.4° 2θ degree as main reaction product, which is in agreement with previous studies [21, 24, 29, 66, 67]. Considering Al content in raw materials, this C-S-H type gel may have moderate Al substitution in the structure. Existence of zeolite phases, which are generally derived from the alkaline activation of fly ash, cannot be identified by XRD patterns. Thus, C-S-H type gel is the dominant reaction product formed in alkali activated slag/fly ash binder with various amount of GP replacement. It is believed that inclusion of GP will significantly alter Ca/Si ratio, which may have major impact on C-S-H gel structure. Detailed studies on element distribution will be elaborated in Section 5.6. Hydrotalcite ($Mg_6Al_2CO_3(OH)_{16}{\cdot}4H_2O$, PDF# 00-041-0191) is also detected in reaction products at around 10.2° 2θ degree, which has been confirmed to be from the alkali activation of slag containing Mg [24, 66]. Hydrotalcite is found in all samples with different level of GP replacement, which indicates the formation of hydrotalcite is not highly dependent on available silica and alumina content. Last but not least, Portlandite ($Ca(OH)_2$) is not detected in all alkali activated binders slag/fly ash binders, which may be due to the relative low pH value and limited Ca from dissolution compared with Ca-rich alkali activated slag or OPC [68]. The precipitation of C-S-H is preferred over $Ca(OH)_2$ due to its lower solubility [11], which could also be regarded as one of the reasons.

Compared with XRD pattern of GP, disappearance of peaks for chamosite, tobermorite and tremolite is found in all paste samples with GP replacement. It could be observed that the new amorphous hump associated with reaction products is from 25° to 37° 2θ degree. In case of GP and fly ash, the hump is from approximately 17° to 35° 2θ degree. This range is found in between 25° to 35° 2θ degree for slag. Along with Intensities decline of peaks like calcite, these findings indicate GP is involved in the alkaline activation. Quartz, mullite and hematite peaks in reacted blends are identified as remnant crystalline phases of incompletely reacted fly ash, intensities of which change with different level of GP replacement.

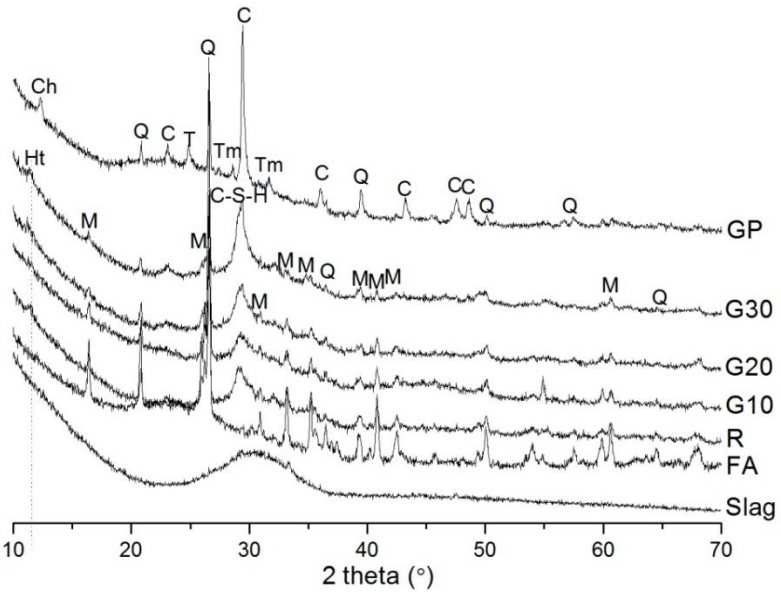

Figure 5.2 XRD pattern of alkali activated slag/fly ash paste with various amount of GP as replacement for fly ash at 7 days with XRD patterns of unreacted precursors

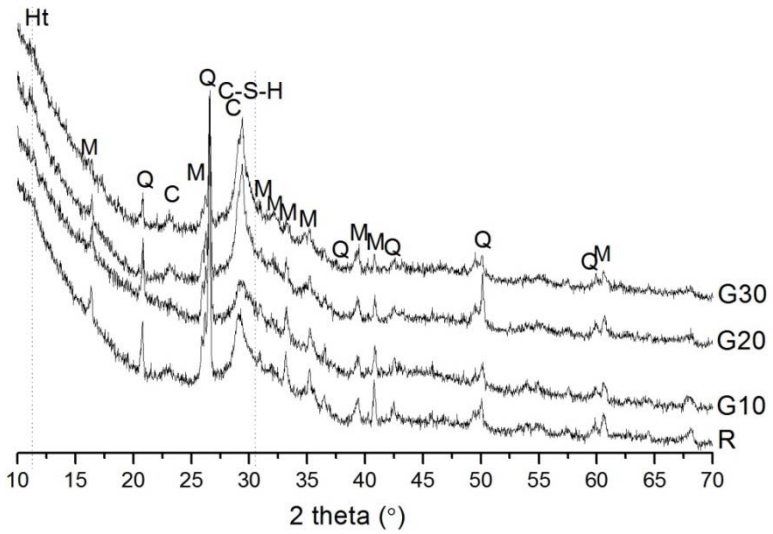

Figure 5.3 XRD pattern of alkali activated slag/fly ash paste with various amount of GP as replacement for fly ash at 28 days

As discussed before, there is no significant change in XRD patterns for each mixture over different curing age. Crystalline phases are found to be identical in both 7-day and 28-day XRD patterns. Nonetheless, increases in the relative intensities of C-S-H peaks (in comparison within XRD each spectra) along with sharpening of the peaks are observed with growing amount GP replacement. This may imply that replacing fly ash in the mixture by GP affects the reaction kinetics of alkali activation of slag. Although direct comparison of intensities of amount cannot be made among different peaks in different XRD patterns, it is believed that higher amount of gel formation is achieved with increasing amount of GP replacement. In order to further substantiate such assumption, other testing technique is applied which will be elaborated in section 5.3 and 5.4.

5.2.3 Conclusion

XRD gives important information regarding crystalline phases in alkali activated binders with GP replacement. However, due to highly amorphous state of reaction products, the development of reaction products needed to be further examined by other techniques. Based on the XRD patterns and discussion, the following conclusions can be drawn:

1. The reaction product of alkali activated slag/fly ash paste with different GP replacement is mainly amorphous C-S-H type phase.
2. GP is involved in the alkaline activation and may have impact on the reaction kinetics of alkaline activation of slag.
3. Formation of zeolite phases from alkaline activation of fly ash is not identified, which indicates aluminosilicate gel does not exist in the structure up to 28 days.

5.3 Heat Evolution

5.3.1 Introduction

Like in cement hydration, the heat release during alkaline activation process is an important factor affecting the setting and other properties of alkali activated materials. Slag has been reported to be highly reactive to alkaline solution which often leads fast setting and higher water demand. GP as highly reactive precursor replacement of fly ash in the mixtures may have heat contributions both in the dissolution stage and the reaction stage, both of which may have impacts on total heat release and reaction rate.

The heat release generated by the blended paste causes inner heating in the structures. A temperature gradient from the inside to the surface is created by inhomogeneous heat conduction through structure. This temperature gradient may generate thermal stresses which lead to generation of microcracks and deterioration of mechanical properties and durability. Thus, understanding the heat evolution of alkali activated slag/fly ash with GP replacement can provide useful information for future application of this material.

5.3.2 Results and discussion

Figure 5.4 shows the heat flow of binders of sole precursor: slag, fly ash and GP with L/S ratio 0.6 during the first 60 hours. Curves after 60 hours are considered to be in the stable period since they reflect no sign of further reaction.

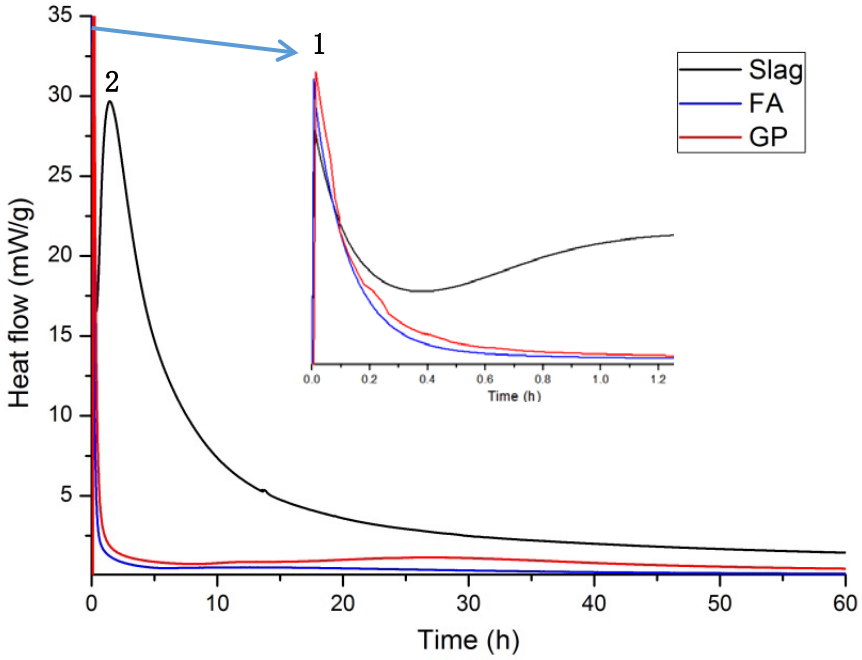

Figure 5.4 Heat flow of single precursor alkali activated mixtures (slag, fly ash and GP), with L/S ratio 0.6

Two calorimetric peaks are found in each curve. The initial sharp peak during the first several minutes correlate with wetting and dissolution of precursors and the second one represent reaction of dissolved species like silica, alumina and calcium units. The heat flow for newly

formed reaction products from these dissolved species is quite different among three precursors. It is well acknowledged that slag has the highest activity with formation large amount of reaction products (C-A-S-H gel). It is illustrated that GP has higher reactivity than fly ash. Fly ash also shows limited reactivity like GP. Thus the peak intensities for both fly ash and GP are much lower than that for slag while the widths of peaks are quite broad.

The cumulative heat evolution for three precursors: slag, fly ash and GP with L/S ratio 0.6 during the first 120 hours are shown in Figure 5.5. It is obvious that slag has much higher total heat release compared with GP and fly ash. The reason is that as for slag, the heat not only comes from dissolution heat release but also come from alkali activation and further hydration reaction of slag. From the curves, it is clearly indicated that GP has a higher heat release than fly ash. The results on heat evolution of binders from sole precursors provided theoretical basis for analyzing heat evolution of blended systems.

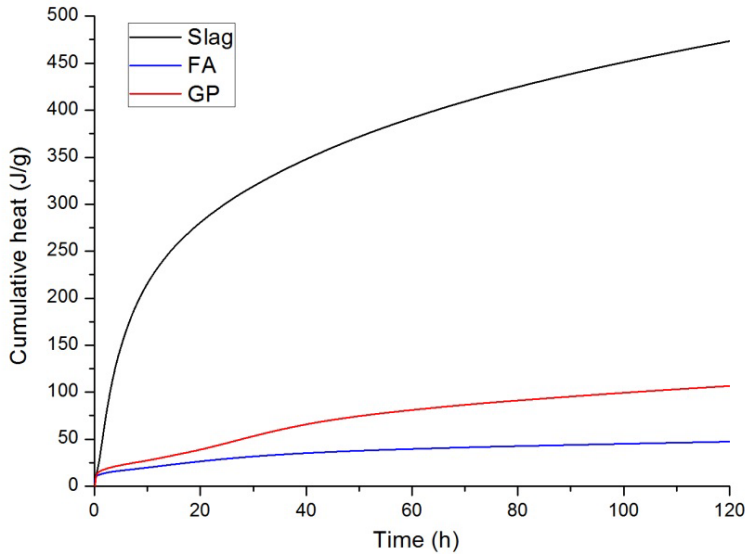

Figure 5.5 Cumulative heat evolution of single precursor alkali activated mixtures (slag, fly ash, GP), with L/S ratio 0.6

The heat flow curves of alkali activated slag/fly ash paste as a function of different replacement level during the first 120 hours are plotted in Figure 5.6. It is observed that two peaks exist in all four mixtures: an initial sharp peak with extremely high heat flow during the first several minutes after mixing and a relative broad peak with much lower heat flow intensity. The occurrence of these two peaks is in agreement with the heat evolution curves of silicate activated slag or slag/fly ash blends in previous studies [69-71]. The first sharp peak is due to the wetting and dissolution of precursors and immediately followed by the second peak which corresponds to the massive reaction product formation. Considering the same L/S ratio and preparation route for all mixtures, changes in peak height and delay of appearance of the second peak is highly likely to be related with the replacement level of GP to fly ash.

Induction period refers to an initial slow stage of a chemical reaction; after which the reaction accelerates. A longer induction period is found with higher amount of GP replacement. The appearance of induction period is due to the fast formation of initial

reaction products around the unreacted slag or fly ash particles [72], as GP react really fast because of smaller particles size and higher specific area. With higher amount of GP replacement, it is believed that the thickness of reaction products layer is increasing thus leads to an increase in time required for available alkali and other useful species to penetrate through the layer. Therefore, longer induction periods are expected for higher GP replacement. Similar results have been found in previous studies in alkali activated slag/fly ash mixtures [71, 73]. The reaction began to accelerate after the ionic concentration reaches a critical concentration [74].

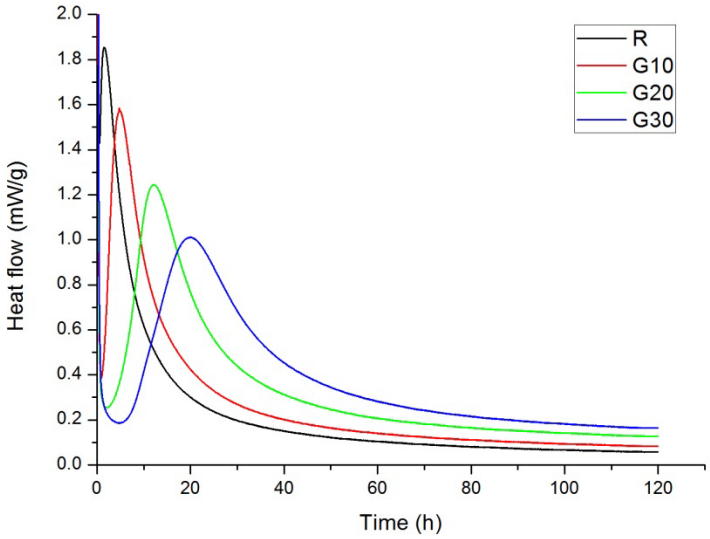

Figure 5.6 Heat flow rate alkali activated mixtures, with L/S ratio 0.42

The cumulative heat evolution of alkali activated slag/fly ash pastes with different GP replacement during the first 120 hours is shown in Figure 5.7, with an L/S ratio of 0.42. In general, an increase of GP replacement for fly ash leads to a higher total heat release of mixtures. It is well known that total heat release can reflect the extent of reaction of cementitious materials. As has been discussed in heat flow rate in Figure 5.6, the total heat comes from summation of heat from wetting and dissolution along with heat from formation of reaction products. Considering that the first part of heat release of GP is higher than that of fly ash, it implies that this could be one of the reasons for the increase of cumulative heat release with more GP replacement.

By comparison between heat evolution of sole precursors in NaOH solution in Figure 5.5 and paste in Figure 5.7, it is possible that the higher reacting heat of GP may not be the only reason for the increase in cumulative heat. One proof is that in G30, the cumulative heat after 120 hours is 167.44 J/g while it is 102.98 J/g for R. From the cumulative heat evolution of sole precursors in Figure 5.5, this value is 106.58 J/g and 47.45 J/g for GP and FA respectively. As in Figure 5.5 the L/S ratio is higher, it is impossible for GP to contribute to all increase of 64.46 J/g in total heat of paste at 120 hours, since it is higher than 59.13 J/g. This implies that another reason also exist which has contribution to the cumulative heat evolution.

It is found in that a more dominant part is the second part for reaction products formation. The reaction of GP with NaOH yields sodium silicate which provided soluble silica monomers.

These silica monomers is confirmed to be quite similar to soluble silica from the addition of water glass [51]. In addition, both of the dissolution rates and potential of silica from GP is higher than FA, which has been confirmed in section 4.2.7. In fact, the calorimetric curves of mixtures with increasing GP replacement share the same trend with those of alkali activated slag/fly ash mixtures using NaOH and solid sodium silicate as alkaline activator with increasing silicate moduli [69]. Therefore, the increase of cumulative heat release with higher amount of GP replacement can be also due to the enhanced reaction of slag by more available soluble silica induced by the GP dissolution. However, taking consideration of the complexity of these ternary binder systems, further confirmation is necessary.

It is also worth noting that the higher total heat release may be correlated with strength development. A detailed discussion is given in Section 6.3.

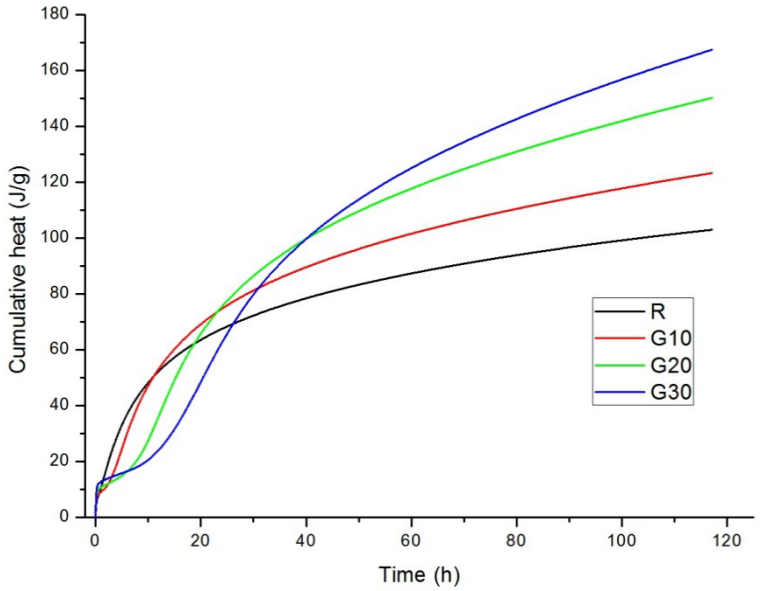

Figure 5.7 Cumulative heat evolution of alkali activated mixtures, with L/S ratio 0.42

5.3.3 Conclusions

The effect of different level of GP replacement for fly ash on heat evolution in alkali activated slag/fly ash binders are studied by isothermal calorimetry. The following conclusions are drawn from this study:

1. For both alkali activated binders with sole precursors and alkali activated slag/fly ash binder with GP replacement, two typical peaks, the first depicting the wetting and dissolution processes and the second one as the formation of reaction products were found.
2. Higher replacement of fly ash by GP leads to longer induction period, because the layer of fast formation of initial products around the slag particles. The reaction is retarded by the increasing time of ionic unit penetration through the initial products layer.
3. Replacement of fly ash by GP may facilitate the reaction of slag, which leads to higher reaction degree of slag and generating a larger amount of total heat release. The mechanism of this facilitation is explained by the higher amount of available silica

species for gel formation, which is similar to the effect of higher silicate moduli in alkali activated slag/fly ash binder. Further confirmation is recommended for this conclusion.

5.4 Thermogravimetric Analysis

5.4.1 Introduction

Thermogravimetric analysis was performed on all mixtures in order to estimate the amount of reaction product formed with specific focus on the amount of gel formation. Both thermogravimetric (TG) curves and differential thermogravimetric (DTG) curves are investigated.

5.4.2 Results and discussion

DTG curves of all mixtures at a curing age of 28 days are presented Figure 5.8. The maximum weight loss peaks for all mixtures are found between temperature 105 and 300 °C while the rate of weight loss stabilized gradually after 300 °C. Actually, all four DTG curves share great similarities indicating formation of same kind reaction products in all mixtures.

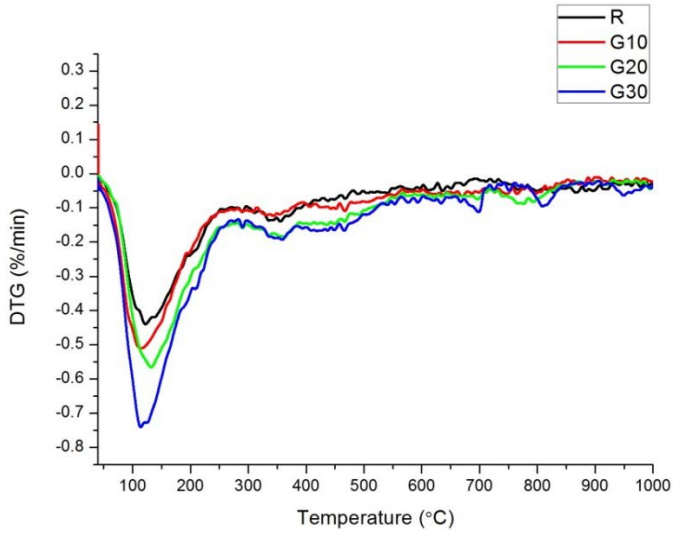

Figure 5.8 Differential thermogravimetric analysis of alkali activated slag/fly ash paste with GP replacement

The TG curve shown in Figure 5.9 reveals only minor decline before 105 °C because all samples have been dried in oven at temperature 105 °C and most of the evaporable water in the system has already been removed. Again, all mixtures exhibit a significant mass loss from 105 to 300 °C. It is believe that the mass reduction in this region represents the decomposition of C-S-H type gel which is in good agreement with previous studies: As the dehydration of C-S-H gel is found lying between 180 to 300 °C in OPC [75]and 105 to 300 °C in AAS binders [71]. It has also been found that decomposition of C-S-H gel occurs between 105 °C and 300 °C; C-A-S-H gels show same thermal behavior [76]. Accordingly, these results may indicate that C-A-S-H type gel is the dominant reaction products in all investigated mixtures. The presence of the peak at 300 to 400 °C in Figure 5.8 and the corresponding peak shoulder in Figure 5.9 can be attributed to the dehydration and decarbonation of hydrotalcite-type phase [66], which has also been detected by XRD. Very weak peaks are observed between 500 to 700 °C which may represent the decomposition of carbonate phases. Further mass loss from 750 to 800 °C may come from decomposition of calcite in

raw materials or from possible carbonation. It is also worth noting that after 800 °C, the gel structure is destroyed and new crystalline phases begin to form, thus contributing to further mass loss. Therefore, these thermal characteristics in Figure 5.9 are combined action of gels and other reaction products.

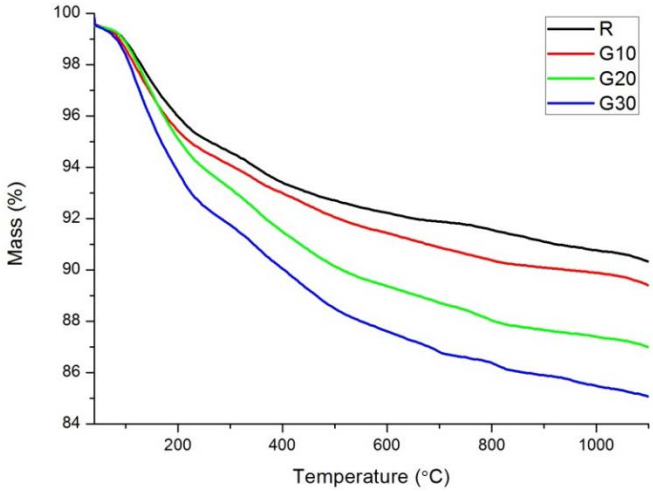

Figure 5.9 Thermogravimetric analysis of alkali activated slag/fly ash paste with GP replacement

It is also illustrated in Figure 5.8 that the weight loss increases with increasing amount of GP replacement. The amounts of gels formed in four mixtures are compared from the TG curves shown in Figure 5.9 by calculating the percentage of mass reduction in the region from 105 to 300 °C. The calculation is made with an assumption that in the region 105 to 300 °C, the dominant reason for the mass loss is by the dehydration process of amorphous gel phases. The results of the calculation are listed in Table 5.1.

Table 5.1 Amount of gel formation with different GP replacement

Mixture	R	G10	G20	G30
Amount of gel formation (%)	4.16	4.33	5.50	6.36

It is obviously that the sequence of amount of gel in the mixture is G30>G20>G10>R. This indicates introduction of GP into system may facilitate the reaction of gel formation and finally yields more amount of gel in the structure. This result is reasonable in consideration of higher amount of available silica from GP dissolution. In addition, this result is in line with the studies on calorimetry which prove that GP replacement enhanced the total reaction of precursors and provide higher total heat release.

5.4.3 Conclusion

Based on the experimental results and discussion, the following conclusions can be drawn:

4. The reaction products of alkali activated slag/fly ash paste with different GP replacement are mainly of amorphous C-S-H type phase.
5. The replacement of fly ash with GP in alkali activated slag/fly ash binder facilitate gel formation and in the end provide higher amount of gels formed in the structure.

5.5 Chemical Bonds Development

5.5.1 Introduction

Fourier transform infrared spectroscopy (FTIR) analysis is considered as an appropriate method to analyze the structural evolution of amorphous reaction products in cementitious materials which exhibiting high heterogeneity. By identification and monitoring of infrared absorption bands in FTIR spectra, development of reaction products can be studied by attributing to specific molecular components and structures.

In this section, the FTIR spectra of alkali activated slag/fly ash mixture with different GP replacement level are studied in order to further understand the process of gel formation and nature of reaction products. The shifts of the main bands are analyzed after chemical bonds assignment of different bands in the spectra.

5.5.2 Results and discussion

FTIR spectra of alkali-activated slag/fly ash binder without different GP replacement: R, G10, G20 and G30, along with spectra of unreacted precursors are shown in Figure 5.10, Figure 5.11, Figure 5.12 and Figure 5.13, respectively. The main bands in the spectra are marked with their position in wavenumber cm^{-1}. Although not shown here, FTIR spectra exhibit only identical band at around 3400 cm^{-1}, which corresponds with stretching and deformation modes of OH^-. Therefore, all FTIR spectra were plotted in the range from wavenumber 600 to 2000 cm^{-1} with the specific interests in the changes in T-O bands, which reveal more significant information about gel formation. Since it is observed that all spectra for both unreacted precursors and binders with different GP replacement level share certain similarities, band assignment is done with respect to all spectra.

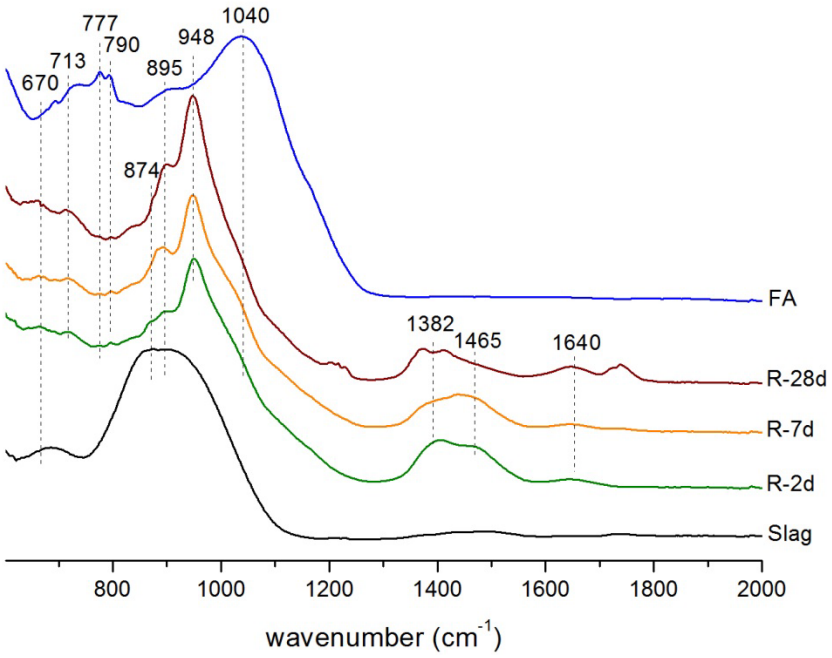

Figure 5.10 FTIR spectra of alkali-activated slag/fly ash binder (R) as a function of curing time

The very small band observed at around 1640 cm^{-1} is associated with bending vibration modes of molecular water. In unreacted fly ash spectrum, typical asymmetric stretching band at wavenumber 777 cm^{-1} and symmetric stretching band at approximately 790 cm^{-1} is associated with quartz [61, 62]. Existence of carbonate is confirmed in both slag and binders, with identification of broad absorption band at approximately centered at 1450 cm^{-1}, which is associated with asymmetric stretching of O-C-O bonds in CO_3^{2-} group [29, 30, 62]. Carbonation is also detected with a vibration band at 713 cm^{-1} corresponding to in-plane bending vibration of CO_3^{2-} group [30]. The traces of quartz and carbonates are well consistent with XRD results. Some authors also attribute this band to tetrahedrally coordinated Al in the structure [77], which is also likely since both fly ash and slag contain considerable amount of Al. Band appeared at 670 cm^{-1} and 874 cm^{-1} could be also assigned to the stretching vibrations of Al-O bonds in AlO_4 tetrahedral groups present in the glassy phase [29, 30].

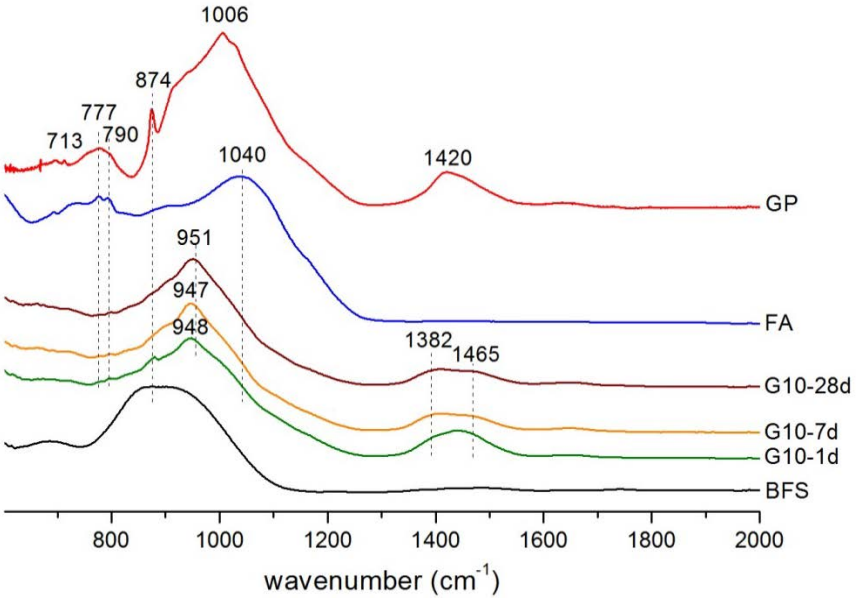

Figure 5.11 FTIR spectra of alkali-activated slag/fly ash binder with 10% GP replacement (G10) of fly ash at different curing time

Carbonates are also found in unreacted GP with the absorption appeared at 1420 cm^{-1} and 713 cm^{-1} [61]. Both the sharp peak at 874 cm^{-1} and the relative broad hump at 1420 cm^{-1} are associated with presence CO_3^{2-} with different vibration mode: out-of-plane bending of $v_2[CO_3]^{2-}$ for 874 cm^{-1} and asymmetric stretching of $v_3[CO_3]^{2-}$ for 1420 cm^{-1} respectively [62]. They possibly exist in calcite detected in XRD patterns. Some authors alleges that peak at 874 cm^{-1} could be correspond to the tetrahedral coordinated Al, however, taking into consideration of limited Al content, this peak is more likely to come from bonds vibration of carbonates. Band at 1005 cm^{-1} may be in correlation with asymmetric stretching of Si-O-Si bonds in amorphous glasses [63]. Stretching of Si-O-M (M as alkali metal or alkali=earth metal) is found at wavenumber 919 cm^{-1} [63]. Considering GP is rich in calcium, it is highly likely they could be Si-O-Ca bonds.

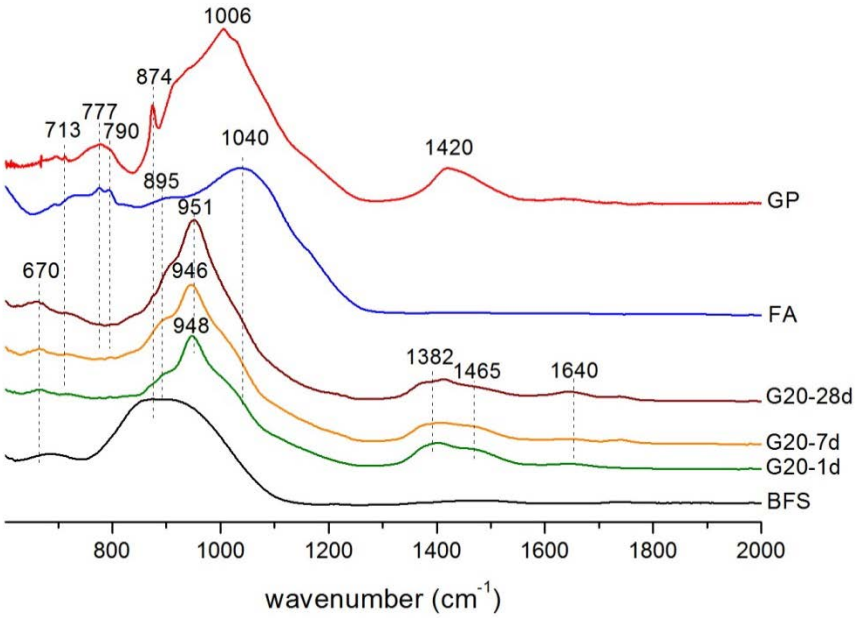

Figure 5.12 FTIR spectra of alkali-activated slag/fly ash binder with 20% GP replacement (G20) of fly ash at different curing time

Broad bands in both precursors and binders are found between 800 and 1200 cm^{-1}, which are due to bands overlapping of both crystalline and amorphous phases. This has been widely accepted as the main T-O asymmetric stretching band by many studies and has been intensively used to study the changes of the gel structure (Ca/Si or Al/Si ratio) in alkali activated materials [78, 79]. The main T-O band for binders at all ages is broad and includes all the response of the unreacted fly ash, slag, GP and reaction products. Although differentiating among them cannot be achieved due to its complexity, the different positions of main T-O band imply a difference in the structural and elemental nature in the precursors and binders. Here the main T-O stretching bands in all FTIR spectra are found to be centred all approximately at around 950 cm^{-1}, which are assigned to asymmetric stretching vibration of Si-O bonds, and can also corresponds to Si-O-M bonds (M being alkali metal or alkali earth metal) [80]. More specifically, this absorption band approximately centred at 950 cm^{-1} could be associated with the Si-O-Si stretching vibrations of SiO_n units for n=2 [81]. This is the representative vibration bands of alkali activated slag indicating the formation of C-A-S-H type gels with short chain structures, in which Si has dominant Q^2 structure. It is worth noting that this main T-O band in each binder spectra is independent from the influence of GP replacement. This indicates that the GP replacement doesn't affect the major ultimate reaction products, which is a C-A-S-H type gel.

Absorption band appeared at around 895 cm^{-1} is found in all binder spectra as single band or as band shoulder. This absorption band may correspond with the Si-O-NBO, which formed in the structure is modified by the incorporation of alkali Na and alkali-earth elements Ca. It has been reported that the stretching modes Si–O with one non-bridging oxygen per SiO_4 tetrahedron (Si–O–NBO) is often observed at 890–975 cm^{-1} [82]. The absorption band of Si-OH is also located in this region with an overlap from 900 to 980 cm^{-1} [83]. However, it is highly unlikely that big amount of hydroxyl ion can exist in unreacted fly ash taking consideration of its production process.

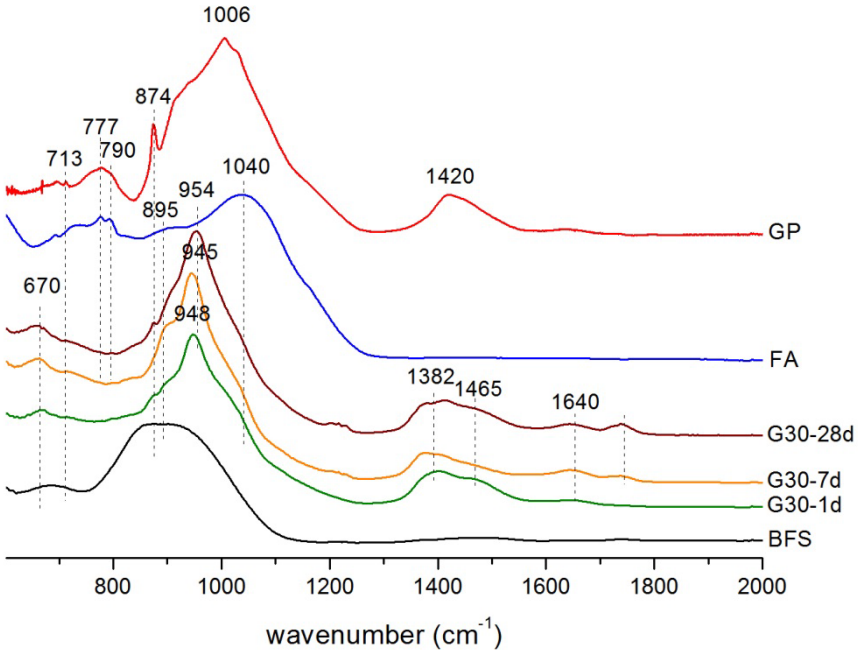

Figure 5.13 FTIR spectra of alkali-activated slag/fly ash binder with 30% GP replacement (G30) of fly ash at different curing time

By careful scrutinizing on the changes with main T-O bands, slight spectra shifts of the wavenumber of main T-O band as a function of time could be observed. A detailed shifts of the center of main band in each binder spectrum as a function of time is illustrated in Figure 5.14. It is observed that the T-O main band has a tendency to first slight to lower wavenumber from 1 or 2 days to 7 days. Afterwards, the centers of main bands gradually shift to higher wavenumbers. For instance, the main band for G30 cured for 1d is at 947.64 cm^{-1}, which shift lower to 946.30 cm^{-1} at 7d and then higher to 953.74 cm^{-1} at 28d.

It is commonly acknowledged that FTIR spectra can reflect two types of bonds vibrations in aluminosilicate molecules, the first of which being inner bonds vibration inside the T-O tetrahedral (T=Si or Al) and the second being the bonds vibration between T-O tetrahedral [84]. Basically, molecular vibrations can be treated as simple harmonious vibration model within the range of Newtonian mechanics to calculate vibration frequencies using Hooke's law. The frequencies can be calculated by the following equation:

$$\upsilon = \frac{1}{2\pi}\sqrt{\frac{k}{\mu}}$$

Where k is the force constant and μ is the reduced mass. Force constant k can be calculated by the experienced formulation after Badger and Gardy. As atomic mass of Al is similar to Si, they share almost the same reduced mass. Nonetheless, the force constant of Al is lower than Si, which in the end leads to lower vibration frequencies of Al-O bonds. Consequently, the main band shift to lower frequencies is due to the precipitation of the reaction products with an increased substitution of Si with Al [85, 86]. The exact position of this band depends on the Al/Si ratio of the reaction products. It is believed that as Al first dissolve from the structure due to lower binding energy of Al-O bonds; the reaction products have the

tendency to form Al-rich structure in the early age [19, 85]. These findings are in line with previous studies on alkali activated fly ash [55].

After 28 days, the main band shift eventually shifts to higher wavenumbers compared to its position at 7d, indicating that more Si was incorporated in to the gel network, forming a Si-rich structure. It is reported Si-O stretching band shift to higher wavenumber in cementitious systems as hydration proceeds, indicating a higher polymerization degree and/or higher cross-linking of silica network in C-S-H gel [87]. The higher polymerization degree at 28 days also contributes to the shift of the main band.

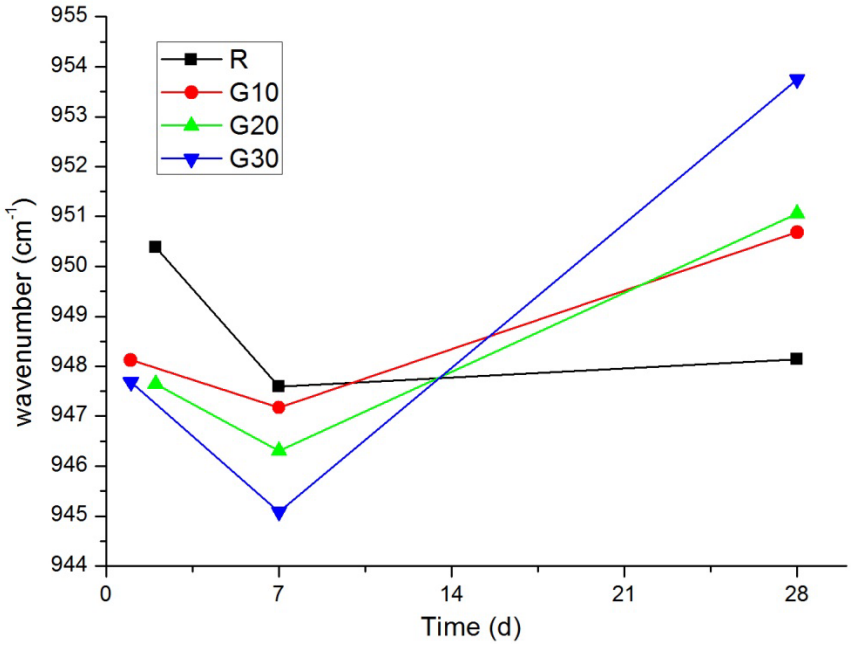

Figure 5.14 Change in wavenumber of the main T-O band for alkali activated slag/fly ash paste with different GP replacement as a function of curing time

The effect of GP replacement level on the chemical bonds can also be revealed from Figure 5.14. With increasing GP replacement for fly ash in the binder, the frequencies of main band vibration at 1d and 7d decreased. For example, the main band for G30-7d is at 945 cm^{-1} while is at 948 cm^{-1} for R-7d. This change can also be related with polymerization degree within the reaction products. Previous studies on alkali activated GP found sodium silicate gel formation in the binder using GP as precursors along [50]. The involvement of GP in the precursors will largely increase amount of available silica for geopolymerization process, which has been discussed in Section 4.2.5. Under these circumstances, the soluble silica in the pore solution of system is more likely to exist as species with lower polymerization like monomer rather than species with higher polymerization degree [88], thus providing more reaction sites for nucleation of available Al or Si to react with the silica monomers. Accordingly, the initial average polymerization degree is lower for higher GP replacement at early age, which eventually conduces to the lower vibration frequencies of main band. Another possible explanation is also concerning the polymerization degree of C-A-S-H type gel. From results in Section 4.2.5, the Al/Si ratio is decreasing taking only reactive Al and Si into consideration. As Al serves as Si substitution in the Q^2 Si chains, the reduced Al amount

works in such a way that leads to the formation of lower polymerized of C-A-S-H type gel [89]. Consequently, lower position of main band with higher GP replacement is found.

It is also worth noting that with higher GP replacement, the frequency of main band changes to higher wavenumber, which in line with findings of other authors [85, 87, 90]. The change indicates a higher crosslinking aluminosilicate formation in the structure.

5.5.3 Conclusion

From the analysis and discussion of FTIR spectra of alkali activated slag/fly ash binders with different proportion of GP to fly ash replacement, following conclusions is made:

1. The major reaction product of alkali activated slag/fly ash binder is C-A-S-H type gels with chain-like Q^2 structure.
2. GP replacement for fly ash in alkali activated slag/fly ash binder doesn't affect the ultimate reaction products, although may has influence in the final polymerization degree.
3. The early age reaction products are Al-rich at 1d and 7d, and Si rich at 28d with higher polymerization degree.
4. The shift of main T-O band in alkali activated slag/fly ash binder with different level of GP replacement is due to two reasons: the Al/Si ratio and polymerization degree of C-A-S-H type reaction products.

5.6 Element Distribution and Gel Formation

5.6.1 Introduction

As a type of electron microscope, scanning electron microscopy (SEM) can apply electron beam on the sample to provide information about the sample's surface topography, chemical composition and phase distribution. In order to determine the nature of the reaction products and to further understand gel formation process in alkali activated slag/fly ash binder with GP to fly ash replacement, samples were examined by ESEM coupled with EDX analysis to give comprehensive information on morphology as well as element distribution of the hardened binder.

5.6.2 Results and discussion

Morphology of hardened binder with GP replacement

Polished binders of R and G30 were examined by ESEM using BSE mode. Representative BSE images for different curing age are shown in Figure 5.15. From results of microstructural and mineralogical characterization by other techniques, it is believed that the nature of main final reaction products is independent from the GP replacement for fly ash (Section 5.2 and Section 5.5). Mainly consists of C-A-S-H type gel, the reaction products have different degree in crosslinking and polymerization with respect to binder with different GP replacement. To better illustrate the effect of GP on gel formation, only R and G30 is studied in this section since a higher GP replacement have more evident influence on microstructure.

Figure 5.15 show the BSE images of alkali activated slag/fly ash samples at all curing ages with no GP replacement (reference sample) and 30 % GP replacement, respectively. Different phases of the paste, i.e. fly ash, slag, GP are marked in Figure 5.15 (a) and (b). In BSE images, the intensity depends on the local atomic number of the area, the higher the atomic number, the brighter the images. Fly ash particles, in light gray color, generally have regular spherical shapes. Some of the fly ash particles are also in irregular shape or hollow shape. Slag particles in shape of irregular polygonal are shown in a brighter color due to the greater amount of Ca and Mg. GP particles after alkali activation can still be recognized by its irregular triangle or polygonal shape. Albeit it is found that GP and slag share similar morphology as have been discussed in Section 4.2.2, however, GP is distinguished from slag by its smaller particles size as well as its chemical composition. Typical EDX spectra determined on precursor particles of GP and slag in the paste are shown in Figure 5.16. It is notable that compared with GP, slag contain more Ca, Al and Mg while less Na in the structure, which can be shown by the atomic ratio of M/Si (M being other cations).

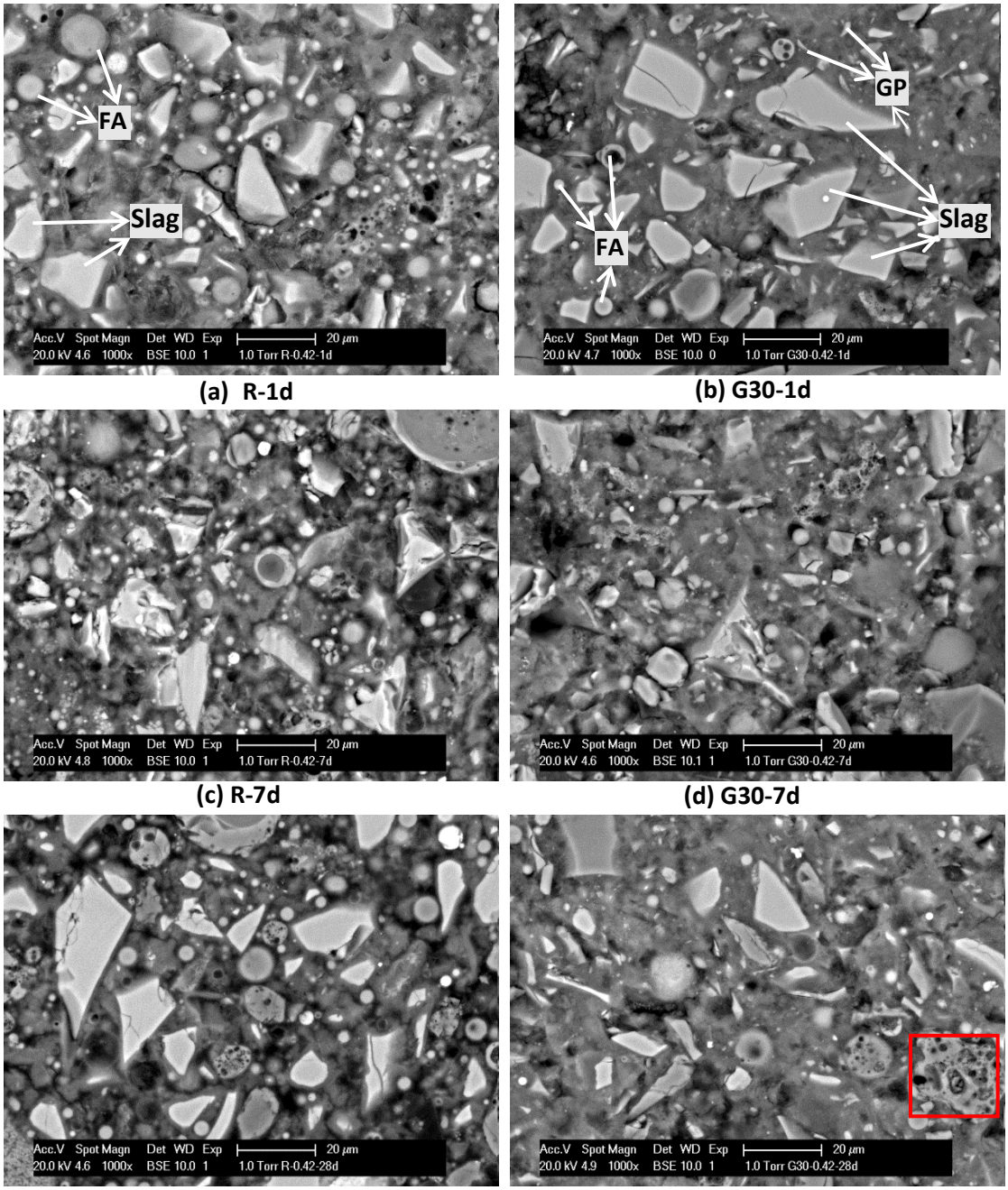

Figure 5.15 BSE images of alkali-activated slag/fly ash binder R and G30 cured for 1 day, 7 days and 28 days

It is clearly shown that the distribution of unreacted slag and fly ash particles embedded in gel formed around particles. The gel phase generally shows a dark grey color with grey level lower than fly ash. Pores, filled with epoxy, are shown in black color due to its dominant carbon and oxygen composition. By comparison between the BSE images of paste R and G30 at the same curing time, it is evident that paste with GP replacement (G30) yields a more homogenous microstructure at all ages with more area of gel phases and less pores. While it is obvious that for reference paste (R), the paste show heterogeneously distributed pores, which indicates a more porous microstructure. This is in line with the findings on amount of

gel formed by thermogravimetric analysis, which indicates increasing of GP replacement facilitate the gel formation.

Compared with previous studies on the similar alkali activated fly ash/slag with 50 wt% slag/50 wt% fly ash [24, 29] and also with systems with sole precursors, the binder system in this study reflects a less dense structure with higher porosity. The former system often exhibits large areas of homogenous gel formation with quite limited amount of pores and unreacted fly ash and slag particles. This can be derived from the low alkali activator concentration and also the curing temperature. A denser structure in previous researches is often acquired by using higher alkali activator concentration or curing in the oven at higher temperature.

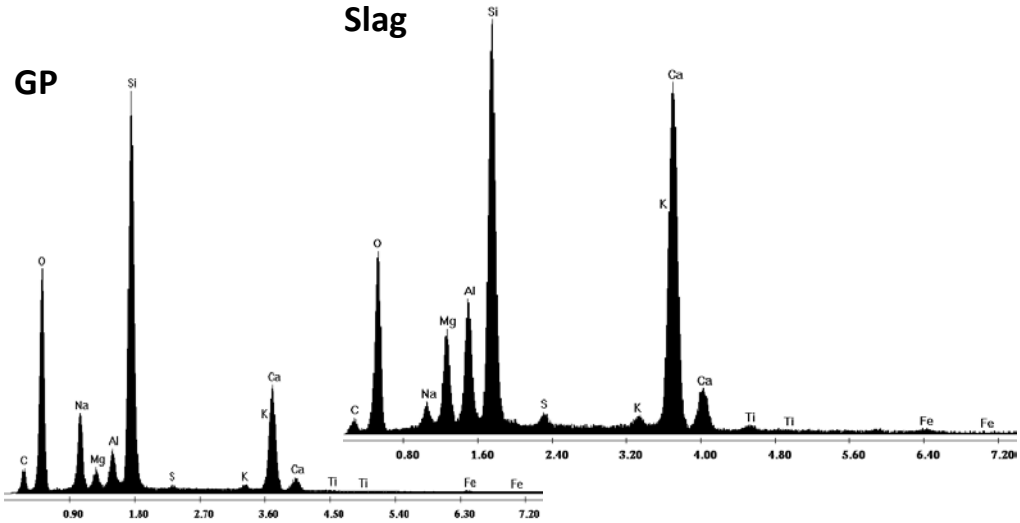

Figure 5.16 Representative EDX micrographs of unreacted GP and slag

It is also observed in BSE images that some fly ash particles after alkali activation exhibit porous structures which may due to the dissolution of fly ash by the attack of OH^-. It has been proved that fly ash with pores inside structure can provide extra space for accommodation of the reaction products. This phenomenon will be further studied in Section 6.1.

Element distribution by EDX point analysis

Quantitative elemental spot analysis is also performed on two samples, i.e. R and G30, in order to conduct the chemical analysis of the reaction products in the system. EDX results of multiple points are selected randomly within the binder region (excluding unreacted precursor particles), a total number of 20 measurements were conducted on each sample at curing age of 1 day and 7 days. 30 measurements were performed on the samples at curing age of 28 days.

In order to further analyze the influence of GP replacement on the chemical compositions of gel formation, CaO-SiO_2-Al_2O_3 ternary diagrams are plotted. Calcium, aluminum and silicon contents of these samples are renormalized to 100% on an oxide basis, which excludes all other elements present in the samples. These ternary diagrams reflect the gel composition

with respect to different GP replacement, which provide useful information to determine the nature of reaction products.

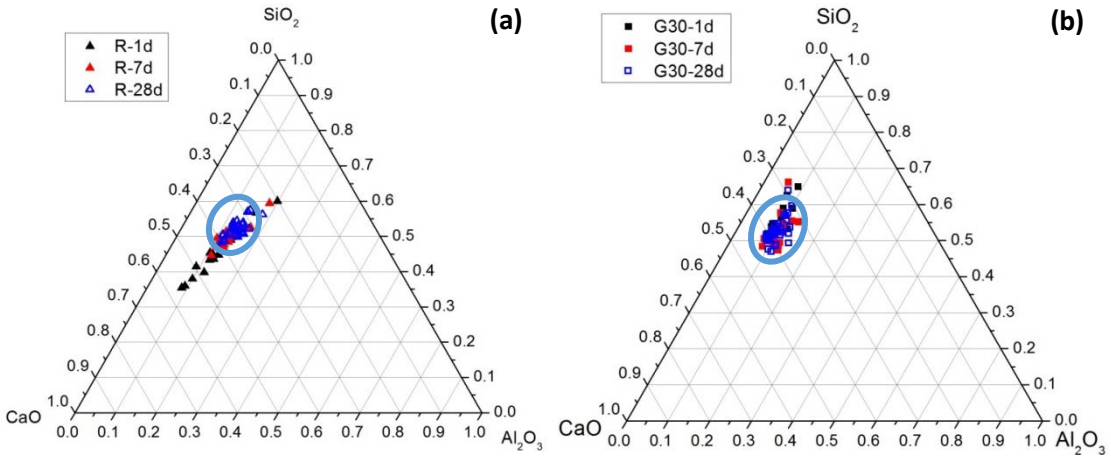

Figure 5.17 Representative ternary diagram of EDX spot analysis for alkali activated slag/fly ash as a function of GP replacement level and curing time: (a) 0% replacement (R), (b) 30% replacement (G30).

From Figure 5.18, it is shown in the ternary diagram that the Ca/Si ratio of gel formed at 28 day is in the range of 0.45-0.9 for G30. For R, this range is 0.5-0.8. The 28 day Al/Si ratio for G30 and R is in the range of 0.3-0.5 and 0.43-0.65, respectively. It is seen from the ternary diagram in Figure 5.17 that all data points of EDX spot analysis for both R and G30 dominantly fall in to the region which is defined by previous studies on alkali activated slag [66, 91, 92] as well as alkali activated slag fly ash mixtures [21, 24, 29, 30, 71, 93, 94]. The reaction products with approximately the same chemical make up at 7 day and 28 day is highly likely to be C-A-S-H type gel. C-(N)-A-S-H gel could also exist if Na is incorporated in to the C-A-S-H type gel, however, due to the limitations of EDX technique and the influence of NaOH in the pore solution in the matrix, it is difficult to confirm the formation of this type of gel. Detailed discussion on gel formation and nature of gel products will be given in Section 6.1, in combination with results from other characterizations in this study. It is worth noting that no N-A-S-H type gel is found within the ternary diagram, which is ordinarily been found near the SiO_2 and Al_2O_3 axis in the ternary diagram due to limited Ca in its structure. N-A-S-H type gel is widely accepted as an 3-dimensional aluminosilicate network from alkali activation of fly ash [55, 95, 96] or alkali activated slag/fly ash binder with dominating fly ash content [29, 71]. More discussion on inexistence of N-A-S-H gel will also be given in Section 6.1.

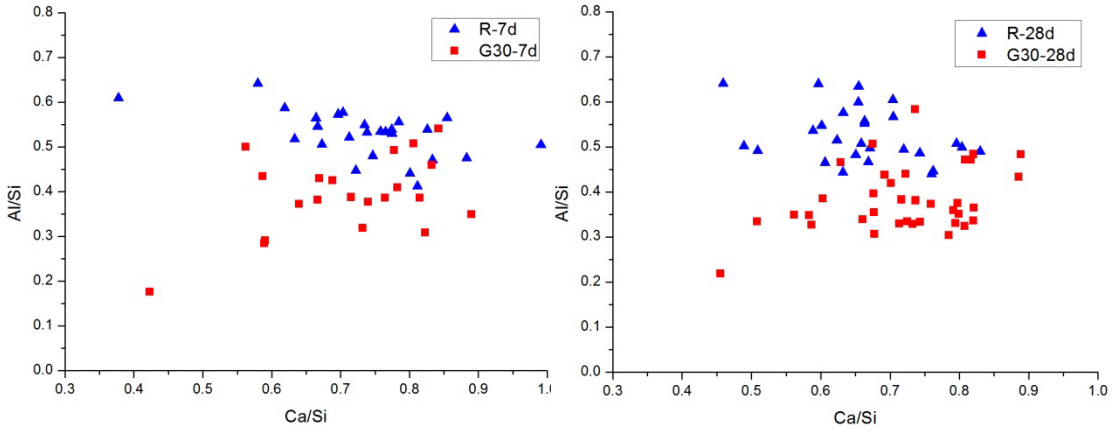

Figure 5.18 EDX analysis on the Al/Si ratio vs Ca/Si ratio of reaction products for R and G30 binder cured for 7 and 28 days

The range of Ca/Si ratio and Al/Si ratio of binder G30 and R cured for 28 days are shown in Figure 5.18. At same curing age, the average Al/Si ratio is generally higher in R than in G30 for sample at all curing age. This may be due to higher fly ash content in the mixture of reference sample, since fly ash have higher amount of reactive Al than GP as has been studied in Section 4.2.5. The Ca/Si ratio of G30 is slightly higher than R, which can be possibly explained by higher Ca content in GP. Amount of Al incorporation into the C-S-H gel is found to decrease with Ca/Si ratio [97, 98], which is in agreement with the findings in this study.

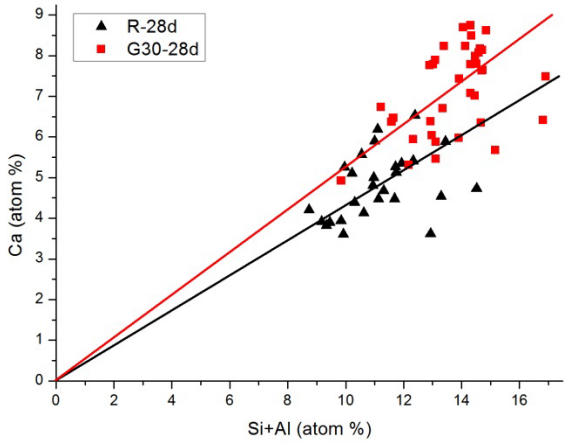

Figure 5.19 A comparison in the Ca/(Si+Al) ratio of reaction products in R and G30

As shown in Figure 5.19, a higher Ca/(Si+Al) ratio of reaction products at 28 day is observed in G30 mixture compare with R. In previous studies on C-S-H gels, Ca/Si ratio is one important factor which influences the mean chain length (MCL) in the gel. The MCL is found to be negatively correlated with Ca/Si ratio, which means increase in Ca/Si ratio shortens MCL in C-S-H gel [97]. In C-A-S-H gel, the part of the Si in the chain is substituted by Al thus forming an aluminosilicate chain, the MCL of which is believed to be correlated with Ca/(Si+Al) like the relation between Ca/Si ratio and MCL in C-S-H gel. The higher the Ca/(Si+Al) ratio, the lower the MCL. Therefore, the higher replacement level of GP may have

impact on the gel structure and shorten the MCL of the aluminosilicate chain in the C-A-S-H type gel.

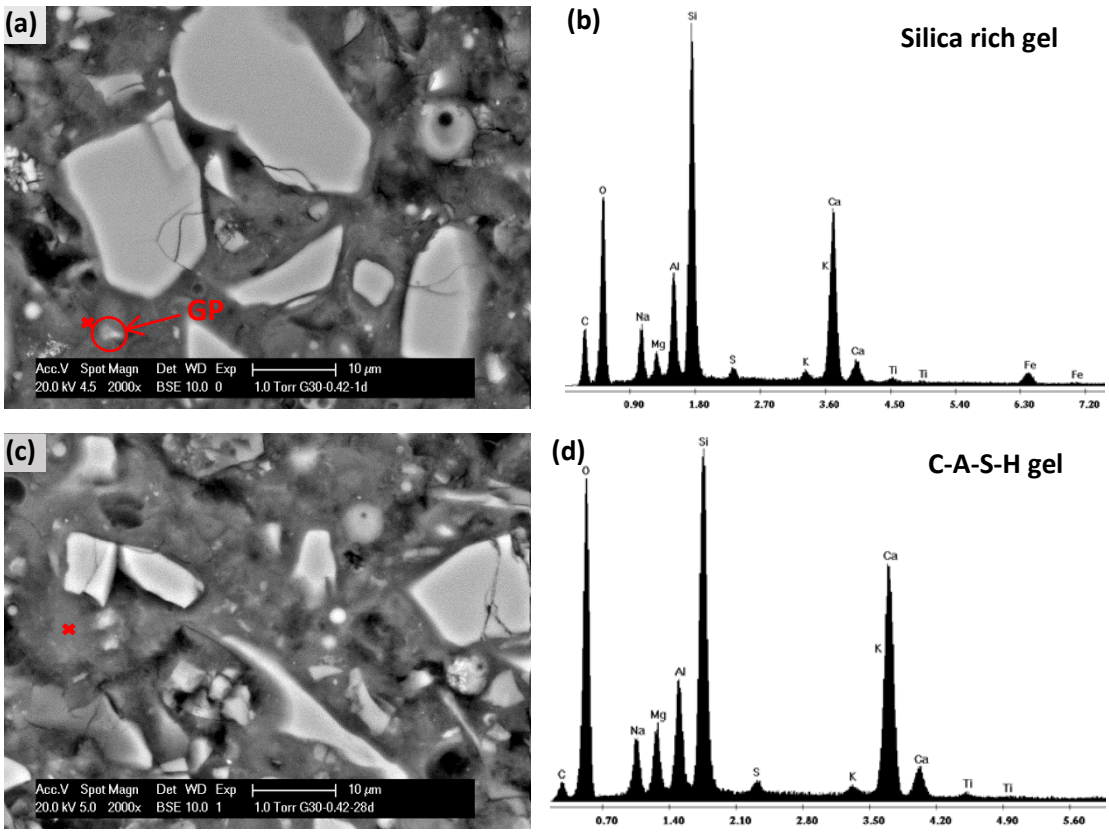

Figure 5.20 Gel formed around individual particles: (a) BSE Micrograph of G30 cured for 1 day, (b) EDX spectra of silica rich gel formed near GP particle; (c) BSE micrograph of G30 cured for 28 days, (d) Representative EDX spectra of C-A-S-H type gel.

Except for the measurements on relatively homogenous region of reaction products, analysis was also performed on specific reaction products formed around individual particles. Figure 5.20 shows BSE images of G30 sample at 1d and 28d with corresponding EDX spectra taken at marked position around precursor particles. It is notable that the EDX result on the spot analysis on the reaction products around GP particles (Figure 5.20 (b)) reveals higher Si/Al ratio and Si/Ca ratio than those in C-A-S-H type gel. This confirms the formation of sodium silicate either in semi-crystalline or amorphous phase, in line with previous studies on binder of alkali activated glass powder [49, 50]. Existence of Al and Ca are detected in EDX spectra of silica rich gel, which may due to possible dissolution of these element from nearby solid precursor particles though diffusion process. It is reported that silicate gels have great affinity for Al since its incorporation into the structure to substitute for Si in silica tetrahedron with Na as charge balancer and/or absorbed in the gel surface [99]. It is believed these silica rich gels mainly exist in the structure at early age, after which the amorphous silica will be further involved in the geopolymerization to form the main reaction product C-A-S-H type gel.

Gel phases in the BSE images in Figure 5.20 (c) is rather homogeneous and in general of similar chemical makeup, which is shown in the representative EDX spectrum of C-A-S-H

type gel in Figure 5.20 (d). C-A-S-H type gel as found in the ternary diagram is believed to be the main reaction products in the mixture.

5.6.3 Conclusion

The following conclusions could be drawn from the analysis of BSE images and EDX spot analysis presented in this chapter:

1. From the morphology of binder by BSE imaging, a more homogenous and denser microstructure is found in binder with GP replacement.
2. Amount of GP replacement does not have major influence on the nature of the reaction product. C-A-S-H type gel is the dominating reaction product formed in all alkali activated slag/fly ash binder with or without GP replacement.
3. Lower Al/Si ratio and lower Ca/Si ratio found in G30 mixture compared with R mixture is due to the replacement of fly ash by GP, which largely altered the initial chemical composition of unreacted precursors.
4. Silica rich gel is formed around GP particles at early age, which also present incorporation of Ca and Al. Higher Si/Ca and the affinity to Al (higher Si/Na) in G30 further strengthen the proof that the silica rich gel is mainly semi-crystalline or amorphous sodium silicate formed by the dissolution of GP.

5.7 Strength Development of geopolymer paste

5.7.1 Introduction

The strength of concrete is defined as its ability of concrete to withstand forces, stresses and pressures without failure. Among all properties of concrete, strength is generally considered one of the most valuable. The strength gives an overview of the quality of the concrete because it is directly related to the hydrated cement matrix. The strength of concrete is separated into flexure, compression, tension and splitting. The strength does not only depend on the strength properties of the materials, but also on the bond strength between the aggregates and binder. The most commonly performed experiments are the compression and flexural tests.

5.7.2 Results and discussion

Compressive strength

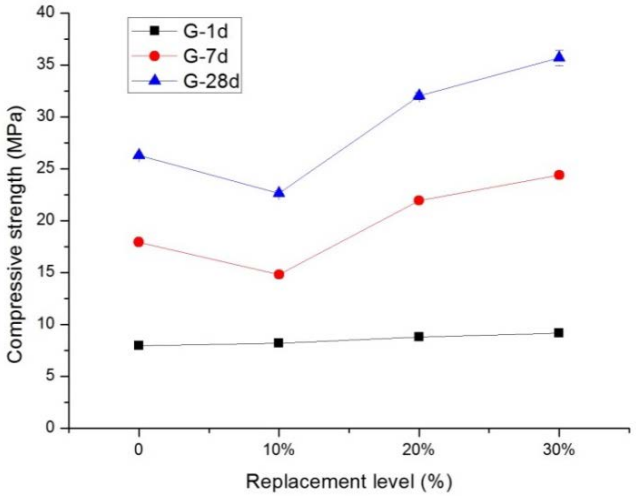

Figure 5.21 Influence of GP replacement for fly ash on compressive strength at 1, 7 and 28 days, L/S ratio=0.42.

Figure 5.21 shows the compressive strength of alkali activated slag/fly ash pastes with GP replacement level from 0, 10%, 20% and 30% at a curing age of 1, 7 and 28 days. The standard deviations are presented as the error bar at each measurement value; some of the STD is so small that it cannot be identified with the error bar. It is found that although the compressive strength at 1 day does not show obvious difference, in general it increases with higher amount of GP replacement after 7 and 28 days curing. It is believed that the increase of compressive strength is due to the facilitating effect by the higher amount of available silica introduced by reaction of GP with NaOH. The use of sodium silicate in conjunction with sodium hydroxide as alkali activator resulted in additional available silica in the system and helps to speed up the geopolymerization [91]. The enhanced reaction kinetics in the end result in an increase in amount of gel formed in the structure at the same curing age, as has been detected by heat evolution discussed in Section 5.3 and TG/DTG analysis in Section 5.4.

However, it is worth noting that a considerable decline in strength is found within mixtures contain 10% replacement. The reason for this reduction is a combination effect of several

factors of both physical dominating properties of fly ash and reaction chemistry, which will be elaborate in Section 6.2.

Flexural Strength

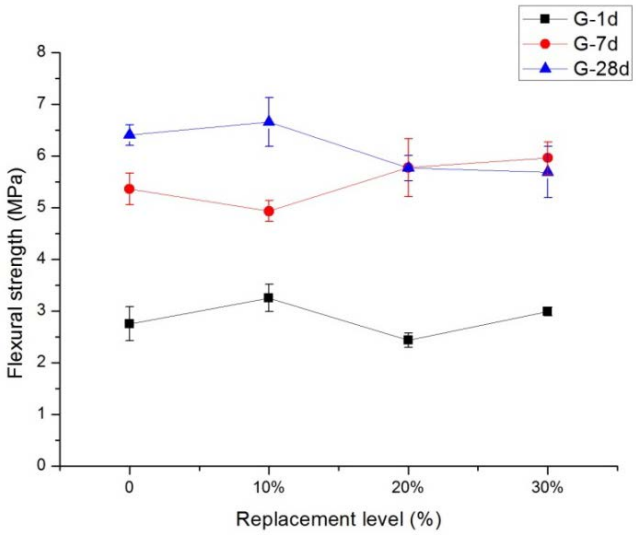

Figure 5.22 Influence of GP replacement for fly ash on flexural strength at 1, 7 and 28 days, L/S ratio=0.42.

Figure 5.22 shows the flexural strength of alkali activated slag/fly ash pastes with GP replacement level from 0, 10%, 20% and 30% at a curing age of 1, 7 and 28 days. Inconsistent trend of flexural strength development could be observed. For binder cured for 1 day and 28 days, the flexural strength fluctuates with replacement level from 10% to 30%. The results at 7 days exhibit an increase in flexural strength with replacement level higher than 10%. However, it is found that the binder with 30% GP replacement suffers a slight reduction in flexural strength at 28 days.

An explanation for this phenomenon may be related to the formation of microcracks in the structure. These microcracks in the structure have more significant influence on flexural strength than compressive strength. The formation of the microcracks may be due to the early age shrinkage within the binder. Up till now the volume stability of AAMs and the mechanism of shrinkage in this system are still largely unknown, therefore, further research on these problems have to be done to clarify this phenomenon comprehensively.

5.7.3 Conclusion

From the compressive and flexural strength results, the following conclusions can be drawn:

1. The replacement of GP for fly ash in alkali activated slag/fly ash binder generally leads to an increase in compressive strength at 7 and 28 days' curing with 20% and 30% GP replacement.
2. The increase in compressive strength is attributed to more available silica introduced by GP replacement and finally a higher amount of gel products in the structure.
3. 10% GP replacement result in a loss in compressive strength at 7 and 28 days.
4. In consistent trend on development of flexural strength is found with different level of GP replacement, which may be due to the formation of microcracks by possible

shrinkage in the structure. The explanation of this phenincrease omenon is beyond the scope of this project and further clarification of mechanisms of shrinkage in AAMs is recommended for future research.

6 General Discussion on Gel Formation and Compressive Strength

6.1 Nature of Final Gel Product

Gel formation in alkali activated slag/fly ash (50 wt %/50 wt %) with GP replacement from 0, 10%, 20% and 30% is discussed in this section taking consideration of the results from a series of analysis done in Chapter 4 and 5.

In Section 5.2.2, XRD detected a poorly crystalline calcium silicate hydrate (C-S-H) phase ($1.5CaO{\cdot}SiO_2{\cdot}xH_2O$, PDF# 00-033-0306), which is found near 29.4° 2θ degree as main reaction product. Broad humps in XRD patterns reveal the amorphous nature of the reaction products. C-S-H phase is confirmed to correlates with amorphous gel formation in previous studies [21, 24, 29, 66, 67], in which it is attributed to C-S-H type gel in OPC and C-A-S-H type gel in AAS. Formation of C-A-S-H type gel is also identified in chemical bonds analysis using FTIR in Section 5.5.2. The main T-O stretching bands centred all approximately at around 950 cm^{-1} are assigned to asymmetric stretching vibrations of Si-O bonds. Absorption bands approximately centred at 950 cm^{-1} is associated with the Si-O-Si stretching vibrations of SiO_n units for n=2 [81], indicating the formation of C-A-S-H type gels with chain structures, in which Si has dominant Q^2 structure.

Except for above proofs on formation of C-A-S-H gel, $CaO\text{-}SiO_2\text{-}Al_2O_3$ ternary diagram of EDX data on gel region is in well agreement of previous studies, in which range of chemical composition of this region is attributed to C-A-S-H gel or C-(N)-A-S-H gel. Later EDX spot analysis also confirmed that Al incorporation into the gel structure as Al mostly presents in tetrahedral bridging sites within the chains. Na^+ cations in general serves as negative charge balancer in between the layered chain structure, however, it is impossible to determine if Na^+ cations have incorporated into the gel structure due to limitations of EDX and influence of NaOH in the pore solution. Therefore, the major reaction product in this kind of alkali activated binder is C-A-S-H type gel.

N-A-S-H gel is not identified in the $CaO\text{-}SiO_2\text{-}Al_2O_3$ ternary diagram. Previous studies show that N-(C)-A-S-H gel, which is N-A-S-H gel modified by Ca into the structure, share the similar chemical composition with C-(N)-A-S-H gel while having lower Ca/Si ratio. It is believed that in this study the N-(C)-A-S-H is not formed in G30 considering the higher initial Ca/Si ratio of unreacted precursors. For R mixture, even if this kind of gel is formed in the structure, the amount would be so limited that it cannot be distinguished by the EDX analysis or other technique like XRD and FTIR. Furthermore, from results of FTIR, no absorption band inside the main band for N-(C)-A-S-H gel is found as this kind of gel is dominated by Q3 and Q4 Si structure generally with absorption band above 1000 cm^{-1}.Additionally, XRD patterns of all alkali activated binders do not indicate the existence of any zeolite phases. Aluminosilicate gel is commonly accepted to be “zeolite precursor” and the correlations exist between alkali activated fly ash and zeolite [23, 27]. In line with results of other techniques, XRD patterns also provide no evidence of formation of N-(C)-A-S-H gel or N-A-S-H gel. To summarize, the traces of N-A-S-H gel is not identified in this study in all mixtures, and it is assumed that no N-A-S-H type gel is formed in the structure.

It is also worth noting that a silica rich gel is identified in the binder with 30% GP replacement at 1 day. Formed around GP particles, this implies the formation Silica rich gel is at early age, which also present incorporation of Ca and Al. Higher Si/Ca and the affinity to Al (higher Si/Na) could be either by incorporation of Ca and Al dissolved from the fly ash and slag or be intermixing with C-A-S-H type gel, although it is hard to distinguish this two kinds of gel phases by EDX analysis at early age. The silica rich gel is not identified in samples at 7d and 28d, which may indicate the consumption of this kind of gel by formation of main product C-A-S-H type gel. Abundant amorphous silica although not all in the form of silica monomer inside this structure may be favorable in geopolymerization process and in the end yields a higher amount of gel formation as measured by isothermal calorimetry in Section 5.3.2 and TG/DTG in Section 5.4.2.

6.2 Effect of GP on Gel formation

It is confirmed by the EDX analysis that GP replacement in the binder does not have significant influence on the nature of gel formed in the structure. In FTIR analysis, the position of main T-O band in each binder spectra is also found to be independent from the influence of GP replacement. This indicates that the GP replacement doesn't affect the major ultimate reaction products. Moreover, there is no significant change in XRD patterns for each mixture over different curing age. All these findings indicate replacement GP doesn't change the nature of the main reaction product.

However, the partial inclusion of GP and removal of fly ash indeed change the chemical composition of initial unreacted precursors, followed by higher Al/Si ratio and lower Ca/Si ratio in R mixture at 28 day. Careful observations on element ratio at 28 days also imply that GP replacement may to some extent affect the polymerization degree and crosslinking.

Like in other polymers, the mean chain length and cross-linking between chain layers in C-A-S-H gel defines the overall polymerization degree of the aluminosilicate polymer network in C-A-S-H type gel. Single aluminosilicate chain with shortened MCL is believed to have lower polymerization degree. As G30 has lower Al/Si ratio, higher Ca/Si ratio as well as Ca/(Si+Al) ratio, a shorter aluminosilicate chain length is formed which implies a lower polymerization degree of single aluminosilicate chain. On the other hand as studied in FTIR analysis, the position of main T-O absorption band shift to higher wavenumber at 28 day, which indicate an increase in the overall polymerization degree in the gel structure. With lower polymerization degree of single chain, the overall polymerization degree has to be results from a higher cross-linking of the C-A-S-H type gel network. It is believed that higher crosslinking density of gel network lead to better mechanical properties, which can also be one of reasons contributing to the increase of compressive strength with GP replacement.

It has to be mention here that although FTIR reveals qualitative results on the overall polymerization degree, it is not a quantitative analysis method on the gel network. The shortened single chain also need to be confirmed by more accurate analysis besides the Ca/Si or Ca/(Si+Al) ratios. Magic angle spinning nuclear magnetic resonance (MAS-NMR) is the very technique to give detailed information about atomic environment of gel network which is essential for comprehensive understanding of gel nature. MCL can also be

calculated using ratios of different Q structure of Si and Al. Therefore, NMR is highly recommended to further clarify the effect of GP on gel network in future research.

6.3 Compressive Strength Development

Discussions in this section focused on clarification of reduction of compressive strength of G10 mixture.

6.3.1 Effect of NaOH treatment on pore structure of fly ash

Although not intensively studied as paste mixture, the pore structure of fly ash, both porosity and pore size distribution is also of great significance when it comes to formation of reaction products.

In reaction kinetics, at constant temperature and pressure, higher concentration of reactants leads to higher reaction rate. That is one of the reasons that the reaction products form on the surface of remaining precursors after dissolution stage and saturation of source element. Since the pore inside precursors may give extra surface and the concentration of reactant (alumina and silica in this case) is first saturated near the surface, it is possible that the gelation products form not only on the outside surface of precursor but also on the inside. It has been confirmed that in cement paste blended with fly ash, the reacted hollow fly ash particles are able to provide extra space for the accommodation of reaction products, including both hydration products of cement and reaction products of fly ash [100]. The reaction product can filled up hollow fly ash particles after long period of reaction.

A reasonable assumption is made that the pores in fly ash as precursor in geopolymer system can also accommodate reaction products.

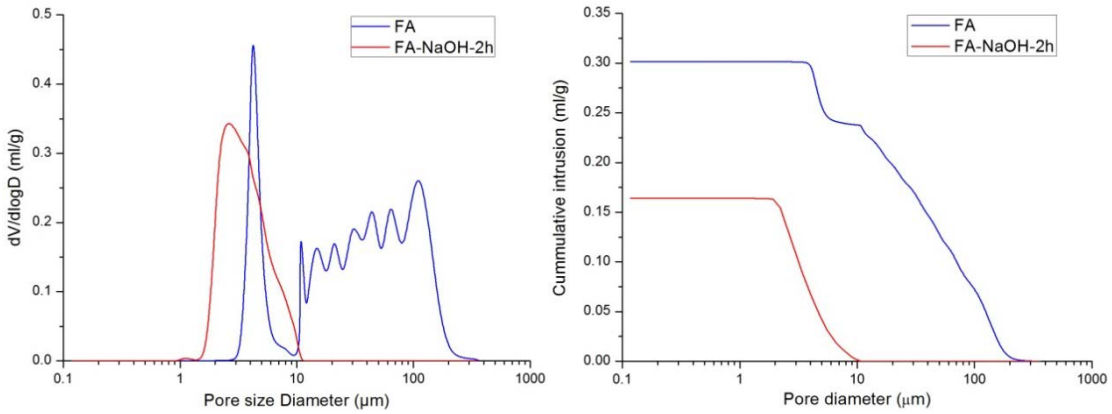

(a) Differential pore size distribution **(b) Cumulative pore size distribution**

Figure 6.1 (a) Cumulative pore size distribution curves and (b) Differential pore size distribution curves of original fly ash and fly ash treated with NaOH solution for two hours

As shown in Figure 6.1 (a), the differential pore size distribution shows distinct differences with pore size diameter above 10 μm. Several sharp peaks are found in the curve for original fly ash and these peaks are known to be corresponding to the threshold (critical) pore diameter, which indicate a higher rate of mercury intrusion at this pore diameter [101]. However, considering the particle size distribution of fly ash particles, D_{90} is only around 80

µm. Therefore, it is impossible for the fly ash to maintain pores with diameters over 100 µm, which is larger than its particle size. Also, taking consideration of the similarities of peaks between 10 to 130 µm and disappearance of such peaks in fly ash treated with NaOH solutions, it is reasonable to believe that these peaks for original fly ash is correlated with the mercury intrusion process into the interstitials or irregular empty space between fly ash particles. The size and volume of these interstitials or empty space vary largely and thus yield a range of critical pore diameter. In addition, the fly ash after NaOH treatment was dried in the oven at 105°C, and afterwards the empty space is somehow eliminated. Therefore, no peaks are found in the range between 10 to 130 µm. In this way, Figure 6.1 is modified as Figure 6.2, in which the part for mercury intrusion into the empty space between fly ash is ignored.

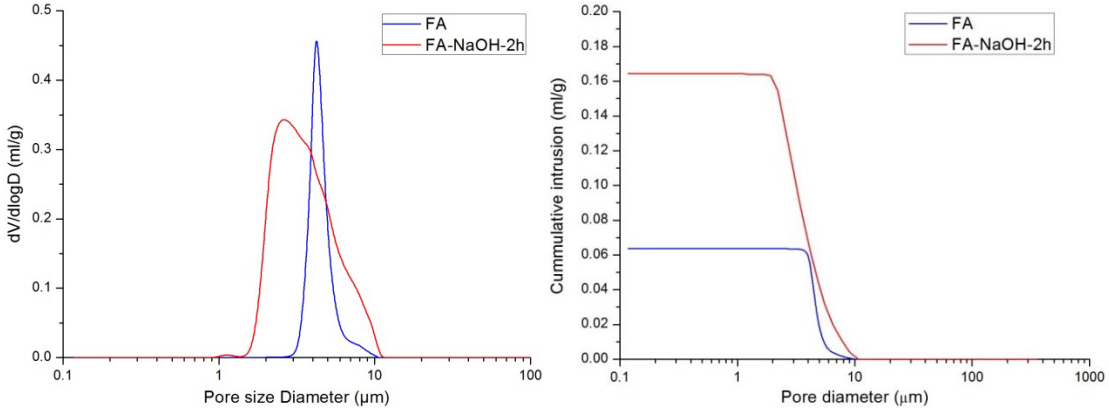

(a) Differential pore size distribution (b) Cumulative pore size distribution

Figure 6.2 (a) Modified Cumulative pore size distribution curves and (b) Modified differential pore size distribution curves of original fly ash and fly ash treated with NaOH solution for two hours

The comparison of pore structure between original fly ash and fly ash treated with 4M NaOH solutions for two hours reveals obvious differences in two systems. Several pore structure parameters could be retrieved from the cumulative and differential pore size diameter curves shown in Figure 6.2.

The total porosity is calculated from the total intrusion volume of mercury divided by the bulk volume of the sample. In this study, the total porosity is accepted as the volume percentage of pores inside fly ash. As shown in Figure 6.2, the total porosity Φ_{total} for original fly ash is recalculated as:

$$\emptyset_{total} = \frac{V_{intrusion}}{V_{bulk}} = \frac{V_{intrusion}}{\frac{m_{bulk}}{\rho_{bulk}}} = \frac{0.06386\ mL/g}{\frac{1}{0.8911}\ mL/g} = 5.6881\%$$

The total porosity for fly ash treated with NaOH for two hours is 17.4241%, indicating a massive increase in the porosity compared with original fly ash. By comparing the pore size distribution derived from Figure 6.2 (a), NaOH treatment of original fly ash particles gives a finer pore structure.

This kind of pore refinement after NaOH attack may due to the opening of hollow fly ash particles by dissolution and consumption of the thin shell. After the surface opening, the inside of fly ash particles become accessible for mercury intrusion while the pores in these fly ash particles before attack are regarded as isolated pores, which has no contribution to the total porosity. The accessibility of fine pores inside fly ash particles largely increase due to the opening up of fly ash surface, and in this way conduce to a refinement of pore structure in fly ash.

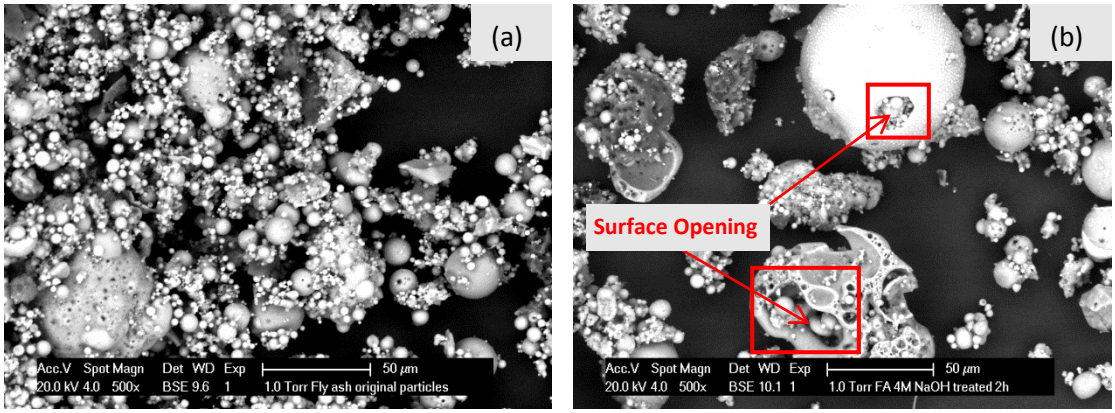

Figure 6.3 Surface opening of fly ash particles: BSE images of (a) original fly ash particles and (b) fly ash treated with 4M NaOH for 2 hours

Proof of surface opening is found in BSE images before and after NaOH solution treatment (see Figure 6.3). Before treatment, large quantities of small fly ash particles are found in Figure 6.3 (a) and original fly ash particles normally have smooth surface. Small fly ash particles disappear after treatment due to dissolution. Except for small particles left from dissolution, it is also believed that some of small fly ash particles come from inside of original hollow fly ash particles after surface opening. Surface opening can be observed in the red rectangular marked in Figure 6.3 (b).

6.3.2 Reduction of compressive strength of G10

Again the compressive strength development as a function of GP replacement level and curing time is illustrated in Figure 6.4.

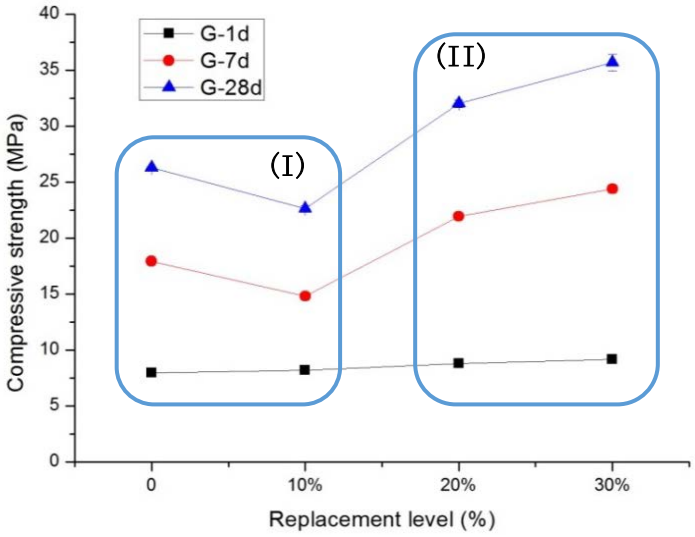

Figure 6.4 Compressive strength as function of GP replacement level and curing age

Although higher compressive is discovered in mixtures with 20% and 30% GP replacement, a notable reduction is found with 10% GP. As is confirmed by heat evolution discussed in Section 5.3 and TG/DTG analysis in Section 5.4, an increase in amount of gel formed in the structure cured for 7 days and 28 days with increasing GP content. If the amount of gel formation is the only major factor with respect to compressive strength development, a near linear relationship should be established. Nonetheless, this inconsistency, which seems somehow abnormal, implies a different mechanism concerning development of compressive strength.

As slag content is fixed constant at 50% and L/S ratio is fixed constant at 0.42 in all mixtures, the only parameters altered by the GP replacement are precursor proportions for both fly ash and GP. As fly ash and GP serves different role in geopolymerization, the reduction and later increase of compressive strength is extremely probable due to the changes in the initial precursor proportions of fly ash and GP. It can be hypothesized that in general three factors may have major influence on gel formation and later compressive strength, which are (1) packing effect of fly ash, (2) accommodation of reaction products by opening pores in fly ash, and (3) enhanced amount of gel formation by GP replacement.

The impact of these three reasons is closely related with GP replacement level, since the properties introduced by these factors is largely determined by the amount of fly ash and GP. Previous studies reported that fly ash incorporation in cement paste improve the compressive strength by increasing the packing density in the structure [102, 103]. The accommodation of reaction products has been discussed in Section 6.3.1, providing proves of the potential for the reaction product to form inside the pores in the fly ash particles after pore opening up by OH^- attack. The reaction product formed in the inner surface of pores in fly ash can be characterized by experimental techniques like TG/DTG and isothermal calorimetry but do not contribute to the compressive strength, which contradict with traditional understanding on positive correlation between amount of reaction products and compressive strength [104]. Facilitating effect of GP replacement is confirmed from the

enhanced amount detected by isothermal calorimetry in Section 5.3.2 and in Section 5.4.2, the reason of which has already been discussed in Section 5.4.2.

Table 6.1 Impact factors on development of compressive strength with increasing amount of GP replacement

Factor	Factor impact by increasing GP	Compressive strength by increasing GP
(1) Fly ash on packing effect	↓	↓
(2) Fly ash recommendation for reaction products	↓	↑
(3) GP facilitating gel formation	↑	↑

Figure 6.4 is divided into two regions, with (I) from 0 to 10% GP replacement and (II) 20% to 30%.The contribution of the factors as well as their impact on compressive strength are shown in Table 6.1 with increasing GP replacement. It is found that with increasing GP replacement (i.e. decreasing fly ash content), factor (1) has negative contribution in compressive strength while factor (2) and (3) enhance the compressive strength. Therefore, the reduction in G10 samples and higher compressive strength in G20 and G30 could be due to the combination effects brought by these three factors, the contribution of which varies according to GP replacement.

In region I, it is believed that the major factor contributes to the reduction of compressive strength is (1) packing effect of fly ash. 10% GP replacement decreases the fly ash content, which minimize the pack density of the mixture. Somehow it is beyond the scope of this research to further explain why contribution of factor (1) dominates in region I.

When the GP replacement reaches 20%, factor (2) together with factor (3) take over and become the dominating impact factors which influence the compressive strength. This alteration in dominating roles is the result of decline of fly ash content by increasing GP replacement. As shown in Table 6.1, the capacity of fly ash accommodation for reaction products decrease with GP replacement since less fly ash is remained in the structure. In this way, the amount of gel that could be formed inside the open up pores in fly ash is diminished. On the other hand, the higher GP replacement leads to a higher amount of gel formed. Consequently, simultaneous contributions of these two factors increase compressive strength with 20% and 30% GP replacement.

7 Fine Glass Aggregate as Sand Replacement in Alkali-activated Slag/Fly ash Mortar

7.1 Introduction

Except for the powder fraction of waste glass gathered after drying process, another fraction of waste glass, generally manufactured by crushing bottled glass into fine glass cullet, also has the potential to be utilized in Alkali-activated slag/fly ash mortars. This fraction of waste glass as fine glass aggregate (GA) is in the size of 1 to 2 mm, which is suitable for partial sand replacement in mortars. This chapter aims to study the possibility of reusing fine waste glass cullet from container glass and flat glass as fine aggregate replacement for preparing mortars. The effects of different replacement level of waste glass in alkali-activated slag/fly ash mortars were studied, mainly focusing on workability and strength.

7.2 Results and Discussion

7.2.1 Workability

When it comes to construction process of structures, the workability of concrete is one of the most important factors. It has a direct influence on the properties of hardened concrete, such as strength and porosity. The workability of mortars is defined by different properties, such as the consistency, plasticity and cohesion. In this study the consistency by the flow table test is applied as a measure for the workability.

The workability is presented as spread diameter against different replacement level of fine glass aggregate to CEN reference sand, which includes 0, 10%, 20% and 30%. Results of spread diameter were acquired after 15 times of free falling from a height of 10 mm on the flow table. The reference and G30 mortar mixtures, as described in Section 3.2.4, were included in workability test initially. However, due to the content of GP already as precursor replacement in G30 mixtures, there is not any difference between the initial diameter and the spread diameter. Therefore, only the reference mortar mixtures were used for workability testing, which contains only 50% slag and 50% fly ash as binder precursors. This is also another proof that GP as precursor has a higher water demand than fly ash or slag.

The effects of GA as replacements of sand on workability of mortar are shown in Figure 7.1. For four different replacements, the initial spread diameter remains unchanged. Thus, the initial spread diameter is not plotted.

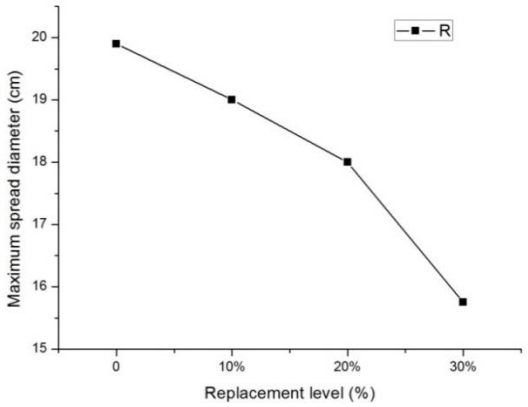

Figure 7.1 Maximum spread diameter of mortar after flow table tests as a function of GA replacement of sand

Increase of sand replacement with GA leads to a reduction of the maximum spread diameter. This suggests that increasing GA content up to 30% as sand replacement give negative impact on the consistency of mortar. The decline of mixture consistency is due to difference of roundness between sand and GA. As one kind of crushed aggregate with well-defined edges, angularity of GA is absolutely higher than that of sand. It has long been accepted that angular fine aggregate with lower roundness generally require more water for a given workability [104]. The sharper edge, more angular shape and higher aspect ratio of GA reduced the flowability of mortar by hindering the movement of paste and other particles [27]. In addition, the increased surface area of glass sand compared to nearly round natural sand would require more water to wet and more paste to coat and lubricate.

7.2.2 Flexural strength

The results of flexural strength, like in paste strength test, are acquired from average measurements of three prisms. The prisms are standard prisms with a size 40x40x160 mm^3. The effects of amount of GA as sand replacement on flexural strength of mortar R and G30 are illustrated in Figure 7.2 and Figure 7.3, respectively.

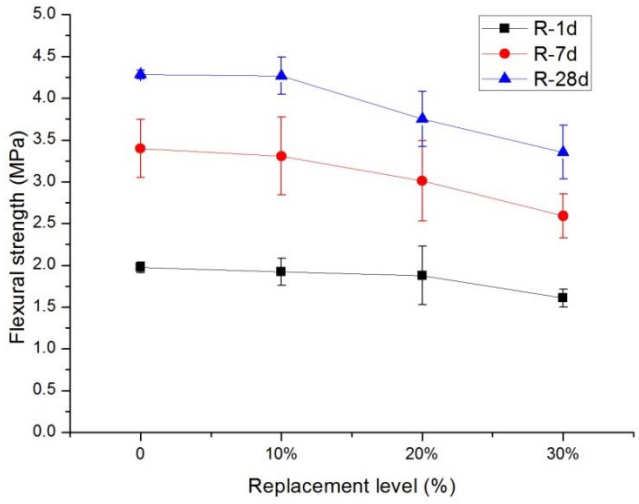

Figure 7.2 Flexural strength of mortar R as a function of GA replacement level

It is obvious that all curves for R mortar indicate a loss in flexural strength with increasing GA content. Only slight reduction is found between replacement levels up to 10%. However, a higher reduction rate of flexural strength is found between 10% and 20% as well as between 20% and 30% for all R mortar mixtures. The decrease in flexural strength may be mainly attributed to the weaker bonding between the smooth surface of the glass particles and the paste [104].

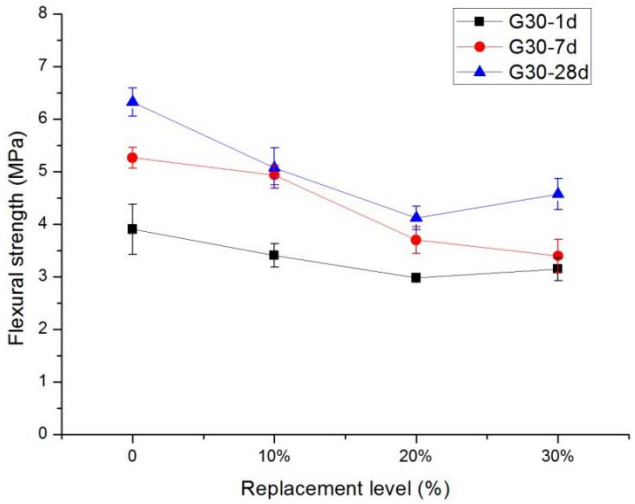

Figure 7.3 Flexural strength of mortar G30 as a function of GA replacement level

Compared with R mortar, an almost 100% increase in flexural strength is identified within G30 mortar. This improvement of flexural strength is due to the higher amount of gel products formed in G30 in agreement with previous findings in this project, which provides enhanced binding properties in G30. G30 mortar also shows a reduction in flexural strength with increasing GA content up to 20%. However, all curves except for 7d sample exhibit an increase in flexural strength when the GA content is further increased to 30%.

Fine glass cullet, which is detected to be partially dissolved and participate in the formation of geopolymeric matrix, is found to have positive effect on mechanical strength in alkali-activated calcareous fly ash mortars [105]. As is discussed in Section 4.2.7, GA also has potential to release Si into the system from dissolution process. Si dissolved does not impose major impact on gel formation when the content of GA is lower than the threshold value. It is believed when content of GA increase to 30%, the gel formation is enhanced by more available silica incorporation into the C-A-S-H type gel, thus leads to higher flexural strength with 30% GA.

7.2.3 Compressive strength

The results of compressive strength are acquired from average measurements of 6 half-prisms after flexural strength test. The effects of amount of GA as sand replacement on compressive strength of mortar R and G30 are illustrated in Figure 7.4 and Figure 7.5, respectively. For some groups of data, the standard deviation is so small that it cannot be seen in the figure.

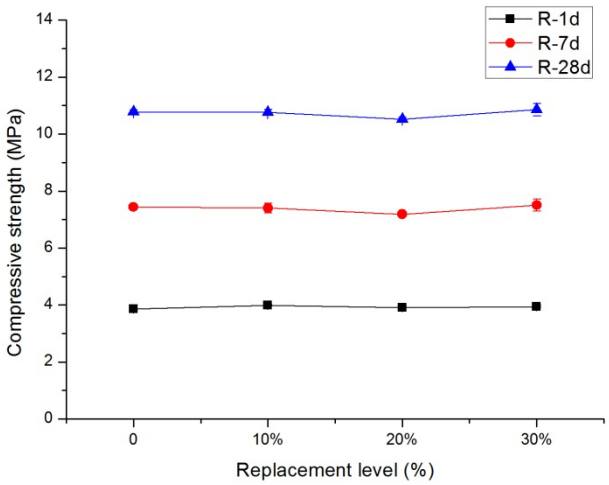

Figure 7.4 Compressive strength of mortar R as a function of GA replacement level

For mortar R, the results of compressive strength at different GA replacement level are quite similar to each other.

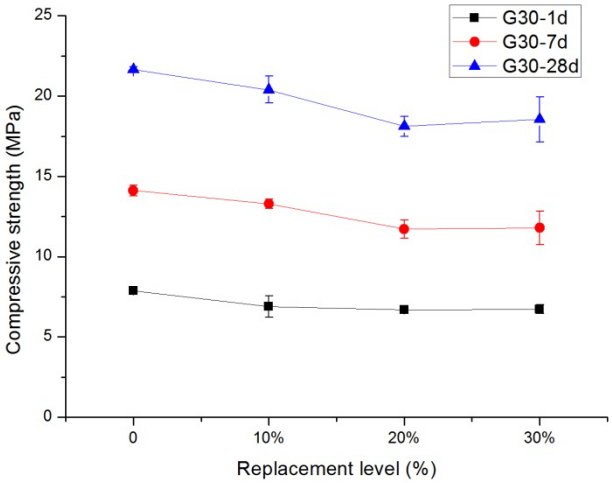

Figure 7.5 Compressive strength of G30 as a function of GA replacement level

By scrutinizing of the curves in Figure 7.5, it seems that the curves for all replacement level first have a tendency toward a slight drop from 0 to 20% followed by a slight increase in compressive strength between 20% and 30%. The compressive strength for each corresponding mortar G30 is almost two times higher compare to mortar R, which fits well with compressive strength measurements in paste mixtures. In Figure 7.5, It is found that this trend of strength reduction become more pronounced at 7 and 28 days. Compared with mortar with only reference sand as aggregate, mortar cured for 28 days with 10% and 20% GA replacement for reference sand suffers a strength loss of approximately 16% and 14%, respectively. From the view of mechanical strength, it seems that such reduction is comparably small and could be accepted.

The reduction of compressive strength between 0 and 20% may be due to the decrease in adhesive strength between the surface of the waste glass aggregates and the paste. Like results for flexural strength, slight strength increase is again found with GA replacement higher than 20% in G30 mortar. Considering the identical tendency of flexural and

compressive strength development as a function of GA replacement level, the same mechanism is used to explain the increase of compressive strength. The gel formation is enhanced by incorporation of more available silica into the C-A-S-H type gel.

It is worth noting that although GA has the potential to replace part of fine aggregate (reference sand) in alkali activated mortars with acceptable strength decrease, further research on other factors concerning volume stability, durability and permeability are still necessary to give further evaluation for real application of this replacement.

7.3 Concluding Remarks

1. From the results and discussions, it follows that the increase in GA from 0% to 30% leads to a substantial decrease in workability. The sharper edge, more angular shape and higher aspect ratio of GA compared with reference sand reduced the flowability of mortar by hindering the movement of paste and other particles, thus decrease the workability
2. GA replacement for reference sand in alkali activated slag/fly ash mortar generally reduces the mechanical strength. The percentage of strength reduction is comparably small and could be accepted when only taking influence of compressive strength into consideration.
3. A slight increase of both flexural and compressive strength in mortar G30 is due to more available Si from GA dissolution. It is believed as the when content of GA increase to 30%, the gel formation is enhanced by more available silica incorporation into the C-A-S-H type gel.
4. Further studies upon other aspects for further application of GA replacement are recommended.

8 Conclusions and Recommendations

8.1 General Conclusions

The following general conclusions can be summarized from this work:

Characterization of waste glass powder (GP)

- GP, generally of irregular polygonal morphology, has much finer particles size distribution and compared with fly ash and slag a larger specific surface area, which leads to a higher water demand within binders containing GP as precursor.
- GP contain high amount of amorphous phases. Quartz and calcite are main crystalline phases in GP with minor crystalline phases introduced in the GP recycling process.
- GP is rich in Si (65.60%) and Ca (22.06%) and has limited Al content (2.37%). The reactive Si content is higher than that of fly ash, which is up to 54.31%. Due to these reason, the dissolution potential of Si and Ca is higher in GP than in fly ash.
- Reactive chemical bonds in amorphous phases in GP and fly ash characterized by FTIR spectra subtraction mostly corresponds with (Si, Al^{IV})-O-Si bonds or (Si, Al^{IV})-O-M (M=Na or Ca) bonds, which are highly reactive and largely determine the activity of precursors.

Waste glass powder as partial replacement for fly ash in alkali activated slag/fly ash binder

- The replacement of GP for fly ash in alkali activated slag/fly ash binder generally leads to an increase in compressive strength at 7 and 28 days' curing with 20% and 30% GP replacement. An increase
- Fly ash after dissolution in alkaline solutions has an increased total porosity as well as a finer pore size distribution. The opening up of the fly ash surface makes the pores inside fly ash particles accessible. Fly ash after alkaline solution attack can provide space for accommodation reaction products with increased pore volume.
- The increase in compressive strength is attributed to more available silica introduced by GP replacement and finally a higher amount of gel products in the structure. With increasing GP content, the decline of fly ash potential to accommodate reaction product also contribute to the increase of strength, as the gel formed inside the pores of fly ash does not contribute to the compressive strength.
- 10% GP replacement result in a loss in compressive strength at 7 and 28 days. The reduction of fly ash content replaced by GP leads to lower packing effect.
- Inconsistent trend on development of flexural strength is found with different level of GP replacement, which may be due to the formation of microcracks by possible shrinkage in the structure. The explanation of this phenomenon is beyond the scope of this project and further clarification of mechanisms of shrinkage in AAMs is recommended for future research.
- C-A-S-H type gel is the main reaction product in alkali activated slag/fly ash 50 wt%/50 wt% with 0 to 30% of GP to replace fly ash. A silica rich gel is identified at early age in the mixture with GP replacement. It is assumed that no N-A-S-H gel is formed all mixtures.

Fine glass aggregate as sand replacement in alkali activated slag/fly ash mortar

- From the results and discussions, it follows that the increase in GA from 0% to 30% leads to a substantial decrease in workability. The sharper edge, more angular shape and higher aspect ratio of GA compared with reference sand reduced the flowability of mortar by hindering the movement of paste and other particles, thus decrease the workability
- GA replacement for reference sand in alkali activated slag/fly ash mortar generally reduces the mechanical strength. The percentage of strength reduction is comparably small and could be accepted when only taking influence of compressive strength into consideration.
- A slight increase of both flexural and compressive strength is due to more available Si from GA dissolution. It is believed as the when content of GA increase to 30 %, the gel formation is enhanced by more available silica incorporation into the C-A-S-H type gel.

In summary, the characterization of GP confirms its high reactivity and suitability for alkali activation. It has been found in this study that GP serves as a highly effective binder precursor replacement for fly ash in alkali activated slag/fly ash binder. Regardless of 10% replacement, the increase in compressive strength is the highest with 30% GP replacement to be 35.8%. GA as fine aggregate replacement can be accepted considering the comparably small decline in mechanical strength. Care should be taken when utilizing GA replacement to have suitable workability for the mixture.

8.2 Recommendations for Future Research

Although it is believed that waste glass powder has the potential to be alkali activated to produce AAMs, its utilization as binder precursor in alkali activated materials is rarely studied before. This master thesis contributes to the understanding of using waste glass powder as partial binder precursor in alkali activated slag/fly ash systems, with specific focus on the reactivity of waste glass powder, the nature of reaction products and effects on gel formation. For the future application of this kind of mixtures, a more comprehensive understanding of waste glass powder in the alkali activated systems is necessary and the following research aspects are recommended for further work.

The microstructural analysis on ternary binder as in this study is tricky. The complexity in chemical compositions and gel formation of the ternary binder hinders elucidation on the reaction mechanism and comprehensive understanding of effect of glass powder replacement. Therefore, it is of great importance to carry out investigation on alkali activated binder solely on glass powder and follows up by a binary system binder.

More precise analytical techniques are necessary to be used to accurately determine the gel network structure. Magic angle spinning nuclear magnetic resonance, abbreviated as MAS-NMR, is recommended to study the gel formation and influence of GP replacement on the reaction products as it provides detailed atomic environment of Si and Al in the network which is closely linked with different gel types. The changes of MCL can also be confirmed by this technique.

Last but not least, it is found in this study that an inconsistency tendency for flexural strength development in mortar with fine glass aggregate. Although assumption is made that the inconsistency is the result of formation of microcracks by possible shrinkage in the mixture, however, the mechanism of shrinkage in AAMs is still largely unknown. As the early age volume stability is of great significance when it comes to real application of this kind of material, the study on the mechanism of shrinkage in alkali activated binder contain waste glass powder is highly recommended.

References

1. *2013 Report on the State of the Environment in China*. 2013: Ministry of Environmental Protection, People's Republic of China.

2. Freeman, H.M., *Standard handbook of hazardous waste treatment and disposal*. 1998: McGraw-Hill.

3. *Published on www.feve.org. These data are published as industry estimates based on latest available figures at country level.*

4. Keulen, A., *Report on waste minerals and solutions*, in *Waste minerals SEMBRES project*. 2013, Van Gansewinkel Minerals.

5. Federico, L.M. and S.E. Chidiac, *Waste glass as a supplementary cementitious material in concrete – Critical review of treatment methods.* Cement and Concrete Composites, 2009. 31(8): p. 606-610.

6. Shi, C. and K. Zheng, *A review on the use of waste glasses in the production of cement and concrete.* Resources, Conservation and Recycling, 2007. 52(2): p. 234-247.

7. Jani, Y. and W. Hogland, *Waste glass in the production of cement and concrete – A review.* Journal of Environmental Chemical Engineering, 2014. 2(3): p. 1767-1775.

8. Duxson, P., et al., *The role of inorganic polymer technology in the development of 'green concrete'.* Cement and Concrete Research, 2007. 37(12): p. 1590-1597.

9. Regourd, M., *Slags and slag cements.* Cement replacement materials. Department of Mechanical Engineering, University of Sheffield, 1986: p. 73-99.

10. Fernández-Jiménez, A. and A. Palomo, *Characterisation of fly ashes. Potential reactivity as alkaline cements ☆.* Fuel, 2003. 82(18): p. 2259-2265.

11. Shi, C., D. Roy, and P. Krivenko, *Alkali-activated cements and concretes*. 2006: CRC press.

12. Provis, J.L. and J.S. van Deventer, *Alkali Activated Materials*. 2014: Springer.

13. Davidovits, J. and M. Morris, *The pyramids: An enigma solved*. 1988: Hippocrene Books.

14. Purdon, A., *The action of alkalis on blast-furnace slag.* Journal of the Society of Chemical Industry, 1940. 59(9): p. 191-202.

15. Glukhovsky, V., *Soil silicates.* Gostroiizdat Publish. Kiev, USSR, 1959.

16. Palomo, A., et al., *Alkaline activation of fly ashes: NMR study of the reaction products.* Journal of the American Ceramic Society, 2004. 87(6): p. 1141-1145.

17. Davidovits, J., *Geopolymers.* Journal of Thermal Analysis and Calorimetry, 1991. 37(8): p. 1633-1656.

18. Davidovits, J. *Chemistry of geopolymeric systems, terminology*. in *Geopolymer*. 1999.

19. Duxson, P., et al., *Geopolymer technology: the current state of the art.* Journal of Materials Science, 2007. 42(9): p. 2917-2933.

20. Kumar, S., R. Kumar, and S. Mehrotra, *Influence of granulated blast furnace slag on the reaction, structure and properties of fly ash based geopolymer.* Journal of materials science, 2010. 45(3): p. 607-615.

21. Puertas, F., et al., *Alkali-activated fly ash/slag cements: strength behaviour and hydration products.* Cement and Concrete Research, 2000. 30(10): p. 1625-1632.

22. Lloyd, R.R., *The durability of inorganic polymer cements.* 2008.

23. Provis, J.L. and J.S.J. Van Deventer, *Geopolymers: structures, processing, properties and industrial applications*. 2009: Elsevier.

24. Puertas, F. and A. Fernández-Jiménez, *Mineralogical and microstructural characterisation of alkali-activated fly ash/slag pastes.* Cement and Concrete composites, 2003. 25(3): p. 287-292.

25. Bernal, S.A., et al., *High‐Resolution X‐ray Diffraction and Fluorescence Microscopy Characterization of Alkali‐Activated Slag‐Metakaolin Binders.* Journal of the American Ceramic Society, 2013. 96(6): p. 1951-1957.

26. Yip, C.K., G.C. Lukey, and J.S.J. van Deventer, *The coexistence of geopolymeric gel and calcium silicate hydrate at the early stage of alkaline activation.* Cement and Concrete Research, 2005. 35(9): p. 1688-1697.

27. Alonso, S. and A. Palomo, *Alkaline activation of metakaolin and calcium hydroxide mixtures: influence of temperature, activator concentration and solids ratio.* Materials Letters, 2001. 47(1): p. 55-62.

28. Yip, C. and J. Van Deventer, *Microanalysis of calcium silicate hydrate gel formed within a geopolymeric binder.* Journal of Materials Science, 2003. 38(18): p. 3851-3860.

29. Ismail, I., et al., *Modification of phase evolution in alkali-activated blast furnace slag by the incorporation of fly ash.* Cement and Concrete Composites, 2014. 45: p. 125-135.

30. Puertas, F., et al., *A model for the C-A-S-H gel formed in alkali-activated slag cements.* Journal of the European Ceramic Society, 2011. 31(12): p. 2043-2056.

31. Bernal, S.A., et al., *Gel nanostructure in alkali-activated binders based on slag and fly ash, and effects of accelerated carbonation.* Cement and Concrete Research, 2013. 53: p. 127-144.

32. Garcia-Lodeiro, I., et al., *Compatibility studies between N-A-S-H and C-A-S-H gels. Study in the ternary diagram Na2O–CaO–Al2O3–SiO2–H2O.* Cement and Concrete Research, 2011. 41(9): p. 923-931.

33. Lee, W. and J. Van Deventer, *Structural reorganisation of class F fly ash in alkaline silicate solutions.* Colloids and Surfaces A: Physicochemical and Engineering Aspects, 2002. 211(1): p. 49-66.

34. Mikuni, A., R. Komatsu, and K. Ikeda, *Dissolution properties of some fly ash fillers applying to geopolymeric materials in alkali solution.* Journal of materials science, 2007. 42(9): p. 2953-2957.

35. Chen‐Tan, N.W., et al., *Determining the reactivity of a fly ash for production of geopolymer.* Journal of the American Ceramic Society, 2009. 92(4): p. 881-887.

36. Chancey, R.T., et al., *Comprehensive phase characterization of crystalline and amorphous phases of a Class F fly ash.* Cement and Concrete Research, 2010. 40(1): p. 146-156.

37. Criado, M., et al., *An XRD study of the effect of the SiO2/Na2O ratio on the alkali activation of fly ash.* Cement and Concrete Research, 2007. 37(5): p. 671-679.

38. Ibáñez, J., et al., *Quantitative Rietveld analysis of the crystalline and amorphous phases in coal fly ashes.* Fuel, 2013. 105(0): p. 314-317.

39. Fernández-Jimenez, A., et al., *Quantitative determination of phases in the alkali activation of fly ash. Part I. Potential ash reactivity.* Fuel, 2006. 85(5): p. 625-634.

40. Hamilton, J.P., et al., *Dissolution of nepheline, jadeite and albite glasses: toward better models for aluminosilicate dissolution.* Geochimica et Cosmochimica Acta, 2001. 65(21): p. 3683-3702.

41. Crundwell, F.K., *The mechanism of dissolution of minerals in acidic and alkaline solutions: Part II Application of a new theory to silicates, aluminosilicates and quartz.* Hydrometallurgy, 2014. 149(0): p. 265-275.

42. Snellings, R., *Surface Chemistry of Calcium Aluminosilicate Glasses.* Journal of the American Ceramic Society, 2015. 98(1): p. 303-314.

43. Oelkers, E.H. and S.R. Gislason, *The mechanism, rates and consequences of basaltic glass dissolution: I. An experimental study of the dissolution rates of basaltic glass as a function of aqueous Al, Si and oxalic acid concentration at 25 C and pH= 3 and 11.* Geochimica et Cosmochimica Acta, 2001. 65(21): p. 3671-3681.

44. Antonić, T., A. Čižmek, and B. Subotić, *Dissolution of amorphous aluminosilicate zeolite precursors in alkaline solutions. Part 2.—Mechanism of the dissolution.* J. Chem. Soc., Faraday Trans., 1994. 90(13): p. 1973-1977.

45. Oelkers, E.H., *General kinetic description of multioxide silicate mineral and glass dissolution.* Geochimica et Cosmochimica Acta, 2001. 65(21): p. 3703-3719.

46. Corkhill, C.L., et al., *Dissolution of UK High-Level Waste Glass Under Simulated Hyperalkaline Conditions of a Colocated Geological Disposal Facility.* International Journal of Applied Glass Science, 2013. 4(4): p. 341-356.

47. Bunker, B., *Molecular mechanisms for corrosion of silica and silicate glasses.* Journal of Non-Crystalline Solids, 1994. 179: p. 300-308.

48. Tashima, M., et al., *Alkali activation of vitreous calcium aluminosilicate derived from glass fiber waste.* Journal of Sustainable Cement-Based Materials, 2012. 1(3): p. 83-93.

49. Ana Balaguer Pascual, M.T.T., Arezki Tagnit-Hamou, *Waste glass powder-based alkali-activated mortar*, in *NTCC2014: International Conference on Non-Traditional Cement and Concrete*. 2014.

50. Redden, R. and N. Neithalath, *Microstructure, strength, and moisture stability of alkali activated glass powder-based binders.* Cement and Concrete Composites, 2014. 45: p. 46-56.

51. Torres-Carrasco, M., J. Palomo, and F. Puertas, *Sodium silicate solutions from dissolution of glasswastes. Statistical analysis.* Materiales de Construcción, 2014. 64(314): p. e014.

52. Puertas, F. and M. Torres-Carrasco, *Use of glass waste as an activator in the preparation of alkali-activated slag. Mechanical strength and paste characterisation.* Cement and Concrete Research, 2014. 57(0): p. 95-104.

53. EN, T., *196-1. Methods of testing cement–Part 1: Determination of strength.* European Committee for standardization, 2005.

54. NEN, E., *196-2; Methods for Testing Cement*, in *Chemical Analysis of Cement (European Standard), Delft, the Netherlands*. 1994.

55. Ma, Y., *Microstructure and Engineering Properties of Alkali Activated Fly Ash*. 2013.

56. NEN, E., *7375.* Leaching characteristics of moulded or monolithic building and waste materials, Determination of leaching of inorganic components with the diffusion test, 2004.

57. EN, B., *1015-3: 1999.* Methods of test for mortar for masonry part 3: Determination of consistence of fresh mortar (by flow table), 1999.

58. Ye, G., *Experimental study and numerical simulation of the development of the microstructure and permeability of cementitious materials*. 2003: TU Delft, Delft University of Technology.

59. Hajimohammadi, A., J.L. Provis, and J.S.J. van Deventer, *The effect of silica availability on the mechanism of geopolymerisation.* Cement and Concrete Research, 2011. 41(3): p. 210-216.

60. Puligilla, S. and P. Mondal, *Co-existence of aluminosilicate and calcium silicate gel characterized through selective dissolution and FTIR spectral subtraction.* Cement and Concrete Research, 2015. 70(0): p. 39-49.

61. Tuchman, D.P., *Research toward direct analysis of quartz dust on filters using FTIR spectroscopy*. 1992: US Department of the Interior, Bureau of Mines.

62. Reig, F.B., J.G. Adelantado, and M.M. Moreno, *FTIR quantitative analysis of calcium carbonate (calcite) and silica (quartz) mixtures using the constant ratio method. Application to geological samples.* Talanta, 2002. 58(4): p. 811-821.

63. Taylor, W., *Application of infrared spectroscopy to studies of silicate glass structure: Examples from the melilite glasses and the systems Na2O-SiO2 and Na2O-Al2O3-SiO2.* Proceedings of the Indian Academy of Sciences-Earth and Planetary Sciences, 1990. 99(1): p. 99-117.

64. Zhang, Z., H. Wang, and J.L. Provis, *Quantitative study of the reactivity of fly ash in geopolymerization by FTIR.* Journal of Sustainable Cement-Based Materials, 2012. 1(4): p. 154-166.

65. Kouassi, S.S., et al., *Dissolution of waste glasses in high alkaline solutions.* Ceramics-Silikáty, 2010. 54(3): p. 235-240.

66. Wang, S.-D. and K.L. Scrivener, *Hydration products of alkali activated slag cement.* Cement and Concrete Research, 1995. 25(3): p. 561-571.

67. Escalante‐García, J.I., et al., *Hydration Products and Reactivity of Blast‐Furnace Slag Activated by Various Alkalis.* Journal of the American Ceramic Society, 2003. 86(12): p. 2148-2153.

68. Oh, J.E., et al., *The evolution of strength and crystalline phases for alkali-activated ground blast furnace slag and fly ash-based geopolymers.* Cement and Concrete Research, 2010. 40(2): p. 189-196.

69. Ravikumar, D. and N. Neithalath, *Reaction kinetics in sodium silicate powder and liquid activated slag binders evaluated using isothermal calorimetry.* Thermochimica Acta, 2012. 546(0): p. 32-43.

70. Chithiraputhiran, S. and N. Neithalath, *Isothermal reaction kinetics and temperature dependence of alkali activation of slag, fly ash and their blends.* Construction and Building Materials, 2013. 45(0): p. 233-242.

71. Gao, X., Q.L. Yu, and H.J.H. Brouwers, *Reaction kinetics, gel character and strength of ambient temperature cured alkali activated slag–fly ash blends.* Construction and Building Materials, 2015. 80(0): p. 105-115.

72. Rimer, J.D., R.F. Lobo, and D.G. Vlachos, *Physical basis for the formation and stability of silica nanoparticles in basic solutions of monovalent cations.* Langmuir, 2005. 21(19): p. 8960-8971.

73. Brough, A., et al., *Sodium silicate-based alkali-activated slag mortars: Part II. The retarding effect of additions of sodium chloride or malic acid.* Cement and Concrete Research, 2000. 30(9): p. 1375-1379.

74. Provis, J. and J. Van Deventer, *Geopolymerisation kinetics. 2. Reaction kinetic modelling.* Chemical Engineering Science, 2007. 62(9): p. 2318-2329.

75. Alarcon-Ruiz, L., et al., *The use of thermal analysis in assessing the effect of temperature on a cement paste.* Cement and Concrete research, 2005. 35(3): p. 609-613.

76. DeJong, M.J. and F.-J. Ulm, *The nanogranular behavior of CSH at elevated temperatures (up to 700 C).* Cement and Concrete Research, 2007. 37(1): p. 1-12.

77. Ye, J., W. Zhang, and D. Shi, *Effect of elevated temperature on the properties of geopolymer synthesized from calcined ore-dressing tailing of bauxite and ground-granulated blast furnace slag.* Construction and Building Materials, 2014. 69: p. 41-48.

78. Criado, M., A. Fernández-Jiménez, and A. Palomo, *Alkali activation of fly ash: Effect of SiO_2/Na_2O ratio: Part I: FTIR study.* Microporous and mesoporous materials, 2007. 106(1): p. 180-191.

79. Rees, C.A., et al., *Attenuated total reflectance fourier transform infrared analysis of fly ash geopolymer gel aging.* Langmuir, 2007. 23(15): p. 8170-8179.

80. Lee, W. and J. Van Deventer, *Use of infrared spectroscopy to study geopolymerization of heterogeneous amorphous aluminosilicates.* Langmuir, 2003. 19(21): p. 8726-8734.

81. Clayden, N., et al., *Solid state 27 Al NMR and FTIR study of lanthanum aluminosilicate glasses.* Journal of non-crystalline solids, 1999. 258(1): p. 11-19.

82. Aguiar, H., et al., *Structural study of sol–gel silicate glasses by IR and Raman spectroscopies.* Journal of Non-Crystalline Solids, 2009. 355(8): p. 475-480.

83. Brinker, C.J. and G.W. Scherer, *Sol-gel science: the physics and chemistry of sol-gel processing*. 2013: Academic press.

84. Gadsden, J.A., *Infrared Spectra of Minerals and Related Inorganic Compounds*. 1975: Butterworths.

85. Fernández-Jiménez, A. and A. Palomo, *Mid-infrared spectroscopic studies of alkali-activated fly ash structure.* Microporous and Mesoporous Materials, 2005. 86(1): p. 207-214.

86. Fernández-Jiménez, A., et al., *Quantitative determination of phases in the alkaline activation of fly ash. Part II: Degree of reaction.* Fuel, 2006. 85(14–15): p. 1960-1969.

87. Garcia-Lodeiro, I., et al., *Stability of synthetic calcium silicate hydrate gels in presence of alkalis, aluminum, and soluble silica.* Transportation Research Record: Journal of the Transportation Research Board, 2010(2142): p. 52-57.

88. Provis, J.L., et al., *Modeling speciation in highly concentrated alkaline silicate solutions.* Industrial & engineering chemistry research, 2005. 44(23): p. 8899-8908.

89. García Lodeiro, I., et al., *Effect on fresh C-S-H gels of the simultaneous addition of alkali and aluminium.* Cement and Concrete Research, 2010. 40(1): p. 27-32.

90. Rees, C.A., et al., *In situ ATR-FTIR study of the early stages of fly ash geopolymer gel formation.* Langmuir, 2007. 23(17): p. 9076-9082.

91. Ravikumar, D. and N. Neithalath, *Effects of activator characteristics on the reaction product formation in slag binders activated using alkali silicate powder and NaOH.* Cement and Concrete Composites, 2012. 34(7): p. 809-818.

92. Richardson, I., et al., *The characterization of hardened alkali-activated blast-furnace slag pastes and the nature of the calcium silicate hydrate (CSH) phase.* Cement and Concrete Research, 1994. 24(5): p. 813-829.

93. Lee, N.K. and H.K. Lee, *Reactivity and reaction products of alkali-activated, fly ash/slag paste.* Construction and Building Materials, 2015. 81(0): p. 303-312.

94. Deir, E., B.S. Gebregziabiher, and S. Peethamparan, *Influence of starting material on the early age hydration kinetics, microstructure and composition of binding gel in alkali activated binder systems.* Cement and Concrete Composites, 2014. 48: p. 108-117.

95. Palomo, A., M. Grutzeck, and M. Blanco, *Alkali-activated fly ashes: a cement for the future.* Cement and Concrete Research, 1999. 29(8): p. 1323-1329.

96. Fernández-Jiménez, A., A. Palomo, and M. Criado, *Microstructure development of alkali-activated fly ash cement: a descriptive model.* Cement and Concrete Research, 2005. 35(6): p. 1204-1209.

97. Hunnicutt, W., *Characterization of calcium-silicate-hydrate and calcium-alumino-silicate-hydrate.* 2013.

98. L'Hôpital, E., *Aluminium and alkali uptake in calcium silicate hydrates (C-S-H).* 2014.

99. Stone, W.E., et al., *Association of soluble aluminum ionic species with a silica-gel surface: a solid-state NMR study.* The Journal of Physical Chemistry, 1993. 97(39): p. 10127-10132.

100. Yu, Z., *Microstructure Development and Transport Properties of Portland Cement-fly Ash Binary Systems: in view of service life predictions*. 2015, TU Delft, Delft University of Technology.

101. Katz, A. and A. Thompson, *Quantitative prediction of permeability in porous rock.* Physical review B, 1986. 34(11): p. 8179.

102. Katz, A., *Microscopic Study of Alkali-Activated Fly Ash.* Cement and Concrete Research, 1998. 28(2): p. 197-208.

103. Tangpagasit, J., et al., *Packing effect and pozzolanic reaction of fly ash in mortar.* Cement and Concrete Research, 2005. 35(6): p. 1145-1151.

104. Neville, A.M., *Properties of concrete*. 1995.

105. I. Papayianni, S.K., K. Datsiou, F. Kesikidou, *Products of alkali-activated calcareous fly ash and glass cullet*, in *NTCC2014: International Conference on Non-Traditional Cement and Concrete*. 2014.

Acknowledgements

This research project was carried out in Microlab, Materials and Environment, CiTG, TU Delft, with support from Van Gansewinkel Minerals. Many people have been supporting in this research and are recognized here:

I would like to express my deepest gratitude to my daily advisor Assoc Prof. Dr. Guang Ye for his excellent guidance, caring, patience and encouragements throughout two years' study in TU Delft. Dr. Ye has been supportive ever since I was an undergraduate student trying to apply for graduate schools. I am very grateful to him for giving me many opportunities to be involved in research activities and helping me improve to become a better scientific researcher. I feel lucky to have a mentor like him.

Sincere acknowledgements also go to my co-supervisor Arno Keulen from Van Gansewinkel minerals, for the valuable discussions, continuous suggestions and kind support during my research. I would also like to thank Dr. Kamel Arbi for helping with sample preparation and interesting discussions on the results.

I would like to express my thanks to other committee members, Prof. dr. ir. Klaas van Breugel and Dr. ir. Michael Janssen for their availability and comments on my thesis.

I appreciate the support by the kind technicians Arjan Thijssen, Ger Nagtegaal, John van de Berg, Maiko van Leeuwenon and Ron Penners on my experimental work. Special thanks go to Arjan Thijssen for teaching me the operation of ESEM. I also appreciate the assistance from other employees at university, especially to the secretary in our group, Nynke Verhulst for her kind assistance.

I greatly appreciate all my colleagues and former colleagues of Microlab for their assistance and friendship. Special appreciation goes to Yibing Zuo and Marija Nedeljkovic for their assistance in analyzing experimental results and fruitful discussions. I thank Dr. Siska Valcke from TNO for discussions on FTIR. I am also thankful to Bei Wu who helps me with the XRD and TGA, and also discussions on gel structure; Jiayi Chen who helped me with preparing ESEM samples; Lourdes Silva de Souza for her suggestions in ICP. I am grateful to my Chinese colleagues: Hua Dong, Peng Gao, Xuliang Hou, Xiaowei Ouyang, Xu Ma, Zhipei Chen, Yun Zhang, Hao Huang, Tianshi Lu, Dr. Zhiwei Qian, Dr. Yuwei Ma, Dr. Zhuqing Yu, Dr. Fuhai Li, Dr. Yun Huang and Prof. Jiangxiong Wei etc. for all the care and support they have given me.

I thank all my dear friends here in the Netherlands and in China, for sharing all the sorrow and happiness with me through the entire time. Special gratitude goes to Yongchang Hu and Yuyao Zhang for being amazing friends. Agita and Boudewijn has been supportive from the very start of my application, their warmth made me feel less homesick abroad.

Last but absolutely not least, I owe the most to my family, especially to my mother and father, who always believe in me. This thesis would not be possible for me without their endless love, encouragements and sacrifice. Deepest acknowledgement also goes to my beloved Kelly, for her everlasting love, companion, patience and understanding. I am so blessed to have her by my side in this vast experiment called life.

张世哲

Shizhe Zhang

Delft, the Netherlands

September, 2015